Enhancing offshore service vessel concept design by involving seakeeping

Developing a framework to efficiently design high-performance offshore service vessel concepts

P.D.H. Bronkhorst

TU Delft

C-JOB
DEDICATED NAVAL ARCHITECTS

Enhancing offshore service vessel concept design by involving seakeeping

Developing a framework to efficiently design high-performance offshore service vessel concepts

by

P.D.H. Bronkhorst

to complete the thesis in process of obtaining the degree of Master of Science
at the Delft University of Technology,
to be defended publicly on Friday August 20, 2021 at 10:00 AM.

Student number:	4405102	
Project number:	SDPO.21.024.m	
Thesis duration:	November 23, 2020 – August 20, 2021	
Thesis committee:	Ph.D. A. A. Kana,	TU Delft, supervisor and chairman
	Ph.D. H. C. Seyffert,	TU Delft, committee member
	Ph.D. L. van Biert,	TU Delft, committee member
	M.Sc. M. Slagmolen,	C-Job, supervisor

An electronic version of this thesis is available at http://repository.tudelft.nl/.
Cover photo is the sea tug 'Abeille Bourbon' in heavy seas, photo from https://www.pecheurdimages.com/gb/3402-the-high-sea-tug-abeille-bourbon.html.

TU Delft

Preface

Before you lies the thesis *'Enhancing offshore service vessel concept design by involving seakeeping: Developing a framework to efficiently design high performing offshore service vessel concepts'*. This thesis is the product of a need by the offshore wind industry for vessels with high seakeeping performance. C-Job recognized this need and provided the initial spark for this thesis topic. I am incredibly grateful for C-Job for providing me with the opportunity to further evolve this spark into a full-fledged thesis. I could not have done this by myself, and I have to thank many people who helped me along the way. In particular, I would like to thank the following individuals, without whom this thesis simply would not be where it is today.

Firstly, I would like to thank Maarten Veldhuizen for presenting me with the initial problem. Your experience and knowledge helped me incredibly with setting out the initial direction of my thesis. Secondly, I would like to thank Mark Slagmolen for his support throughout this thesis. I am thankful for the time you took to provide me with advice, as well as a reality check on my own thoughts during our weekly progress meetings. Thirdly, I would like to thank Austin Kana for providing clarity and helping me determine the appropriate academic direction for this thesis. The clarity in which you are able to present your thoughts regarding ship design is something I hope to achieve someday in my own professional career. Lastly, I would like to thank all my C-Job and TU Delft colleagues, whom I found inspiration, motivation as well as a lot of fun. You know who you are.

In my personal life, I have many people to thank. My parents, who have supported me throughout my studies. My sister, with whom my student life would not have been the same. My friends and housemates, who have always supported me, but also provided the necessary distractions. And my girlfriend, for the support and laughs I have had these past few months.

Philip Dick Henri Bronkhorst
Delft, August 2021

Abstract

The growth in the offshore wind industry sees an increased demand for offshore service vessels (OSVs). These vessels often operate in harsh conditions, and their performance is heavily dependant on their seakeeping characteristics. Conventional ship design processes fail to effectively consider seakeeping early in the design process, leading to sub-optimal vessel design. A design framework has been developed in the software 'NAPA' to efficiently design high-performing OSV concept designs.

The developed framework is able to optimize a hull shape -specifically the main particulars and length of different hull sections- to maximize performance in certain objectives. These objectives are seakeeping, ship resistance, lightship weight, and station keeping power requirements. Regarding seakeeping, the attainable percentage operability is calculated for each iteration, although the Operability Robustness Index (ORI) is optimized. The ORI is a more robust seakeeping key performance indicator (KPI) than percentage operability, which is advantageous when facing concept design uncertainty [42]. The framework maximizes ORI, thereby seakeeping performance, for a particular loading condition, motion sensitive criteria, and operational area. The ORI is evaluated based on the area of operation's scatter diagram and wave spectrum, governing motion limits, and iteration-specific RAOs. Designs are required to satisfy an initial stability constraint, to ensure feasibility.

The framework's output is a Pareto-frontier showing the trade-offs between different KPIs, and the corresponding variable combinations. Thereby, the naval architect can evaluate what design offers the best overall performance.

A 'feeder' OSV, designed to transport wind turbine components to wind installation vessels has been optimized to validate the framework. This OSV is currently being developed as a concept by C-Job naval architects. The ship has been optimized for maximum operability of an Ampelmann motion compensated platform. A single optimization run took three and a half hours to complete 300 iterations, thereby finding the Pareto-frontier. Comparing the Pareto-optimal solutions with the base vessel, the ORI can be increased up to 3.6%, the lightship weight decreased by 21.1% and the ship resistance decreased by 13.0%. The framework showed that smaller vessels can still attain good seakeeping performance, leading to a substantial reduction in lightship weight. The increase in seakeeping performance allows for the use of less expensive motion compensated equipment while maintaining high operability. The framework showed that there is a trade-off to be made with regard to seakeeping, and lightship weight, and ship resistance. The framework presents what variables and ship attributes cause these trade-offs. This information allows naval architects to determine the optimal design direction during concept design. Clients and naval architects can decide what trade-off in performance provides the ideal combination to achieve the ship's mission. Consequently, besides producing high-performance designs, the framework substantially increases early design knowledge. Thereby, the overall design process becomes more efficient.

The framework showed to be a valuable tool for OSV concept design. By the extensive incorporation of seakeeping early in the design process, naval architects can design high-performance OSVs efficiently. The produced designs maximize performance in any of the KPIs, ensuring vessels have a high operability, but do not weigh more, or have higher fuel costs than is needed.

Contents

Nomenclature

Abbreviations

2D	Two-dimensional
3D	Three-dimensional
ACD	Accelerated concept design
AHTS	Anchor handling tug supplier
CAD	Computer aided design
CAPEX	Capital expenses
CFD	Computational fluid dynamics
CoB	Center of buoyancy
CoG	Center of gravity
DoF	Degrees of freedom
FEM	Finite element methods
GA	Genetic algorithm
GM	Metacentric height
JONSWAP	Joint North Sea wave observation project
KPI	Key performance indicator
NSGA-II	Non-dominated sorting genetic algorithm II
OPEX	Operational expenses
ORI	Operability robustness index
OSCV	Offshore subsea supply vessel
OSV	Offshore service/support vessel
PercOp	Percentage operability
PSV	Platform supply vessel
RAO	Response amplitude operator
ROV	Remotely operated vehicle
SAMO-COBRA	Self-Adaptive algorithm for Multi-Objective Constrained Optimization by using Radial Basis Function Approximations
SKF	Station keeping force
TSHD	Trailing suction hopper dredger
W2W-vessel	Walk-to-work vessel

Greek symbols

α Angle [°]

α Wave steepness factor [°]

β Wave angle [°]

μ Direction of waves with respect to forward direction of vessel $[rad]$

μ Viscosity $[kgm^{-1}s^{-1}]$

∇ Volume $[m^3]$

ν Kinematic viscosity $[m^2s^{-1}]$

ω Wave frequency $[rad/s]$

ω_n Natural roll frequency $[rad/s]$

ϕ Roll position $[rad]$

ψ Yaw position $[rad]$

ρ Density $[kg/m^3]$

σ_j Motion limit $[m]$

θ Pitch position $[rad]$

Math operators

$\ddot{}$ Second derivative with respect to time

$\dot{}$ Derivative with respect to time

Roman symbols

A Area $[m^2]$

B Beam $[m]$

C_B Block-coefficient $[-]$

F Force $[kN]$

F Force or moment $[N]$ or $[Nm]$

Fr Froude number $[-]$

g Gravitational acceleration $[m/s^2]$

GM Metacentric height $[m]$

H Wave height $[m]$

$HBILGE$ Height bilge keel $[m]$

K_{xx} Radius of gyration $[m]$

KG Distance keel-centre of gravity $[m]$

KM Distance keel-metacentre $[m]$

L Length $[m]$

L_{PP} Length between perpendiculars $[m]$

$LBILGE$ Length bilge keel $[m]$

LSW Lightship Weight $[t]$

M Mass or inertia $[kg]$ or $[kgm^2]$

M Moment $[Nm]$

m (First) Spectral moment $[rad \cdot m^2 \cdot s]$

N_{qc} Quadricubic number $[-]$

ORI Operability Robustness Index $[-]$

$PercOp$ Percentage Operability $[\%]$

R_T Total ship resistance $[kN]$

$RBILGE$ Moment arm bilge keel $[m]$

RLD Critical roll damping factor $[\%]$

$RLD1$ Linear part of roll damping $[Ns]$

$RLD2$ Non-linear part of roll damping $[Ns^2]$

Rn Reynolds number $[-]$

S Wave spectrum $[m^2 \cdot s]$

SR Ship Resistance $[kN]$

t Tonne $[t]$

T_z Zero-crossing period $[s]$

V Velocity $[m/s]$

V_S Ship speed $[kn]$

X Environmental force in X direction $[kN]$

x Longitudinal position $[m]$

x x-direction $[-]$

y Transverse position $[m]$

y y-direction $[-]$

z Vertical position $[m]$

z z-direction $[-]$

Sub-scripts

$_{1/3}$ Highest one third

$_{afts}$ Aftship

$_{air}$ For air

$_{ballast}$ Ballast

$_b$ Relative location to CoG of vessel

$_c$ Current

$_c$ With contingency

$disp$	Displacement
dl	Deck load
$fwds$	Forwardship
$hull$	Hull
$longitudinal$	Longitudinal
ls	Lightship
L	Longitudinal
$midss$	Midship
p	Absolute location of point on vessel
RAO	With respect to response amplitude operator
$roll$	With respect to roll
ss	Superstructure
S	Significant height
tol	Tolerable
tot	Total
$transverse$	Transverse
T	Transverse
$water$	For water
w	Wind
x	X-direction
y	Y-direction

List of Figures

List of Tables

1 Introduction

1.1. Project context

Due to the growing offshore wind industry ([88]), there is a need for specific offshore service vessels, also known as offshore support vessels (OSVs). For some of these vessels, such as crane ships or walk-to-work vessels, motion behavior is one of the key aspects influencing the operability, and therefore the performance of such ships. During the design of a vessel, the motion characteristics are calculated once the main particulars, powering, arrangements, and so forth, have been determined. At this point, there is limited room for adjustment of the vessel design if motion behavior needs to be changed. Hence, to design high-performing OSVs efficiently, there is a need by the industry to consider motion behavior as one of the key design drivers from the start of the design.

In recent years, an effort has been made by the maritime industry to develop methods to effectively maximize performance in certain design objectives during the concept design stage. C-Job has started developing such a design method in the form of 'Accelerated Concept Design' (ACD). ACD is an optimization algorithm built into a software suite developed for ship design applications. Within this software suite, a parametric model can developed and optimized by ACD. Appropriate parametric modeling could enable the naval architect to calculate motion response early in the design stage. As such, ACD could optimize the parametric model on seakeeping performance. Thereby, naval architects can consider motion behavior in early-stage concept design. Hence, ACD could be applied to develop a framework to incorporate motions characteristics during the concept design stage.

C-Job sees an opportunity to design high-performing OSVs by developing a concept design framework around ACD. In the context of OSVs, other design drivers may govern the design, in addition to motion characteristics. The motion optimization objective can contradict these other optimizing objectives. For example, a walk-to-work vessel necessitates both a minimal level of motions and minimal ship resistance, influencing crew transferring and transit operations, respectively. Gutch et al. ([42]) demonstrated that a relatively wider ship shows a decreased motion response against a North Sea ocean wave spectra. Although the wider ship shows a better motion response, the ship resistance and subsequent fuel costs are also increased. The design framework should consider multiple design objectives, ultimately giving naval architects the opportunity to determine balanced optimally performing vessel designs.

To conclude, to design high-performing OSVs, motion characteristics should be considered during concept design. This thesis aims to develop a framework whereby motion behavior is optimized by using ACD. This framework should also consider other design objectives which may be contradictory. Additionally, to develop the framework, this thesis aims to investigate what exactly the design drivers and corresponding design variables are for OSVs.

1.2. Research goal

The primary goal of the research is to develop a design framework allowing naval architects to consider motion characteristics during the concept design stage. Such a framework will be an integrated set of design parameters, analysis tools, and an optimization routine ultimately allowing for a streamlined and efficient concept design process of an OSV. By considering all relevant objectives, the framework can

be considered 'holistic' (from the Greek word 'holos' meaning "all, whole, entire"). This research goal is achieved by both a review of literature, developing a design framework, applying it to a case study and evaluating the results.

1.3. Research questions

To support the primary research goal, the following main research question will be answered:

"***How can a new concept design framework incorporating seakeeping improve the design of offshore service vessels?***"

The following sub-questions provide an answer to the main research question, and form the basis for the literature review:

1. **Why is motion behavior an important characteristic of offshore service vessels?**
2. **What is the state-of-the-art of concept design frameworks?**
3. **What are the main design drivers of offshore service vessels?**
4. **What is the current state-of-the-art in design optimization for ship motion characteristics?**
5. **What are the requirements for a concept design framework involving ship motion characteristics?**
6. **How is a concept design framework incorporating motion characteristics developed?**
7. **How can the new framework be verified and validated?**

By answering the research sub-questions above, this thesis aims to provide an answer to the main research question, thereby achieving the goal of the project. Research sub-question one has partially been answered in section 1.1, though is further touched upon throughout the report. Sub-questions two, three and four are answered in chapters 2, 3 and 4 respectively. Based on these answers, sub-question five is answered in chapter 5. Parametric modeling methods are discussed in chapter 6. Based on the findings of chapters two to six, a framework is developed. Its methodology is discussed in chapter 7. The framework is verified and validated in chapters 8 and 9 respectively. The thesis is ended with a discussion of results and conclusion in chapter 10.

1.4. Report structure

This thesis report consists of a review of literature and a new design framework methodology. The core of the literature review is divided into three parts. Firstly, general ship design processes will be elaborated in chapter 2. With general ship design known, OSVs will further be investigated in chapter 3. Given the prime importance of motion behaviour for OSVs, chapter 4 performs a thorough investigation of this subject. Based on the findings of chapters 2, 3 and 4, the needs for the new framework are discussed in chapter 5. Based on the needs analysis, parametric modeling methods are discussed in chapter 6.

The framework methodology comprises three parts. The needs of the framework, together with the findings of the parametric modelling study, result in a new framework discussed in chapter 7. The framework is verified and validated in chapters 8 and 9 respectively. The report is concluded in chapter 10.

Each chapter begins with a brief explanation of the chapter-specific structure. Additionally, chapters 1 - 9 are ended with a conclusion and summary.

2

Ship design

This chapter concerns an explanation of various facets of ship design, thereby answering the research sub-question *'What is the state-of-the-art of concept design frameworks?'*. Firstly, conventional design methods are elaborated in section 2.1. Concluding the findings in section 2.1, the need for an holistic design approach is discussed in section 2.2. A state-of-the-art account of holistic concept design methods is given in section 2.3. This review includes C-Job's own ACD method in sub-section 2.3.2. Finally, the chapter is concluded and summarized in section 2.4.

2.1. Conventional ship design process

2.1.1. Design spiral

Ship design is a complex multifaceted problem, requiring the integration of many engineering disciplines. The end goal is to design a ship that is able to carry out its designated task, doing so in a cost-efficient way. Many design trade-offs exist, and compromises are made throughout the design process. A successful ship design is the result of good and close cooperation between the designer, the customer, the yard, and the equipment suppliers [92]. In the last 70 years, many new developments have been introduced by academia and industry [92]. These range from developing certain ship design processes, such as the design spiral, to more advanced design and calculation methods with the onset of computer-aided design. The former, known as the 'ship design spiral', is one of the most widely used methods to structure ship design. Developed by Evans et al. ([32]), the design spiral describes an iterative process whereby the ship design progresses towards a converged solution. Figure 2.1 visualizes this process.

In the ship design spiral, the mission requirements form the starting point of the design. After which certain design aspects of the ship follow in a specific order. These aspects include global proportions and preliminary powering, lines and body plans, and so forth. As such, each step forms the input for the next consecutive design step. Additionally, the ship design spiral considers the four typical design phases occurring throughout the design of a ship. The design moves through these phases, and each item is iterated and becomes more final in its design. In theory, this process allows for an ideal converged design solution. In practice, a ship design process tends to differ, which the spiral fails to capture [73]. Shortcomings of the ship design spiral, noted by numerous researches, are:

- The design spiral assumes various aspects of the ship design occur sequentially. As already noted in in 1986 by naval ship designer D. Brown [17]: "*The naval architectural aspects of the design are also difficult to structure and are not properly represented by flow diagrams such as the design spiral.*". In practice, during the design process, the time pressure forces simultaneous engineering of various aspects of the ship design. Regarding the aim of this thesis, ship aspects influencing motion characteristics in particular also influence ship resistance. These ship attributes need to be considered simultaneously as they are principally intertwined.
- The design spiral assumes the iterative process leads to an ideal solution. As noted earlier, each step provides input to the consecutive step. As such, the initial design direction governs each consecutive step. Hence, the spiral constrains the design space rapidly. Rather than converging

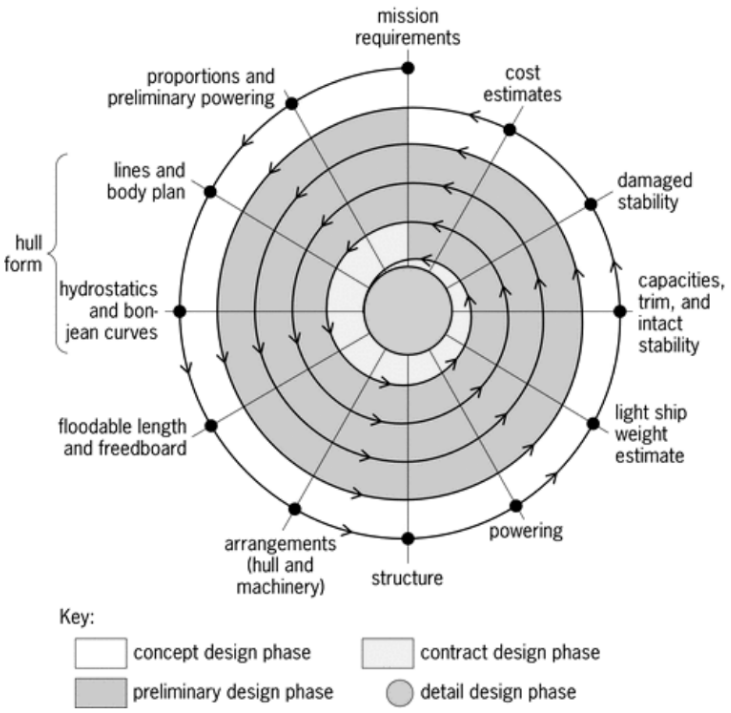

Figure 2.1: Ship design spiral [32]

to an optimal design solution, the design spiral attempts to make the initial design direction 'work'. The majority of the cost implications are decided upon during the early design phase. As a result, a sub-optimal design direction may be decided which may lead to higher costs of the vessel. In the context of this thesis, the design spiral does not consider motion behavior. When applying the design spiral for the design of an OSV, there is a substantial risk of the resultant design having sub-optimal motion characteristics.

- The design spiral was developed during a time when computers were in a fairly infantile phase [67]. This is reflected by the design spiral, as it only addresses design aspects that could be deducted at the time. Since the 2000s, computers are able to extensively assist naval architects in the design of ships. Computer-aided design tools (CAD) enable the naval architect to consider strength optimization with the help of finite element methods (FEM), optimal hull shapes with the help of computational fluid dynamics (CFD), and many more aspects. As such, contrary to making a certain design 'work', naval architects are more than ever enabled to find optimal design solutions.

The design process of a ship tends to happen more 'organically', contrary to the process described by the design spiral. As stated above, the engineering of various aspects happens simultaneously. Today, CAD tools also allow engineers to evaluate many more ship aspects compared to the 1960s. C-Job has developed a formal description of this more natural ship design process. This process is called the 'C-Job Design Circle'.

2.1.2. C-Job Design Circle

The conventional ship design process used by C-Job is called the C-Job 'Design Circle' [20]. The C-Job Design Circle is a concurrent design process whereby multiple engineers design various facets of the ship in parallel. These aspects are intact stability, damage stability, strength, weight & cost, space reservation, resistance, and motions. Development occurs in four levels of detail, specifically:

- Level 1; Results are based on reference databases
- Level 2; Results are on multi-regression analysis
- Level 3; Results are based on simplified simulation analysis such as CFD potential flow analysis

• Level 4; Results are based on accurate simulations such as CFD viscous flow analysis

This process is visualized in figure 2.2.

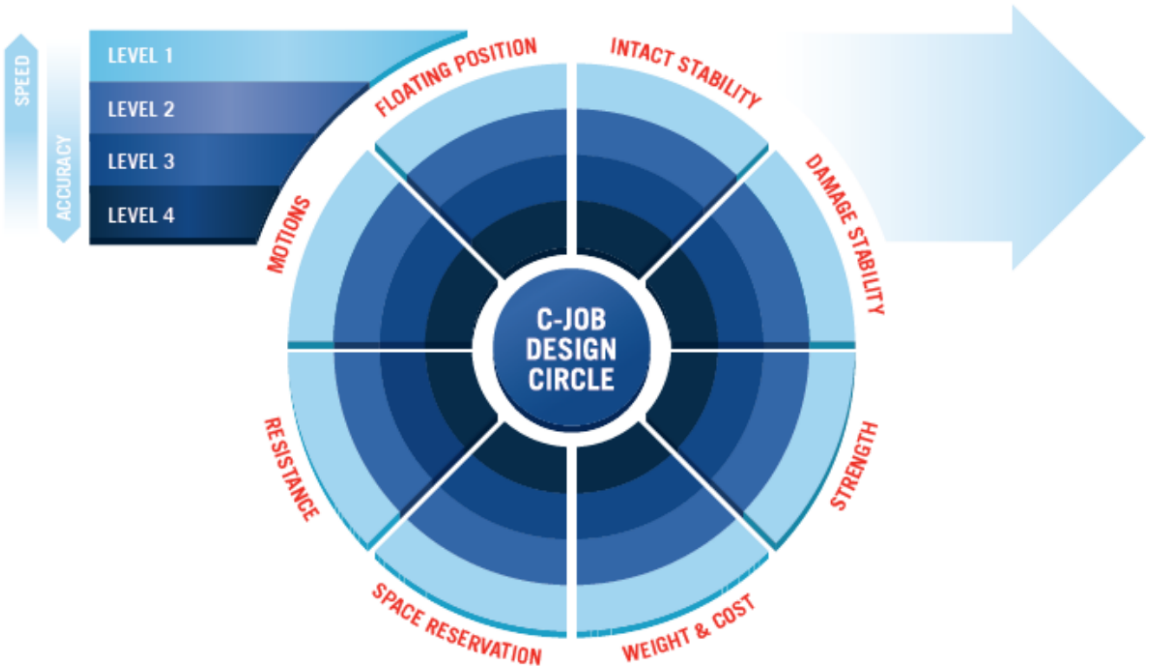

Figure 2.2: C-Job Design Circle [25]

As shown by figure 2.2, the higher the level of detail, the higher the accuracy. The higher accuracy is obtained at the cost of time required for determining the aspect. Inherent to a concurrent design process, C-Job recognizes no order in which any aspect of the ship is designed. The process does still follows certain design phases. These are similar to the design phases as described earlier, and are:

1. Concept design phase
2. Basic design phase
3. Functional design phase
4. Detail design phase

Additionally, C-Job recognizes two developments occurring during the design of a vessel. Firstly, whilst the design developed, the amount of information known about the design increases substantially, visualized by the C-Job 'Design Pyramid', shown in figure 2.3. Secondly, when the ship design matures, it converges towards a single solution and the room for adjustment becomes limited. This is visualized by the 'C-Job design funnel' shown in figure 2.4.

These developments are further confirmed by academic research ([65], [11]). The growing amount of information (figure 2.3) supports a certain design direction (figure 2.4). This information is obtained by spending progressively increasing engineering hours. The information acts as 'luggage', discouraging engineers to make any major changes in later phases of the design, even if those changes improve the performance of the final product. This development emphasizes the need to make the correct design decisions early in the design. Andrews et al. ([11]) argues that the ship design spiral, and many other conventional design processes, attempt to speed up and simplify the concept design process. Given the criticality of this design phase, this simplification has not led to better or faster designs, but limits naval architects from determining optimal performing vessels. To quote Andrews [11]:

"*such a speeding up of an essentially simplified approach to design synthesis is not sensible. Firstly, there is the need to conduct a more sophisticated approach in order to proceed in a less risky manner into the main design process for such complex vessels. Secondly, further advances in computer techniques, particularly those that CAD has adopted from computer graphics advances, now enable*

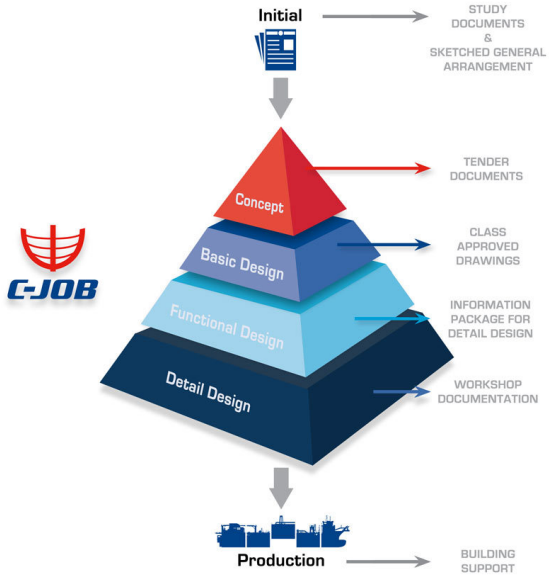

Figure 2.3: C-Job Design Pyramid, indicating the increased amount of knowledge when a design matures [8]

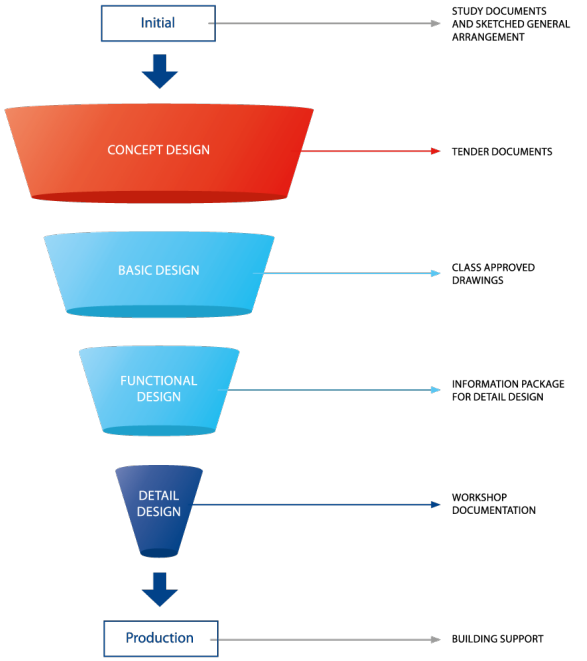

Figure 2.4: C-Job Design Funnel, indicating the restricted design freedom when a design matures [8]

ship concept designers to synthesize more comprehensively and thereby address from the start many more of the likely design drivers"

This notion has been recognized by the industry, and various ship synthesis frameworks or 'holistic design approaches' have been developed. These approaches aim to incorporate all relevant aspects of ship design at design phases when parameters of influence are largely determined. C-Job's ACD method is one of such holistic design approaches.

2.2. Holistic design approach for ship design

2.2.1. Introduction

As discussed in section 2.1, making the correct design decisions early in the design of a vessel is highly important yet challenging. To mitigate this challenge, and facilitate the design of high-performing vessels the concept design phase should consider all relevant aspects ([72], [11]) to the vessel. The development of computing technology has enabled naval architects to approach ship design in such a manner regardless of the complexity [67]. In the last decade, much effort has been made by academia to develop such design methods in the form of ship synthesis models ([11], [67]). These methods have started to gain traction by the industry and are typically called 'holistic' design approaches.

Broadly speaking, these methods optimize a set of design variables to a set of design objectives by the means of various evaluation methods by an optimization algorithm in an iterative process. Additionally, the subsequent design has to satisfy certain constraints. This (simplified) working principle is depicted in figure 2.5.

The outcome of the depicted procedure is a set of 'Pareto-optimal' solutions. These are design solutions on a Pareto-frontier, indicating the trade-offs between two design objectives. Such a Pareto-frontier is shown in figure 2.6.

The Pareto-frontier indicates design solutions with the maximum attainable performance at one objective at the cost of performance in another objective. As such, naval architects can identify the exact trade-offs and determine optimal design solutions.

These efforts have extended to incorporate the estimation of various vessel aspects during the concept design, which was previously only done so in a later phase. C-Job's ACD method also concerns such an approach, as it is able to involve all sorts of objectives [25]. Thereby, the risk of having to make a sub-optimal design 'work' is mitigated during contract and detail design. Ultimately, naval architects

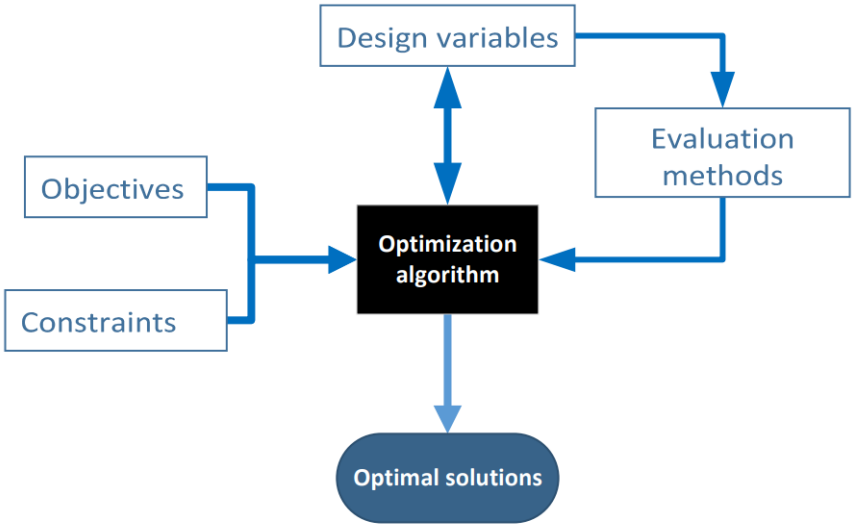

Figure 2.5: Simplified working principle of holistic optimization method

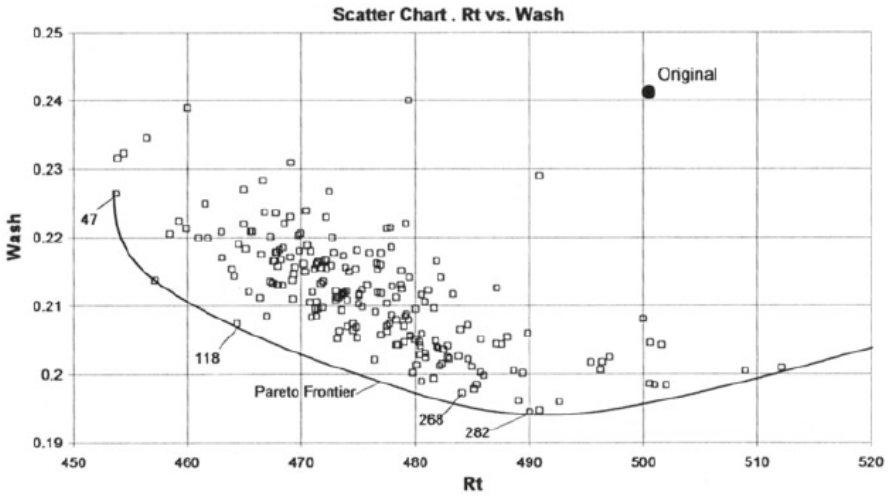

Figure 2.6: Scatter chart with feasible designs for a mono-hull plotted against two objectives, total resistance and wash, showing the Pareto-optimal frontier as the lower envelope [70]

are given the freedom to choose a configuration that best suits the client's demands. In the last decade, a multitude of these methods has been developed for the maritime industry. These are discussed in the next chapter.

2.3. State-of-the-art holistic concept design frameworks

In this section, a state-of-the-art review of holistic approaches as described in section 2.2 is given. Specific attention is given to the differences between these methods in a broader ship design context. That is, the performance and practicality of such methods will be discussed.

Firstly, some methods that have currently been applied will be discussed. Additionally, C-Job's ACD method will be discussed in a separate subsection. Lastly, the research gap will be identified.

2.3.1. Applied concept optimization methods

One of the more prominent examples of an holistic design method, is the earlier discussed 'HOLISHIP' project ([72],[16],[75],[76]). The HOLISHIP project realises a holistic approach to ship design by developing a framework solving multi-objective problems. Within this approach, a parametric model of the ship is created, which is subsequently optimized according to certain KPI's.

An application of HOLISHIP by Priftis et al. ([76]) also introduced a method to account for the uncertainty during concept design. Priftis et al. characterizes a design as robust - with minimal uncertainty - when the final solution does not change much when small modifications in the problem occur. Optimization methods that overlook uncertainty tend to produce non-robust, over-optimized designs that do not correspond to reality. In the case study, uncertainty is accounted for by applying probabilities.

Deb et al. ([27]) applied an evolutionary multi-objective optimization (EMO) method to enhance the knowledge of a designer and give insight in ship design issues. In the paper, a simple optimization problem was approached with different objectives related to cost, weight, performance, and cargo-carrying abilities. Uncertainty analysis in the design was incorporated in a similar fashion as done by Priftis et al. As such, the variables were made 'uncertain' using a Gaussian distribution with a standard deviation proportional to 5%, 10%, and 20% of their values. The effects on the Pareto-fronts, are shown in figure 2.7,

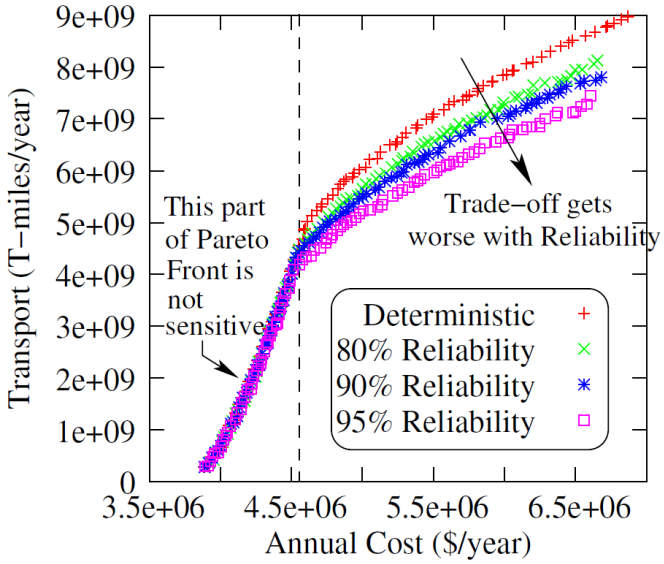

Figure 2.7: NSGA-II obtained trade-off Pareto-optimized solutions for bi-objective ship design problem with uncertainty in three design parameters. [27]

In figure 2.7, it can be identified whether the Pareto front is sensitive to uncertainty, or whether a trade-off gets worse with reliability.

Ljulj et al. ([61]) developed a multi-attribute concept design procedure for generic naval vessels. The procedures allowed for optimizing the life-cycle cost and the overall measure of the effectiveness of a vessel. The final 'best' design was determined based on a weighted sum of the objective scores. Both the weight coefficients and value functions were derived by using Saaty's theory and an analytical hierarchy process method ([79],[80]). Consequently, this method is able to determine a singular optimal design out of the Pareto-frontier.

Hannapel ([44]) dedicated her PhD work to the development of multidisciplinary design optimization algorithms for ship design under uncertainty. Hannapel developed various methods for uncertainty, similar to the ones incorporated in the studies done by de Priftis et al. and Deb et al. ([76], [27]). Additionally, Hannapel discusses surrogate modeling techniques. Surrogate techniques model the expected behavior of a parameter on a certain design objective. When evaluation of the designs requires solving simulation methods, these techniques can substantially save computing time. C-Job's ACD method is another example of a holistic design method that employs surrogate modeling.

2.3.2. C-Job's ACD method

Recently, C-Job has started to develop a holistic design method called ACD [25]. ACD works in a similar fashion to other holistic design methods. Hence, the design method allows for efficient exploration of the design space and finding Pareto-fronts for certain key performance indicators (KPIs). Specifically, the ACD method comprises a framework consisting of two major components:

1. **Software package 'NAPA' where the ship is defined**

   A parametric model of the ship is defined in the NAPA software package. The NAPA software suite allows for the development of simulation tools that can evaluate the parametric model [9]. The parametric model and objectives differ per design problem. Hence, each design problem requires a bespoke ACD framework to be developed.

2. **Optimization algorithm**

   Different algorithms can be selected to optimize constrained multi-objective problems. Some prior holistic design methods saw the application of genetic algorithms. De Winter developed algorithms tailored for efficient optimization within maritime applications. See also appendix D for a paper by de Winter et al. testing the performance of these algorithms.

To prove the concept of the ACD method, C-Job has carried out a case study [25]. In the case study, a trailing suction hopper dredger (TSHD) was optimized for the total cost of ownership. To do so, a parametric model of the geometry of the vessel was created. A visualization showing these parameters with respect to the vessel is given in figure 2.8. Specifically, the model allowed the algorithm to rearrange the bulkheads and the hull shape of the vessel. Rearranging the bulkheads influenced the floating position, intact stability, damage stability, draft, heel, trim, and so forth. Multiple constraints were set to ensure feasible designs. In practice, constraints also allow the naval architect to enable ACD to meet certain client requirements. The total cost of ownership in the case study comprised of various CAPEX- and OPEX-related costs. The experiment used an existing design as a base input. 200 evaluations were done with the ACD method to simulate the time available in a real-world case. The design was run five times independently to prove consistency. The results showed all five independent runs to obtain similar results. On average, 24% of the random design variations turned out to be feasible. Compared to the original design, the final resultant design had a 19% smaller resistance coefficient and 14% lower steel weight.

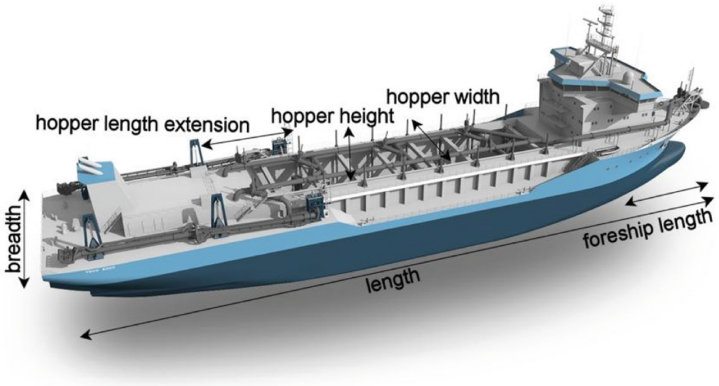

Figure 2.8: TSHD parametric model [25]

Based on the state-of-the-art review of holistic design methods, a research gap can be identified. This is done in the next subsection.

2.3.3. Research gap

The various methods discussed in the previous sections achieved a holistic design approach to the given design problem, although each differed slightly. In the context of this thesis, the efficiency of the method and the ability to determine optimal designs are critical. The former is important due to the likely involvement of computationally expensive motion analysis software. The latter is important if more than two optimization objectives reflect OSV design drivers.

Concerning the efficiency of a method, the algorithm used in the ACD method is most efficient as it applies surrogate modelling and actively recognizes design directions towards optimum points, contrary to the inherent randomness factor of genetic algorithms [25].

The ability to determine optimal designs describes the method's ability to determine *final* optimal designs from the obtained Pareto-optimal solutions. The ACD method forms an attractive candidate

to use, due to the speed and (relative) integration into the NAPA framework. Yet, if more than two objectives are present, an inspection of the Pareto-frontiers may not suffice to determine final optimal design solutions. As such, a method for determining final optimal designs may be required. Many of these methods exist, such as applying an analytical hierarchy process, weighing the different objective scores according to different scenarios.

2.4. Conclusion and summary

To answer the research sub-question, *'What is the state-of-the-art of concept design frameworks?'*, conventional ship design processes fail to efficiently consider all design drivers throughout the design process. Additionally, time pressure warrants naval architects to make design decisions quickly, even if the design space has not yet been fully explored. As such, conventional design processes may lead to sub-optimal design choices. Once a design moves past the concept and preliminary design phases, the majority of the ship aspects are determined and subsequent costs are decided. As such, sub-optimal design decisions may lead to more expensive vessels with decreased vessel performance.

Due to the shortcomings of conventional design processes, various 'holistic' design approaches have been developed. C-Job's ACD method concerns such an approach. A holistic approach considers all important aspects of a ship design from the start of the design process. Such an approach optimizes a set of design variables to a set of objectives. By the means of various evaluation methods, various ship aspects can be considered, even in an early design phase. A holistic design approach may form a solution to incorporate motion behavior efficiently, early in the design process of OSVs. Specifically, C-Job's ACD method is able to efficiently optimize designs, even when computationally expensive evaluation software is required. In comparison to other methods, there may be a development gap with the ACD method if more than two optimization objectives are present. If more than two objectives are present for the concept design of an OSV, a routine to determine final optimal designs should be determined. These objectives are based on the functionalities and design drivers of any vessel type. Therefore, chapter 3: Offshore service vessels will define the OSV vessel type.

3

Offshore service vessels

This chapter further defines the OSV vessel type by answering the research sub-question *'What are the main design drivers of offshore service vessels?'*. To do so, a definition of offshore service vessels and their sub-types are given in section 3.1. Typical OSV design drivers are discussed in section 3.2, directly answering the earlier mentioned research question. The research sub-question *'What is the state-of-the-art of concept design frameworks?'* is also further elaborated with respect to OSVs by giving a brief account of developments in design for OSVs in section 3.3. The chapter is briefly concluded and summarized in section 3.4.

3.1. Definition and OSV sub-types

OSVs are an intricate, complex type of vessels which fulfill unique roles in the maritime industry [11]. Most OSVs serve to support either the oil & gas industry or the rapidly growing offshore wind industry. Within these industries, OSVs carry out a number of activities spanning from construction, towing, sub-sea diving, supplying, servicing, and everything in between. As such, the mission of any OSV can be any of these activities, be it as the ship's single purpose, or a combination of.

Typically, three main types of OSVs are considered: anchor handling tug supplier (AHTS), platform support vessel (PSV), and offshore subsea construction vessels (OSCV) [6]. A newer type of OSV, the walk-to-work vessel (W2W-vessel), is also considered [40]. The W2W-vessel is specifically used for servicing offshore wind farms and can quickly transport technicians to offshore wind turbines by a motion compensated gangway. In the text below, a brief description of each type is given based on a study by Erikstad et al. ([6]) on system based design of offshore support vessels.

- **Platform supply vessel (PSV)**

  PSV's main mission is to provide supplies to offshore platforms. To do so, they feature a large open deck space and the capability to store dry and wet cargo underneath the deck. Typically, they also feature systems to dispose of any (hazardous) waste from offshore platforms. To maneuver around offshore structures, PSVs are highly maneuverable and are often fitted with DP systems. In figure 3.1, a typical PSV is depicted.

- **Anchor handling tug supplier (AHTS)**

  AHTSs assist large floating offshore structures. These assisting activities can be towing the structures or handling the mooring anchors. In addition, they are capable of supply operations, fulfilling a similar role to PSVs. As such, they have a large open deck space, dry and wet storage capacity, and DP functionality. In addition, a powerful propulsion system is fitted for high bollard pull. A typical AHTS is depicted in figure 3.2.

- **Offshore subsea construction vessel (OSCV)**

  OSCVs are designed to carry out offshore construction activities, such as the construction or maintenance of offshore wind farms. They typically feature a large onboard crane, carry a remote-controlled vehicle (ROV) for underwater operations, are fitted with a moon-pool, have a large open

Figure 3.1: PSV 'VOS Patriot' [63]

Figure 3.2: AHTS designed by C-Job [7]

deck-space for construction equipment, have a helicopter platform for the transport of specialized personnel, and have DP functionality for high maneuverability and stationkeeping performance. As such, OSCVs are highly complex vessels. A typical OSCV is depicted in figure 3.3.

Figure 3.3: OSCV 'SKANDI SKANSEN' [3]

Figure 3.4: W2W-vessel 'KASTEELBORG' [2]

- **Walk-to-work vessel**

  The recent growth in the offshore wind industry saw an increased demand for new types of OSVs suited for servicing offshore wind farms ([40], [60]). As servicing wind farms requires visiting many offshore wind turbines, the W2W-vessel type has been created. These types of vessels are specifically suited for efficiently transporting technicians to offshore wind turbines. As such, they are typically fitted with a motion-compensated crane and gangway. In addition, W2W-vessels feature a large accommodation for housing technicians, and an open deck space for servicing equipment or turbine components. In figure 3.4, such a vessel is depicted.

The various subtypes show OSVs span a wide range of vessels, all of service to the offshore industry in some way. To understand the global design governing principles, applicable to any OSV, a study has been done with C-Job naval architects to determine the design drivers that dictate any OSV design. These are discussed in the next section.

3.2. Design drivers OSVs

A design driver is an aspect of the ship that is of such influence that it 'drives' the design [57]. Consequently, to fully satisfy the needs of a design driver, it should be considered from the start of the design of a vessel. C-Job naval architects have been interviewed to derive OSV design drivers [1]. Based on these interviews, and the OSV functionalities, typical design drivers governing the design of OSVs can be determined. See the next page for a list of these design drivers.

[1] An interview report providing this input is available in the appendices

- **Design driver - Mission equipment**

  Inherent to a certain type of OSVs, it has to be able to carry out certain missions. To do so, certain mission equipment needs to be installed onboard. Depending on the type of OSV, this equipment can be motion compensated gangways, cranes, chemical process equipment, and so forth. This equipment may significantly impact the design requirements of an OSV, such as requirements for a large open deckspace, or strong foundations for a large crane, and therefore forms an important design driver.

- **Design driver - Cost**

  An obvious design driver for any new-build ship is the cost. To maximize revenue, any shipowner wants a vessel that generates maximum value at a minimal cost. This cost can be decomposed into capital expenses, CAPEX, and operational expenses, OPEX. These costs consider the acquiring and operating costs of a vessel respectively.

  CAPEX considers the design- and (mostly) building cost of a vessel. Increasing vessel's weight and design complexity increase building cost. During the design of a vessel, the volume is typically correlated with the weight. The design complexity is increased by the number of compartments, intricate ship structures, and advanced equipment. Hence, minimizing building costs requires minimizing the volume and amount of expensive equipment, as well as keeping the layout and general ship design simple. It should be noted that the extent of the complexity is determined during later design phases, namely, during basic design and detail design. For instance, during these phases, the exact structural layout, cable routing, and so forth are determined.

- **Design driver - Lead time**

  The time needed for designing and building ships is also known as lead time and is preferred to be a short as possible for commercial ships. Any ship is only able to full fill its function once it has been launched and sea trials are completed. As such, depending on the function, from there on out it is able to generate revenue for the owner.

  The design time can partially be reduced by the use of efficient design methods. The building time can partially be reduced by keeping the weight and subsequently volume low, thereby reducing the amount of to be fabricated items. Additionally, keeping the ship design simple allows for easier building vessels. As such, the fabrication time can also be reduced.

- **Design driver - Station keeping**

  Many offshore vessels lay stationary to fulfill their functions. Such functions include lifting, walk-to-work activities, and so forth. As such, station keeping capabilities are an important aspect of offshore vessels. Station keeping capabilities are defined by how well a ship can remain stationary in adverse weather conditions. Nowadays, offshore vessels requiring such capabilities are fitted with a DP system. Depending on the redundancy of the system, it can become quite complex. As a result, it may heavily influence the design of the vessel. Station keeping capabilities can be improved by a more powerful DP system. However, this is undesirable from fuel consumption, thus OPEX, perspective. By keeping the vessel compact, the area over which waves, current, and wind can enact a force is minimized. Hence, keeping the ship as compact as possible allows for higher station keeping performance. Additionally, the DP system can ensure station keeping performance with less power, thereby improving fuel costs.

  It should be noted that a ship can also remain stationary using mooring or jack-up systems. For smaller offshore service vessels this is time-consuming and impractical compared to using a DP system.

- **Design driver - Ship resistance**

  For ships that spend much time in transit, a low ship resistance is beneficial. A low ship resistance leads to reduced fuel costs, thus lower OPEX. In practice, this typically steers a design to slenderer ships with optimized hull forms. These factors can heavily impact the total design and are therefore considered design drivers. It should be considered that most OSVs primarily sail at slower speeds (or Froude numbers). At lower Froude numbers, the hull shape is of lesser importance as frictional resistance dominates.

- **Design driver - Seakeeping**

  For any offshore vessel using motion compensated equipment (such as cranes or gangways) to carry out its mission, seakeeping or motion characteristics are of prime importance. Maximum tolerable motions limit the performance of equipment and the comfort of the crew. Motion characteristics of a hull influence how quickly a ship reaches these limits. Hence, these characteristics influence the ship's operation in adverse conditions. As such, an high ability to be operational results in a vessel that is able to operate more often. Consequently, such a ship is able to generate higher revenue.

  The response of a vessel to waves defines its motion characteristics. This response considers any motion in six degrees of freedom (DoF) of the vessel. Additionally, a motion can be decomposed in amplitude, velocity, and acceleration. The response depends on the type of waves encountered and this area of operation. For PSVs, W2W-vessels, and OSCVs in particular, the stationary motion response is important, as they lay stationary when performing supply, walk-to-work, or construction activities.

  C-Job naval architects commented considerations can be taken to minimize motions. Firstly, the transverse metacentric height (GM_T) is necessitated to be kept as low as is safely possible. This results in a large roll period, thus minimal roll accelerations. Additionally, motions can be dampened using appendages and specific damping equipment such as anti-roll tanks. Lastly, the motions of the vessel are also heavily dependant on the size of the ship. A very wide ship leads a (typically) high metacentric height and accelerations, though motion amplitudes will be minimal. A slenderer ship will have higher motion amplitudes, yet slower accelerations. As consequence, the slender ship is more comfortable for the crew. These ship aspects are largely determined during concept and preliminary design phases, emphasizing the need to consider motion behavior early in the design [2].

  This notion by C-Job to consider motion behavior early in the design of OSVs is further supplemented by the work carried out by Gutch et al. ([42]). Gutch et al. argued the offshore industry demand for high reliability and availability for offshore service vessels is by large affected by the vessel's motion behavior. The development of motion compensated equipment has allowed vessels to operate in harsher environments, yet the ability to carry out missions is still largely dependant on the ability to not exceed motion limits. Gutch et al. emphasizes that this requires a holistic design approach and specifically worked on developing a KPI for seakeeping performance [3]. To illustrate this need, figure 3.5.

		Absolute value for beam variation						
	Length [m]	small			mid			large
percOP [%] North Sea	80	84.6	72.2	67.4	65.8	66.7	68.0	72.4
	100	78.4	75.0	74.0	77.5	79.8	82.5	86.7
	120	80.6	81.9	83.7	87.3	89.6	91.8	95.0
	140	88.4	90.0	92.0	94.9	96.3	97.4	98.5
	160	95.1	96.3	97.4	98.5	99.0	99.4	99.6
North Atlantic	80	80.1	65.1	54.8	47.8	44.7	42.4	44.3
	100	66.7	57.6	51.2	50.8	51.5	53.4	56.6
	120	58.2	56.6	56.4	58.3	61.3	65.9	71.0
	140	60.9	62.8	66.5	71.0	75.3	80.0	84.6
	160	71.4	75.4	79.8	84.2	88.0	91.4	93.9

Figure 3.5: Effect of variation length and beam (between $18.3[m]$ and $30.4[m]$ in increments of $\sim 3.0[m]$) on probability of exceeding motion limits (PercOP [%]) [42]

Figure 3.5 shows that the main particulars, which are determined in the early design phases, influence the motion behavior and subsequent probability of exceeding motion limits. Additionally, shown is the significant influence of these parameters on the probability and corresponding mission effectiveness. Furthermore, the figure illustrates that an OSV cannot simply be made 'larger'

[2] The ship aspects of influence to motion behavior are discussed in further detail in section 4.4: Influencing ship motions.
[3] This KPI is further discussed in section 4.3: Operability

or 'wider', yet requires careful consideration of the operational area to determine the optimal dimensions. Hence, considering motion characteristics early in the design of OSVs can improve mission effectiveness, emphasizing the need to do so.

This section answers the research question *'What are the main design drivers of offshore service vessels?'*, which are mission systems, cost, lead time, station keeping, and motion characteristics. The latter two in particular are more specific to the OSV vessel type. C-Job indicated various ship aspects are of influence on motion behavior, some of which are mostly determined at the concept and preliminary design stages and relatively fixed thereafter. Hence, this implies a need for a particular design approach for OSVs.

3.3. State-of-the-art OSV concept design

3.3.1. State-of-the-art review

OSVs are intricate types of vessels that fulfill unique roles and corresponding functionalities. Consequently, unique design drivers govern the design of OSVs. In recent years, numerous efforts have been made to form tailored design methodologies or design drivers for the design of OSVs. Specifically, the research by Gaspar et al. ([35]) and Rehn et al. ([77]) focused on new design methodologies to determine 'optimal' OSV designs.

Gaspar et al. ([35]) quantified the value robustness of OSV design to consider the life cycle performance. To do so, Gasper et al. carried out offshore market forecasts using Epoch-Era analysis. A case study was carried out related to the design of a platform supply vessel. The case study illustrated the complexity involved in striking the correct balance between optimizing the vessel for the first known contract, yet also providing additional capabilities to be competitive in the context of future market requirements. The paper transforms the classical question *'Is this vessel able to fulfill the stakeholder's requirements?'* into *'Is this the right vessel to the right mission?'*. Consequently, it argues that the *right* vessel is not one that is larger, faster, or stronger, but rather a vessel that is able to bring a return of investment regardless of future market uncertainty. By applying an Epoch-Era analysis, a particular vessel design is evaluated on multiple scenarios in terms of place of operation, type of contracts, shifts in policy or the offshore market and so forth. Consequently, these scenarios may represent different circumstances in which the vessel is to operate, or different 'epochs'. A combination of epochs formed an era in which the ship is to operate.

Gasper et al. carried out a case study thereby analyzing different variations of OSVs. Each combination was subsequently weighed to different expected eras. As such, the research by Gaspar et al. resulted in a method for weighing the vessel's life cycle performance.

Rehn et al. ([77]) carried out a holistic optimization study specifically for OSVs. Rehn et al. evaluated the trade-offs between performance, cost, and flexibility for reconfigurable offshore ships. To do so, Rehn et al. evaluated a set of designs with a score indicating the flexibility of an OSV and the acquisition cost. A parametric model containing was created. The parametric model was heavily discretized by having fixed increments between the parametric model. As such, it lacked the fidelity to *optimize* a specific design, but rather broadly identify trade-offs. Design space of 5803 feasible designs was generated and analyzed by obtaining the Pareto-optimal solutions. Exploration of the Pareto-frontier allowed identification of the trade-off between the flexibility of OSVs and acquisition costs. The method proved the use of holistic design methods for OSV design. The results showed OSV ships suitable for retrofitting platforms are characterized by having excess stability, deadweight, and deck area to take on equipment retrofits. Increased platform flexibility does increase capacity, but at the cost of operability, increased resistance, unfavorable roll periods, and high accelerations [4].

3.3.2. Research gap

A difference in the goal of both studies and the goal of this thesis can be observed. The research by Gaspar et al. served to determine OSV designs with increased life-cycle performance. Rehn et al. developed a holistic design evaluation method to determine the trade-offs of re-configurable offshore service vessels which subsequently increase life-cycle performance. Rehn et al. did incorporate

[4] The seakeeping analysis carried out by Rehn et al. is further discussed in section 4.6: State-of-the-art ship motion optimization studies

seakeeping analysis, though with substantial simplifications. The evaluation served to identify global trade-offs for different (reconfigurable) OSV configurations.

Consequently, both methods of Gaspar et al. and Rehn et al. serve to expand the knowledge of OSV designs. Specifically, both methods have been developed to determine OSV designs with increased life-cycle performance.

In the context of this thesis, it is assumed that C-Job designs a vessel for a client which provides certain requirements. The client provides requirements for mission systems or area(s) of operation, which may include considerations for the vessel's life cycle. As such, the method developed by this thesis allows the naval architect to make decisions with respect to the design on how to best achieve the client's requirements.

To conclude, a research gap exists in the fidelity of the existing OSV design approaches, and the fidelity required for determining the optimal design of a specific OSV.

3.4. Conclusion and summary

In the process of answering the research sub-question *'What are the main design drivers of offshore service vessels?'*, this chapter defined OSVs, their sub-types, corresponding functionalities, and design drivers. The design drivers of OSVs are systems, cost, lead time, station keeping, ship resistance, and motion characteristics. These design drivers heavily influence the design of a vessel, but also affect each other's performance. It may impact the dimensions, hull shape, layout, needed equipment, and many more aspects. Consequently, the design drivers for OSVs need to be considered from the start of the design of a vessel.

The research sub-question *' What is the current state-of-the-art in holistic concept design frameworks?'*, has been answered with respect to OSVs. Two studies have been carried out, mostly to determine optimal designs for life-cycle performance. The methods evaluated multiple designs with a low level of fidelity. Consequently, the methods served to determine global trade-offs and optimums. As such, there exists a research gap in design frameworks aimed at determining accurate optimum configurations for a specific to-be-designed OSV.

The motion characteristics design driver may form complex implications on the design of an OSV. As such, this design driver will be further elaborated in chapter 4: Ship Motions.

4

Seakeeping

Chapter 3 illustrated the need to consider motion behavior in the design of OSVs. As motion behavior is the aim of this thesis, an elaboration is given in this chapter. Thereby, a first step is taken towards answering the research sub-question *'What is the current state-of-the-art in design optimization for ship motion characteristics?'*. Specifically, a definition of motion characteristics is given in 4.1. Section 4.2 discusses ship motion limits relevant to offshore vessels. The vessel's response to waves and motion limits forms an input to various measures for operability, discussed in section 4.3. Measures to influence motion characteristics are explained in section 4.4. Methods to calculate ship motions are compared in section 4.5. With this information known, a state-of-the-art review of motion behavior optimization studies is performed in section 4.6. Thereby the research sub-question *'What is the current state-of-the-art in design optimization for ship motion characteristics?'* is fully answered. Finally, the chapter is concluded and summarized in section 4.7.

4.1. Response amplitude operator

This ship motion response due to waves is typically given in the form of response amplitude operators (RAOs) [55][1]. Thereby, it is assumed any ocean sea state considers many individual waves, each characterized by a wave frequency, ω, and an amplitude, ζ_a. The ship is assumed to be a filter, whereby waves form the input, and the ship motions the output. The RAO shows the dimensionless response of the vessel to certain wave frequencies. In figure 4.1, a typical RAO response diagram is shown.

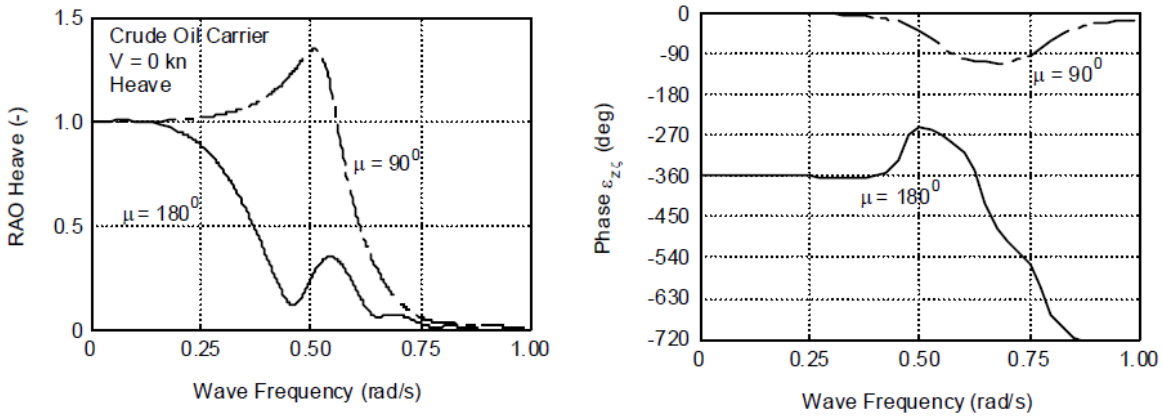

Figure 4.1: Heave RAO of a stationary crude oil carrier for bow head waves (wave angle $\mu = 180°$) and beam waves (wave angle $\mu = 90°$) [55]

In figure 4.1, the heave RAO of a crude oil carrier lying stationary is depicted. Specifically, the RAO shows how much the vessel is excited by waves of a certain frequency. Additionally, the bottom graph

[1] It is assumed the reader is aware of rudimentary ship rigid body dynamics as well as the ship equation of motion, refer to appendix B.

shows the phase of the RAO, indicating the delay between a wave encountering the ship, and the response of the ship itself, or the phase response.

When restoring forces are present, resonance effects can occur. Resonance happens when the natural frequency of the motion coincides with the wave frequency. This results in far greater excitation forces. This is shown by the resonance peak (peak of the bow, $\mu = 90°$ wave RAO at $\omega = 0.5[rad/s]$ in figure 4.1). When designing any vessel, an effort should be made to avoid having the natural frequency of the motions coincide with the most probable wave frequency of the waves found in the area of operation. Especially for roll response, where the damping forces are limited [59].

In determining a vessel's seakeeping performance, the ship motion response is not the only defining factor. If there are no motion limits, the ship can move as freely as possible. However, either because of debilitating crew performance or due to equipment constraints, a vessel is subject to motion limits.

4.2. Motion limits

The prime reason motions are to be minimized is because the ship as a whole, crew, and equipment have tolerable limits for vessel motions. Many studies and guidelines exist aimed at giving value to these limits. A widely used guideline for motion limits has been developed by Faltinsen ([33]). These limits are the result of an extensive study done in the Nordic co-operative project 'Seakeeping performance of ships', also known as 'NORDFORSK' [66]. In this study, the limits ensuring hull safety, operation of equipment, cargo safety, personnel safety, and efficiency have been extensively researched. The result is a set of motion limits applicable to any ship in general. An example of these limits is shown in table 4.1.

In addition to the limits indicated in the NORDFORSK project, any piece of equipment may have its own limits. This holds especially true for OSVs with motion-compensated equipment. This type of equipment makes use of hydraulics and actuator to mitigate the relative motion response of a vessel due to waves. Consequently, the motion-compensated equipment remains static relative to the earth's reference frame. There are mechanical limits to this equipment. As such, this equipment typically has specific motion limits. These limits can include a motion, velocity, or acceleration limit [31].

General Operability Limiting Criteria for Ships (NORDFORSK, 1987)			
Description	Merchant Ships	Navy Vessels	Fast Small Craft
RMS of vertical acceleration at FP	0.275 g (L ≤ 100 m) 0.050 g (L ≥ 330 m)	0.275 g	0.65 g
RMS of vertical acceleration at Bridge	0.15 g	0.20 g	0.275 g
RMS of lateral acceleration at Bridge	0.12 g	0.10 g	0.10 g
RMS of Roll	6.0°	4.0°	4.0°
Probability of Slamming	0.03 (L ≤ 100 m) 0.01 (L ≥ 330 m)	0.03	0.03
Probability of Deck Wetness	0.05	0.05	0.05

Table 4.1: General operability limiting criteria for ships ([33],[66])

For areas of the ship for which motions are critical, such as crew quarters, the bridge, motion compensated equipment, it is beneficial to have the location as close to the CoB as possible (see equation B.1). This remains true for OSVs, although motion compensated gangways may be required to be near the edge of the vessel to minimize the distance between the gangway and to-be-serviced fixed platform (such as a wind turbine) [40]. Cranes often are installed on the side of the vessel to clear the open deck space as much as possible [2]. The bridge is typically a critical point for accelerations since it needs to be at a high location to ensure good visibility. Due to the high location, and subsequently distance from the CoG, the bridge easily experiences large motions.

Based on vessel RAOs and motion limits, naval architects can determine what wave results in the exceedance of the motion limits. If the area of operation is known, an estimate is made on how often these limits are exceeded. Such an estimate is also known as a measure of operability.

[2]This statement is based on input provided by C-Job.

4.3. Operability criteria

Vessel RAOs, motion limits, and area of operation form input for an higher-level assessment of seakeeping performance, reflecting vessel uptime. Widely used by industry, Soares et al. ([34], [83], [78]) developed a linear approach for calculating 'percentage operability', or $PercOp$. Soares et al. defined the percentage operability as 'the percentage of time during which the ship is operational' [34].

Recently, Gutsch et al. ([42], [41]) developed a seakeeping performance indicator called 'Operability Robustness Index', or ORI. The ORI is developed as a robust seakeeping performance indicator. Whereas the percentage operability is heavily dependant on motion limits, the ORI's focus is on the interaction between a ship and the area of operation and is less dependant on the motion limits. An example illustrating this is shown in figure 4.2.

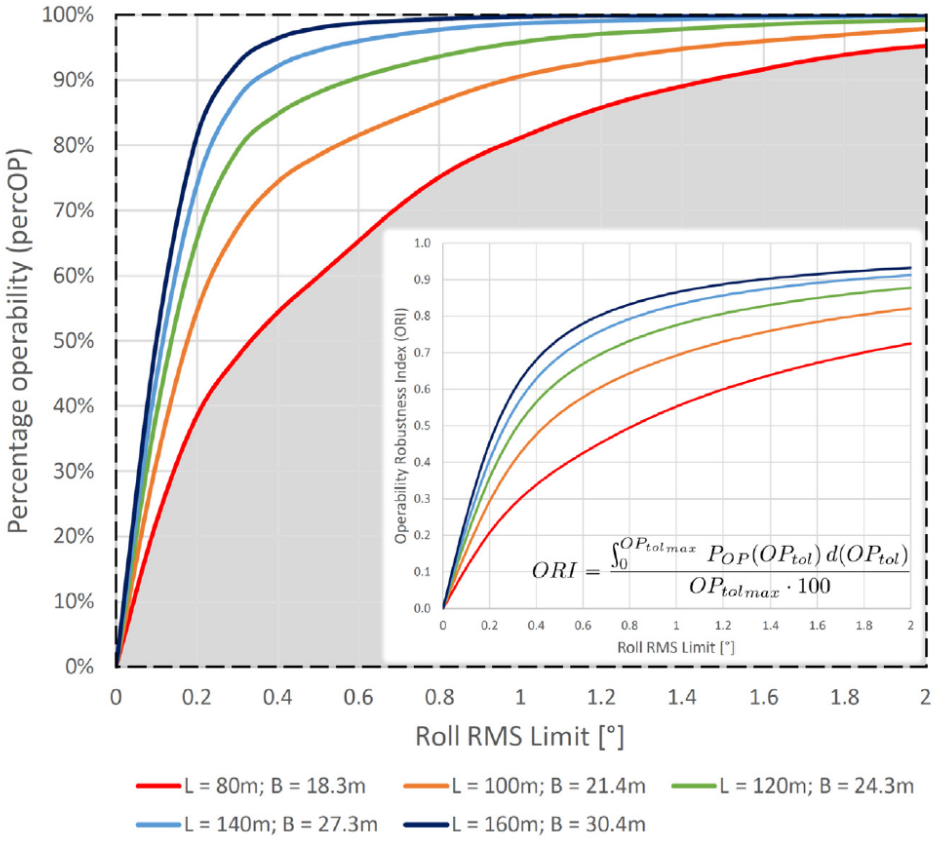

Figure 4.2: Derivation of the Operability Robustness Index from percentage operability [42]

In figure 4.2, the percentage operability ($PercOp$) is plotted as a function of a roll motion limit for five vessels with varying main particulars. When considering the percentage operability for a limit of 2 [°], the difference between all vessels is relatively small. Yet if the roll limit decreases, a steeper decrease of percentage operability is shown for the smaller vessels. As such, the similar percentage operability at a roll limit of 2 [°] does not necessarily mean all vessels have a similar seakeeping performance. ORI aims to be a more robust indicator of seakeeping performance by integrating and normalizing the area under the percentage operability line. Hence, the 'range' of operability values for a specific hull is captured in a single value. Thereby, nuances in the seakeeping performance of varying hull shapes are magnified by capturing the range of percentage operability values. The ORI parameter may therefore be useful for optimization problems in preliminary design stages, uncertainty is a factor. During concept design, the roll limit may not be fully known, which can significantly influence the final percentage operability.

Naval Architects employ various methods to influence ship motions, and thereby improve the seakeeping performance of any ship. These are discussed in the next section.

4.4. Influencing ship motions

In this section, methods to influence ship motions are discussed. These can be categorized by findings from academia, as well as recommendations from C-Job Naval Architects. Both are discussed in subsections 4.4.1 and 2.1.2 respectively.

4.4.1. Findings from academic studies

Methods to influence ship motions have been studied extensively for the past few decades. In particular, Beukelman et al. ([13]), Lloyd ([62]) and Gutsch et al. ([42]) researched the effects of different vessel aspects on ship motion response.

Beukelman et al. ([13],[3]) investigated the influence of the following parameters: forebody section shape, ship length, longitudinal center of buoyancy, block coefficient, and weight distribution on the pitch and heave motions. The study concluded that:

- Heave response increases with increased ship speed
- V-shaped forebodies reduce heaving motion compared to U-shaped forebodies. The influence of forebody shape on the pitch is minor.
- The heave and pitch motions are reduced significantly by an increased ship length.
- The block coefficient causes a rather strong reduction of motions and accelerations.
- The increase of the radius of inertia shows higher heaving and pitching motions.

Lloyd further investigated the effect of hull size and form on seakeeping [62]. Specifically, the effects of changing the hull size, draught/length ratio, beam/length ratio and forward waterplane area coefficients on the heave response were investigated. The effects were studied for an experiment considering a typical North-Sea wave profile. Lloyds made the following conclusions:

- In general, increasing the ship size whilst keeping the shape the same shows a decrease in heave motion response both for amplitude and accelerations.
- Increasing the draught/length ratio shows the increased response in both heave amplitude and accelerations due to a decrease in the added mass and damping terms.
- Increasing the beam/length ratio shows an increased displacement, added mass, and damping coefficients. The excitation from waves is also increased due to a large waterplane area. Consequently, the heave accelerations are reduced whilst motion amplitudes are increased.
- Increasing the forward waterplane area reduces the heave motion amplitude and acceleration.

Both Beukelman et al. and Lloyd implied that simply increasing a certain parameter will increase or decrease a certain motion response. If these guidelines are to be implemented in a design framework adequate freedom should be given to the parametric model to influence these parameters. Both authors simplified this by predetermining a set of varying hull shapes. The variations were modified from a standard hull shape without regard for aspects such as stability, ship resistance, and so forth. Beukelman et al. and Lloyd applied the same wave spectrum and scatter diagram for their experiments.
Gutsch et al. ([42]) found in a recent publication that different ocean areas result in different optimal vessel configurations with regard to seakeeping. Specifically, by adjusting the principal dimensions of a vessel, the frequency of the resonance peaks can be shifted to maximize operability for a certain area of operation. This is illustrated in figure 4.3.

In figure 4.3, the roll RAOs of various vessel configurations are plotted. Specifically, the RAOs of a standard OSV hull shape for various lengths have been computed. Each hull has been analyzed with a metacentric height of $GM_T = 4.5[m]$. The RAOs are plotted against the probability of a certain wave peak period. This has been done for both the North Atlantic (right figure) and the North Sea winter season (left figure). Comparing both plots, it can be seen that a smaller ship will have better roll motion behavior when operating in the North Atlantic. A smaller ship will have its resonance peak occur at a lower period compared to that of the most probable waves. On the contrary, the waves on the North Sea tend to have a shorter wave period. Consequently, a larger ship will have less risk of its natural roll period coinciding with the most probable wave periods.

[3] Even though this academic work is older (year of publication being 1977 and 1989), it remains in use by more recent studies on seakeeping

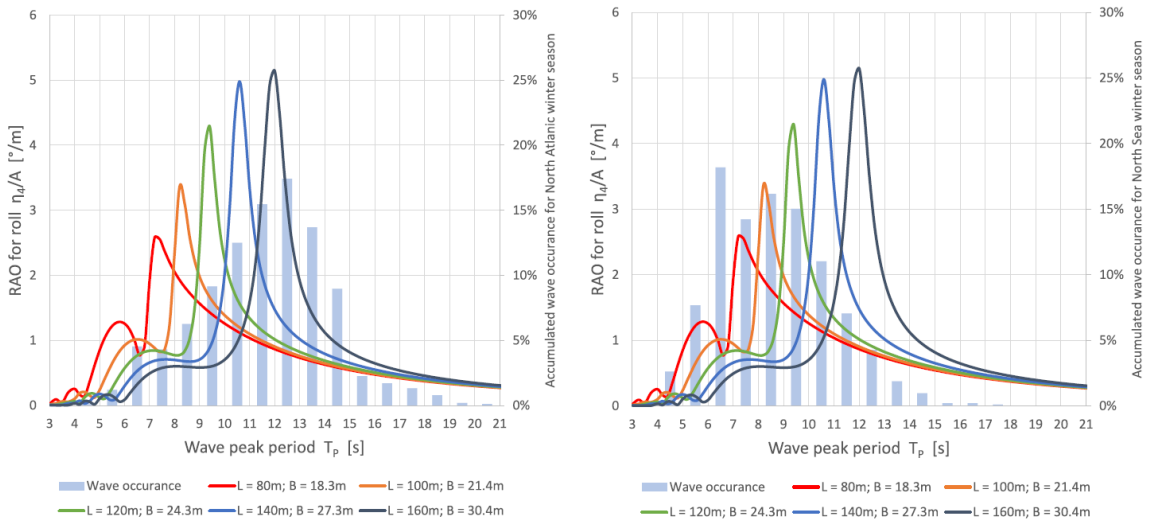

Figure 4.3: Roll motion RAO in relation to the wave occurrence accumulated over the wave height per peak period [42]

Concluding figure 4.3, Gutch et al. showed that the area of operation should be considered when optimizing vessel motions. Regardless, similarly to Beukelman et al. and Lloyd, Gutch et al. developed a predetermined set of hull designs that were to be tested. As such, the hull shapes were developed without regard for the needs of other design drivers, applicable during the design of a to-be-built and operated vessel. Hence, the aim of the three works was of experimental nature regarding seakeeping rather than developing a new design method. The three works of research did indicate which parameters should be considered if a vessel's motion behavior is important. Yet in a to-be-used *holistic* framework, seakeeping forms just one aspect.

4.4.2. Recommendations from C-Job

C-Job naval architects provided information on ship parameters used in practice to control ship motions [4]. The effect of each of these parameters can be related to the ship EoM (see equation B.2). Below, a brief account is given of each of these ship attributes.

- **Hull shape**

  A well-understood way of adjusting ship motions is by adjusting the hull shape. The hull shape is defined by the main particulars, and 'fullness' of the hull, characterized by prismatic coefficients in different areas. Adjusting the hull shape or configuration allows for manipulating the added mass, damping, and mostly (heave) restoring force terms.

- **Appendages**

  Appendages concern protruding parts of the hull such as rudders, thrusters, and bilge keels. The latter of which is specifically added to ships to influence motion characteristics. A bilge keel is a fin mounted on the hull to reduce roll motions. An example of a typical bilge keel configuration is shown in figure 4.4.

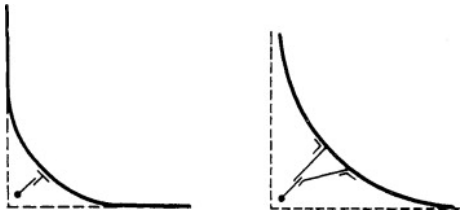

Figure 4.4: Typical bilge keel location on a ship hull [18]

[4] An interview report providing this input is available in the appendix A

A bilge keel increases the amount of added mass that is to be accelerated when the ship undergoes a roll motion. Consequently, accelerations are minimized. Additionally, when undergoing a roll motion, the bilge keel will generate a vortex and cause fluid separation effects [59]. Hereby, some energy of the roll motion is dissipated, damping the roll motion of the ship. A bilge keel does not require forward speed to function and is considered a passive roll damping device.

Ikeda et al. ([53], [54], [49], [50], [51]) showed that the bilge keel size is heavily dependant on the hull shape and size. As such, the effectiveness of a bilge keel is partially dependant on the hull form. A hull shape particularly suitable for bilge keels might have worse motion behavior compared to another hull shape without bilge keels. If both are fitted with bilge keels, the former might actually have the better motion response. No research on this particular notion has been carried out, nor have bilge keels been incorporated with such fidelity in early ship design frameworks. Yet, given the hull form is determined in early design phases, a concept design framework incorporating appendages can lead to better performing vessels.

Active roll damping devices are gyroscopes, rudders, and active fins. As OSVs are of a larger size, and motions are to be minimized in stationary activities, these damping devices are not concerned.

- **Anti-roll tanks**

  Anti-roll tanks consider a pair of partially filled tanks that extend across the beam of the ship [59]. The tanks are constructed in such a way to allow the liquid to slosh from side to side in response to the roll motions of the ship. As such, the anti-roll tanks enact a moment on the ship. By adjusting the phase response of the anti-roll moment, it can dampen the moment enacted by a wave, and thereby the roll motion.

- **Mass distribution**

  The mass distribution of a vessel specifically influences the mass term in equation B.2. As such, the accelerations and natural frequency of the heave, pitch, and roll motion can be adjusted [55]. Though, as indicated by Beukelman et al. ([13]), the influence is limited. C-Job mentioned that naval architects are typically more concerned with adjusting the mass distribution to match the CoB and CoG. Consequently, naval architects refrain from adjusting the mass distribution purely to improve motion characteristics.

- **Metacentric height**

  The behavior of a vessel's pitch and roll motions are largely dependant on the pitch and roll restoring force components (see equation B.2). As the restoring force for the roll is given by,

$$c_{roll} = \rho g \nabla \overline{GM}_T \tag{4.1}$$

  where GM_T is the transverse metacentric height, it is GM_T heavily influences the roll motion. By increasing GM and thereby restoring force terms, the ship roll and pitch amplitudes are decreased. Respective accelerations are increased, as are the natural periods of the motions well as vice versa.

Concluding both subsections 4.4.1 and 2.1.2, the ship hull significantly influences motion behavior. Additionally, the appendages, anti-roll tanks, mass distribution, and metacentric height are also of influence on ship motion behavior. The experiment by Gutch et al. (see figure 4.3)showed that specific dimensions are optimal for specific areas of operation. Additionally, a relation exists between the effectiveness of bilge keels and the hull shape. This implies the need to consider appendages early in the concept design phase as the hull shape is largely determined thereafter. Some of these aspects are also influenced by other design drivers. Section 3.2 showed that design drivers lead time, cost, ship resistance, and station keeping capability are also affected by the hull shape. As such, trade-offs might arise between design driver-related objectives.

A holistic design approach forms a solution to incorporate motion behavior, the ship aspects of influence, effective area, but also other design drivers. Consequently, few researchers have considered a holistic approach to incorporate motion behavior early in the design process. These studies are discussed in section 4.6. Yet first, it is important to consider methods to calculate ship motion response.

4.5. Calculating ship motions

4.5.1. Methods

Analyzing ship motions has been of great interest to naval architects, as elaborated in section 3.2, and is critical for designing good performing OSVs. Classically, ship motions have been analyzed with model tests. The recent increase in computing power has greatly enlarged the toolset for naval architects to analyze motion criteria. For commercial vessel designs, during the concept design stage, naval architects typically employ strip theory or potential flow methods to calculate vessel motion behavior. Unsteady computational fluid dynamics (CFD) methods and model-testing are typically too expensive. Different strip theories and potential flow methods exist to determine ship motion behavior. These solvers solve the Navier-Stokes (NS-) equation, though ignore terms reflecting unsteady effects. In the text below, a brief description is given of each method.

- **Strip theory**

  The majority of ship motion or seakeeping analyses are done by strip theory. Within strip theory, the hull is comprised out of a finite number of rigidly connected transverse two-dimensional 'strips'. Thereby, the required computing time is greatly reduced.

  Strip theory allows for fast and reliable solutions of enough accuracy for conventional hull forms [12]. Yet, additions have been made to strip theory to further improve the accuracy and mitigate the discrepancies occurring in experiments with forward speed. Such methods are called 2.5D strip theory methods [87]. 2.5D strip theory codes do not offer the accuracy of potential flow methods, though are typically for engineering applications sufficiently accurate.

  Strip theory is applied by C-Job engineers as part of the NAPA software suite for which C-Job has a license. It should be noted that this 2.5D strip theory code ([9]) is not integrated into the ACD framework. It is a separate piece of software that is called upon manually in the NAPA software suite. If it is to be applied in a partially automated holistic design method, the appropriate interfaces need to be developed. When provided with a hull shape, the strip theory code can calculate the corresponding motion RAOs.

- **Potential methods**

  Within panel methods, the hull and free surface are described by many panels. Consequently, more intricate hull shapes can be analyzed compared to strip theory methods. Additionally, panel methods solve the problem in 3D.

  Panel methods are applied by C-Job engineers in the form of ANSYS AQWA software, for which C-Job has a license. Additionally, the NAPA software suite employed by C-Job also contains the possibility to carry out panel method seakeeping analyses. Like the available strip theory code, it is not integrated into the ACD framework. To do so, appropriate interfaces need to be developed. When provided with a hull shape, the panel method code can calculate the corresponding motion RAOs.

Both strip theory methods are not able to accurately model the effect of appendages on motion RAOs, as the working principle employs viscous flow effects ([52],[84]). Accurate modelling of bilge keels requires NS-solvers with accurate viscous flow modeling, which is too computationally expensive for everyday commercial use. However, the empirical methods developed by Ikeda et al., which have been further refined by many researchers, show a good approximation for the effect of appendages ([53], [54], [49], [50], [51], [52], [84]).

4.5.2. Benchmark studies

Various research has been done on comparing the different methods for seakeeping analysis. Below, a brief summary of the results of some of this research is given.

Dhavalikar ([29]) compared three different seakeeping software tools for both zero speed and forward speed analysis of a Wigley hull. The three different methods concerned 2.5D strip theory and two potential flow methods. In head seas, the surge, heave, and pitch RAOs are in good agreement. The methods generally are close for zero speed cases. Generally, the strip theory-based tool gives fast and quite reliable results, yet non-linear problems can be handled more efficiently by panel methods.

Software	Method
AQWA	Radiation/diffraction panel code
GL Rankine	Rankine-source patch code
MOSES	Radiation/diffraction panel code
OCTOPUS	Strip theory code
PDStrip	Rankine-source strip theory code
WAMIT	Radiation/diffraction panel code

Table 4.2: Compared seakeeping tools in study done by Gourlay et al. [37]

In an extensive study done by Gourlay et al. ([37]), numerous commercially available seakeeping tools were compared. These tools are shown in table 4.2.

A seakeeping analysis was done on three different cases, each concerning a ship in various sea and transit conditions. The benchmarking generally showed good agreement of numerical predictions with model test results.

Concluding this section, a relation between the four methods in speed and accuracy is observed. In essence, there is a trade-off between speed and accuracy for each of the methods. In the context of a design framework that requires rapid evaluation of many different design configurations. For evaluation and subsequent optimization of ship aspects such as the prismatic coefficient, a sufficiently accurate evaluation method is needed. The relation between accuracy and speed for the four methods and the requirements for fidelity and speed are shown in figure 4.5.

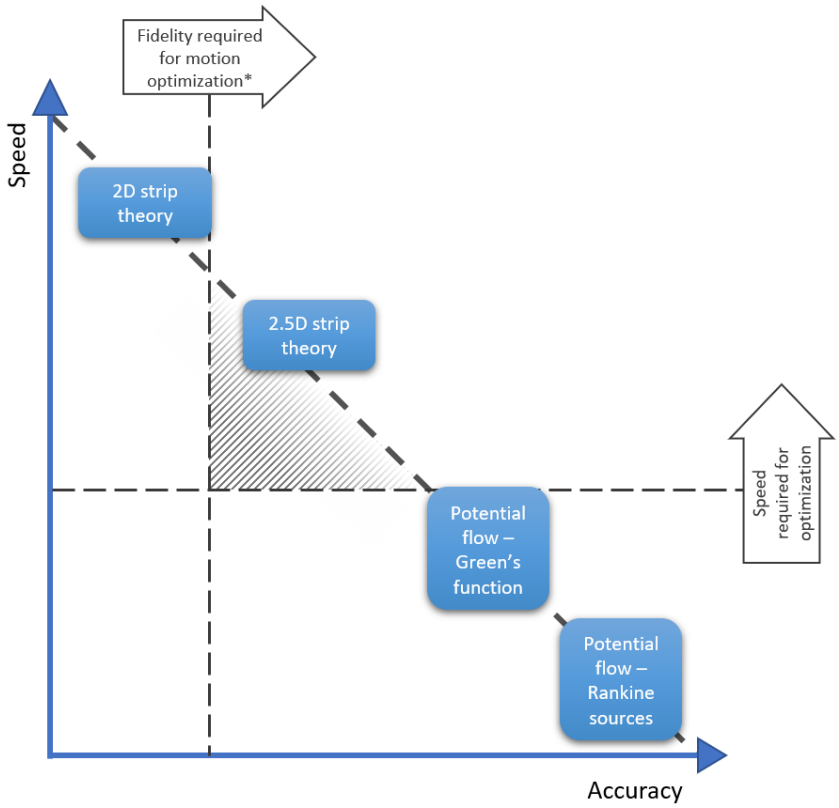

Figure 4.5: Relationship between accuracy and speed for different seakeeping evaluation methods, and requirements for seakeeping optimization and applying holistic design methods. *The required fidelity would be far higher if the behaviour of bilge keels is simulated, methods capable of doing so are too computationally expensive for holistic design methods ([52], [84]).*

Figure 4.5 shows that the 2D strip theory does not provide the required fidelity for seakeeping optimization. Both potential flow methods lack the required speed for efficient (iterative) holistic design optimization. Consequently, 2.5D strip theory provides adequate speed and accuracy, the latter of which is further by numerous benchmarking studies ([87], [29], [37]). Additionally, simulating the

effects of bilge keels requires simulation methods involving viscous effects. These methods are computationally expensive to such a degree, that they are not suited for iterative optimization processes, therefore these are not considered. The bilge keel should be modeled by empirical methods, of which Ikeda et al. have shown to be in good agreement with experiments ([52], [84]).

With the methods for calculating ship motions known and the ship aspects of influence determined in the previous section (section 4.4), a state-of-the-art review can be performed in which ship aspects and evaluation methods are applied to optimize vessel's motion behavior.

4.6. State-of-the-art seakeeping optimization studies

4.6.1. State-of-the-art review

Chapter 4 has so far introduced various definitions to describe ship motion behavior, attributes affecting ship motions, and software to calculate ship motion response with the aim of providing the necessary information to design for ship motion behavior. Recently, Huang et al. ([48]), Scholcz et al. ([81], De Gaaij ([24]), and Rehn et al. ([77]) have performed studies aimed at optimizing motion behavior in the form of seakeeping. In the text below, subsequent findings are briefly summarized.

Huang et al. ([48]) carried out a hull form optimization study for reduced drag and improved seakeeping. The variables influenced the finer geometry of the hull and the main dimensions varied only slightly. The effect of appendages, anti-roll tanks, mass distribution, or metacentric height was not incorporated. With respect to ship motions, the framework only focused on improving heave and pitch motion response. These responses were improved by reducing the corresponding RAO's natural frequency peak. As such, optimizing motion behavior for a particular area of operation or stationary operation was not considered. Additionally, the study was done for an S60 series hull. The S60 series hull is a standard hull type developed in the 1960s. For validation purposes, this hull type is very suitable, as lots of experimental data are available. Yet for more practical optimization studies, modern hull shapes may offer better performance.

Scholcz et al. ([81]) carried out surrogate-based multi-objective optimization for powering and seakeeping. Three frigate-type hulls were selected and used as basis designs for shape parameterization. The selected hulls differed in shape, hydrostatics properties, length, width, and draught.

A pitch and a roll seakeeping objective were defined and applied alongside a powering objective in the multi-objective optimization procedure. The pitch and roll objectives comprised of reducing the area under the RAOs. A set of designs was generated and evaluated on ship resistance and seakeeping. The hull designs were based on 'blending' three different parent hulls. Each hull design was evaluated with a fixed metacentric height. Roll damping was implemented by having a fixed critical roll damping coefficient. Final Pareto-optimized results were verified by CFD software.

By only considering pitch and roll RAOs, the method failed to involve a specific area of operation. The heave response was also not considered. The method only involved appendages to a limited extend. Like the study done by Huang et al. other objectives applicable to the design of OSVs were not considered.

De Gaaij ([24]) carried out a parametric optimization study for, amongst other objectives, seakeeping for his MSc. thesis. De Gaaij defined a base hull whereby the draft, LOA, beam, forward hull entrance angle at the waterline, and stem distance defined the geometry of the to-be-analyzed hull. A genetic algorithm was applied to optimize the parametric model. The seakeeping objective comprised minimizing the maximum heave acceleration, maximum relative heave movement, for head waves only for a vessel with forward speed. No appendages, varying prismatic coefficients, anti-roll tanks, mass distribution, or variable metacentric height were involved. Similar to the other seakeeping optimization studies, other objectives applicable to the design of OSVs were not considered.

Rehn et al. ([77]) performed parametric modeling and evaluation of OSVs, thereby having the focus on reconfigurability (see also sub-section 3.3.1 for a review focused more on the design method). The design variables, which were the main particulars, the inclusion of a moonpool or not, main crane capacity, and light well intervention tower capacity, were varied by fixed increments. For example, the length of the vessel increased with increments of $10[m]$. Ship aspects such as the block coefficient were fixed, as were environmental parameters such as wave peak period and significant wave height. The latter parameter thereby involves the area of operation to a limited extend. The seakeeping analysis remained limited to stationary heave response and a roll and pitch period. A simplified box-shaped hull was analyzed using 2D strip theory. The heave response formed an input for an operability measure.

The seakeeping analysis was limited to such an extent that it allowed for a global evaluation of a set of different vessels. The method lacked fidelity to accurately optimize the motion behavior of a single to-be-designed vessel.

4.6.2. Research gap

Based on the state-of-the-art review, requirements for the OSV design framework, and subsequently a research gap can be identified. With respect to seakeeping optimization, substantial differences can be observed in the two areas. The extent of both the motion characteristics involved and the design variables incorporated differ substantially between the different studies and requirements for an OSV design framework. This is shown in figure 4.6, where the different studies are weighed according to the extent in both areas.

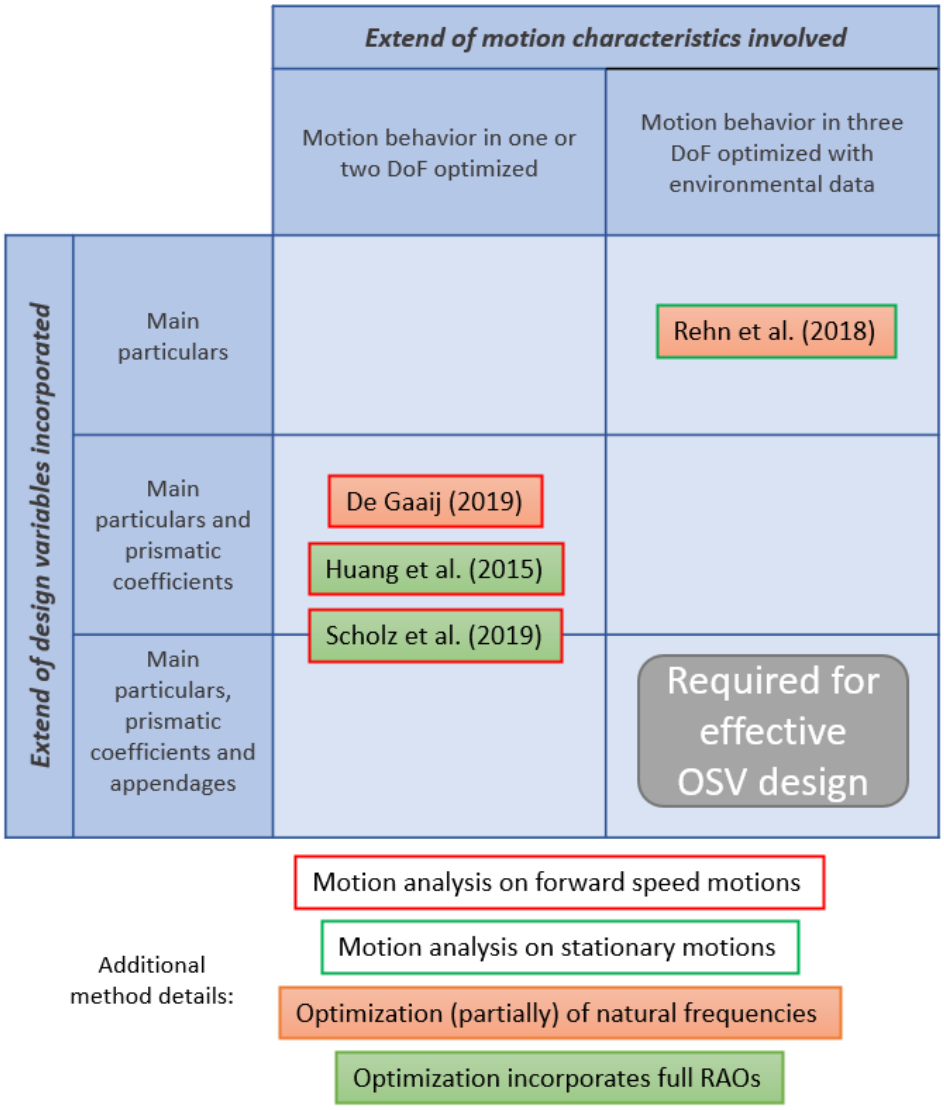

Figure 4.6: Research gap matrix between different seakeeping optimization studies

Figure 4.6 shows that only the study by Rehn et al. ([77]) incorporated motions in three DoF and environmental data. The study did only consider these motions and the area of optimization to a limited extent. Additionally, the study by Rehn et al. only considered a greatly simplified box-shaped hull for the analysis. Thereby, only the main particulars were varied. The studies by De Gaaij, Huang et al. incorporated the main particulars, prismatic coefficients, and Scholz et al. also appendages to a certain extend ([24], [48], [81]). The latter two only optimized the RAOs. All three methods only considered two DoF to evaluate the motion behavior upon, and only at forward speed. Section 4.4 discussed main

particulars, prismatic coefficients, and appendages that should be considered to effectively incorporate motion behavior as a driver. Section 4.2 showed that motion limits in all three DoF are present, hence they all influence a vessel's performance regarding motions and subsequently operability. As such, all three should be considered as does the area of operation. Hence, a research gap exists between incorporating all ship aspects of influence and the full extent of motion behavior for an OSV. For motion behavior to be effectively considered, and enabling better performing OSVs, all aspects should be considered as shown by the grey box.

4.7. Conclusion and summary

This present chapter discussed ship motion behavior. In a first step towards answering the research sub-question *'What is the current state-of-the-art in design optimization for ship motion characteristics?'*, namely RAOs to characterize the response to waves. Motion limits, together with ship-specific RAOs and a certain wave profile, form an input to various operability measures, indicating year-round seakeeping performance. Gutch et al. ([42]) demonstrated that, depending on the area of operation, the optimal hull form for seakeeping may vary. Thereby, Gutch et al. showed that the ORI measure of operability is particularly suitable for optimization studies.

Various ship aspects are of influence on ship motions. These are:

- Hull form, including main particulars and prismatic coefficients
- Appendages, specifically bilge keels
- Anti-roll tanks
- Mass distribution
- Metacentric height

The hull form and bilge keels were significantly influenced by the concept and preliminary design phases. Hence, the motion behavior is determined to an extent in these design phases.

Based on various benchmarking studies, 2.5D strip theory was proven to have adequate speed and accuracy for optimization of hull form. Bilge keels require more advanced CFD methods but can be incorporated by empirical modeling with sufficient accuracy ([52], [84]).

A review of seakeeping optimization studies was conducted to fully answer the research sub-question *'What is the current state-of-the-art in design optimization for ship motion characteristics?'*. No optimization method has been developed involving all three motions, and all ship aspects which are largely influenced in preliminary design phases. For a design method optimizing motion behavior to be efficient, heave, roll, and pitch motions, environmental data, and ship aspects of influence should be considered.

5

Needs OSV design framework

In this present chapter, the needs of the new concept design framework will be discussed. Thereby, a first step towards answering the research sub-question *'What are the requirements for a concept design framework involving ship motion characteristics?'* is made. To do so, the research gap will be deliberated in section 5.1. Based on the research gap and the literature study done in prior chapters, the needs of the new framework are discussed in section 5.2. More specifically, the scope, general method requirement, and specific design driver requirements are discussed in subsections 5.2.1, 5.2.2 and 5.2.3 respectively. A brief conclusion and summary is given in section 5.3.

5.1. Research gap analysis

Chapter 2 showed that conventional concept design processes fail to capture all design drivers governing the design of modern vessels. Holistic concept design methods solve this problem by having the ability to optimize a ship design to a set of design objectives. C-Job's ACD method should be able to involve all relevant objectives applicable during concept design. Chapter 3 discussed the OSV vessel type and its subsequent design drivers. These design drivers are mission systems, cost, lead time, ship resistance, station keeping, and motion characteristics. Some design approaches have been developed specifically for designing OSVs, but mostly to expand the knowledge of what OSVs are most efficient for life-cycle performance. These methods are able to develop global vessel requirements, yet do not determine the best vessel design for a to-be-designed OSV thereby satisfying specific client requirements. Chapter 4 deliberated ship motions. It was concluded that to design OSVs effectively for motion behavior, motions in six DoF, motion limits of equipment and crew, and the area of operation need to be considered. Additionally, main particulars, hull shape, and appendages are influenced by design decisions made during the early design phases. Hence, to involve motion behavior effectively, all these elements need to be incorporated. A state-of-the-art review has shown this has not been done by existing seakeeping optimization studies. Based on the identified gaps in these three chapters, the needs for the new design framework will be elaborated on in the next section.

5.2. Framework requirements

5.2.1. Scope analysis

Before deliberating the framework needs, it is important to consider what is in and out of scope for this thesis. Involving all design drivers to the fullest extent will not be possible, given the time frame of the thesis. The primary aim of this thesis is to have the design framework involve motion characteristics. The requirements of the framework focus upon doing so to an adequate degree, based on the findings of chapter 4. Other design drivers indirectly influencing motion behavior are also sufficiently considered. Design drivers related aspects with no substantial influence on ship motion behavior are beyond the scope of this thesis, these aspects are:

- **Layout**

  For the cost and lead time design driver, the layout is required to be kept simple. The KBE approach by Charisi et al. ([20]) showed the advantage of considering the layout early in the

design. As the influence on seakeeping is minor (the layout influences mass distribution, but its effect was shown to be minor on ship motions [13]), the layout is not considered.

- **DP systems**

  For the station keeping design driver, C-Job noted DP systems with high redundancy might be needed, which may influence the design of the vessel substantially. Yet for this thesis, it is assumed that such advanced DP systems are not required. Therefore, incorporating DP systems is considered beyond the scope.

- **Modelling of anti-roll tanks**

  Anti-roll tanks are complex devices to model and simulate. Lewis and Gawan et al. ([59], [36]) that certain non-dimensional parameters may be followed to determine optimal anti-roll tank behavior. This may be done after concept design, thus modeling of anti-roll tanks will not be considered.

With the scope known for the design framework, the requirements can be determined.

5.2.2. General framework requirements

In general the framework should be able to do:

- Applying C-Job's ACD method requires bespoke modeling of design variables, objectives, and constraints applicable for OSVs and developing appropriate evaluation methods.

- The ACD algorithm can select the design variables to optimize the objectives and satisfy constraints, yet to do so appropriate interfaces need to be developed. A benefit of ACD is that it is built into the NAPA software suite. Thereby, a variety of tools are offered to the naval architect for evaluating the design. Within NAPA, interfaces need to be developed between these tools, as they are stand-alone packages [9]. As such, a general requirement of the framework is appropriate interfaces within the design framework.

5.2.3. Design driver specific requirements

According to the OSV design drivers as discussed in chapter 3, the necessary objectives, constraints, and design variables can be determined:

- **Design driver - Mission systems**

  The mission systems design driver ensures any OSV is able to carry out its mission by having the required systems onboard. Sufficient space for all required systems that are to be installed should be ensured. Since the primary aim of this thesis is motion behavior, this space constraint can be limited to minimum requirements for the main particulars. Additional constraints are formed by the need for the design to satisfy class safety requirements. This includes (intact) stability requirements.

- **Design driver - Cost**

  The CAPEX is kept low by reducing the steel weight (or lightship weight) and design complexity. The weight is correlated by volume. A clear resulting objective is minimizing the ship's volume. The complexity of a design is mostly determined by the design phases after concept design ([71]) and does not form a design objective.

  CAPEX is also kept low by minimizing the amount of expensive motion-compensated equipment onboard. The higher the amount of compensation a piece of equipment offers, the more lenient the motion limits, although this typically increases the cost [4]. By improving the vessel's motion behavior, the required amount of motion compensation and related costs are also kept to a minimum.

  The OPEX is (partially) kept low by satisfying other design drivers. Namely, improving station keeping performance and ship resistance improves the OPEX by minimizing the required powering for station keeping and sailing.

- **Design driver - Lead time**

  It is necessary to design and build the ship in as short a time as possible. The building time of a vessel is minimized by keeping the steel weight low and the design simple, as both form a measure for the number of fabrication steps required. The former is achieved by the design objective 'minimize lightship weight'. As mentioned, the design framework does not need to involve a method for determining design complexity.

- **Design driver - Station keeping**

  The station keeping design driver ensures the vessel's ability to remain stationary under adverse conditions. As mentioned in section 3.2, this is typically achieved by fitting the vessel with a DP system. DP systems do not influence the hull shape (in aspects of relevance to motion behavior) or the ship structure to the extent that it needs to be considered during concept design. Station keeping can be improved however, by keeping the ship as 'compact' as possible, thereby reducing the effective area over which waves, currents, and wind apply force on the vessel. Methods exist to further correlate this area with station keeping force. Hence, the performance in the station keeping design driver can be measured by the required station keeping force.

- **Design driver - Ship resistance**

  To minimize OPEX, minimizing fuel costs and subsequently ship resistance forms an important design driver. The ship resistance is influenced by the main particulars and the hull shape, including main particulars and prismatic coefficients. The hull shape should be represented with enough fidelity to accurately calculate ship resistance.

  To evaluate the ship resistance, an appropriate method should be developed. Depending on the method used it may be computationally expensive and time-consuming. For the holistic method to be efficient, this computational time should be minimal.

- **Design driver - Seakeeping**

  The last design driver, and the primary focus of this thesis, is the vessel's motion behavior. Gutsch et al. ([42]) showed that using the ORI forms a particular robust measure for seakeeping performance.

  Section 4.4 discussed numerous ship attributes of influence on ship motions. The main particulars, prismatic coefficients, metacentric height, and appendages were found to be of influence and are determined during concept design. As such, they need to be involved in the design framework.

  To use the ORI objective, the framework needs to be able to calculate RAOs and incorporate the wave spectra/scatter diagrams of the area of operation. To calculate RAOs, the application of the 2.5D strip theory should be included in the framework. It should be noted that the area of operation does not form a design variable but rather input to the optimization.

  To illustrate how the ORI objective relates to various ship aspects of influence to motion behavior, the elements of influence to the ORI value are visualized in figure 5.1.

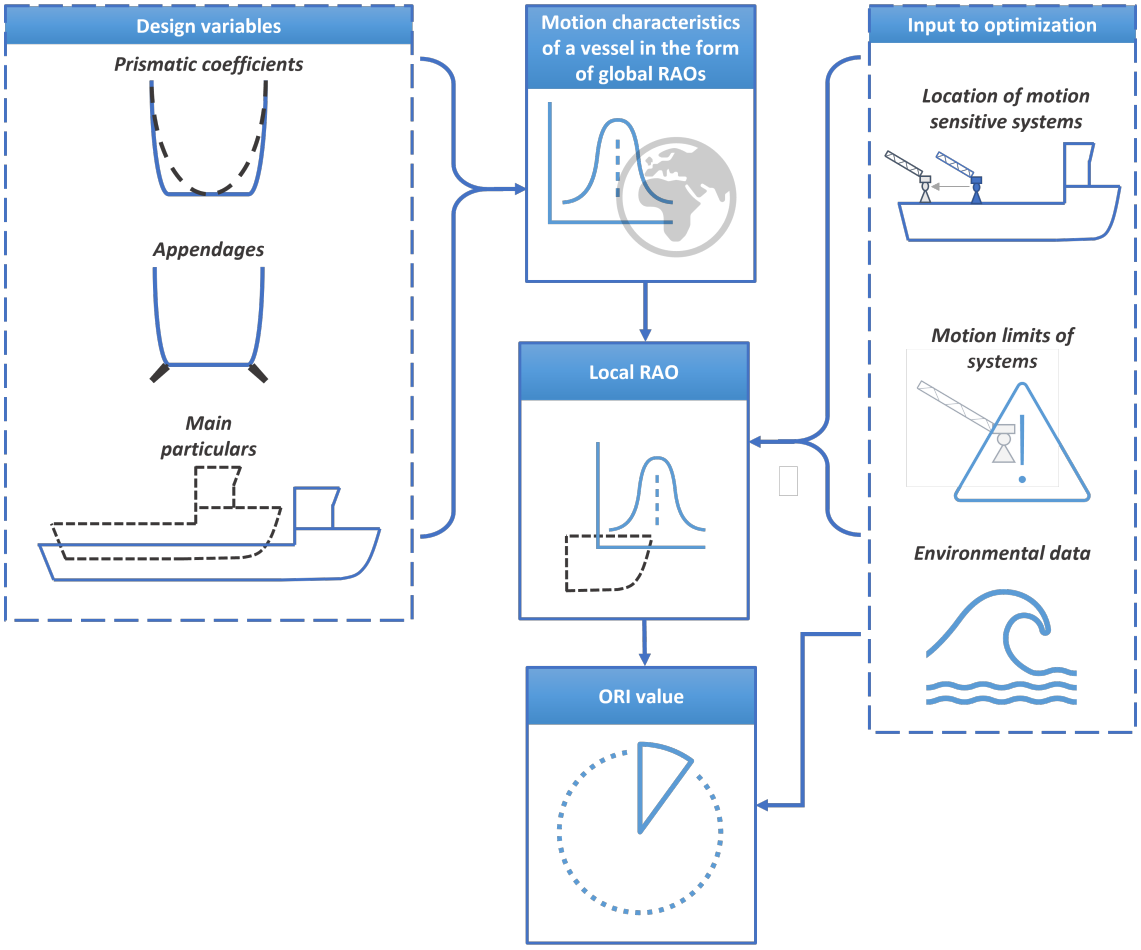

Figure 5.1: Steps involved in determining objective 'ORI', thereby optimizing the vessel's motion behaviour

5.2.4. Resulting framework

The various analyses per design driver result in a set of required objectives, constraints, variables, and evaluation methods of the OSV design framework. The resulting design framework is shown in table 5.1.

Requirements design framework				
Primary objectives	**Constraints**	**Optimization input**	**Design variables**	**Evaluation methods**
- Minimize lightship weight - Minimize station keeping force - Minimize ship resistance - Maximize ORI	- Ensure enough space for mission equipment - Meet initial stability requirement	- Area of operation - Specification of motion sensitive equipment	- Main particulars - Prismatic coefficients - Bilge keels dimensions	- Efficient calculation of objective and constraint KPI's - Meet concept design accuracy requirements

Table 5.1: Summarized framework needs based on design drivers

This table forms the input to an update of figure 2.5, which is shown in figure 5.2. In figure 5.2, additional design input is also shown.

Shown by figure 5.2 are the constraints and objectives providing input to the optimization algorithm. The algorithm steers a set of design variables according to the objectives and constraints. Each set is evaluated according to the evaluation methods. Design input provides additional information needed for the evaluation of variables. The ACD algorithm develops a surrogate model, hence the back and forth interaction between design variables and the optimization algorithm. Finally, after a number of iterations, the algorithm provides a set of Pareto optimal solutions.

Some design drivers share the same objectives, which may share the same constraints share the same design variables. These relationships are shown in figure 5.3.

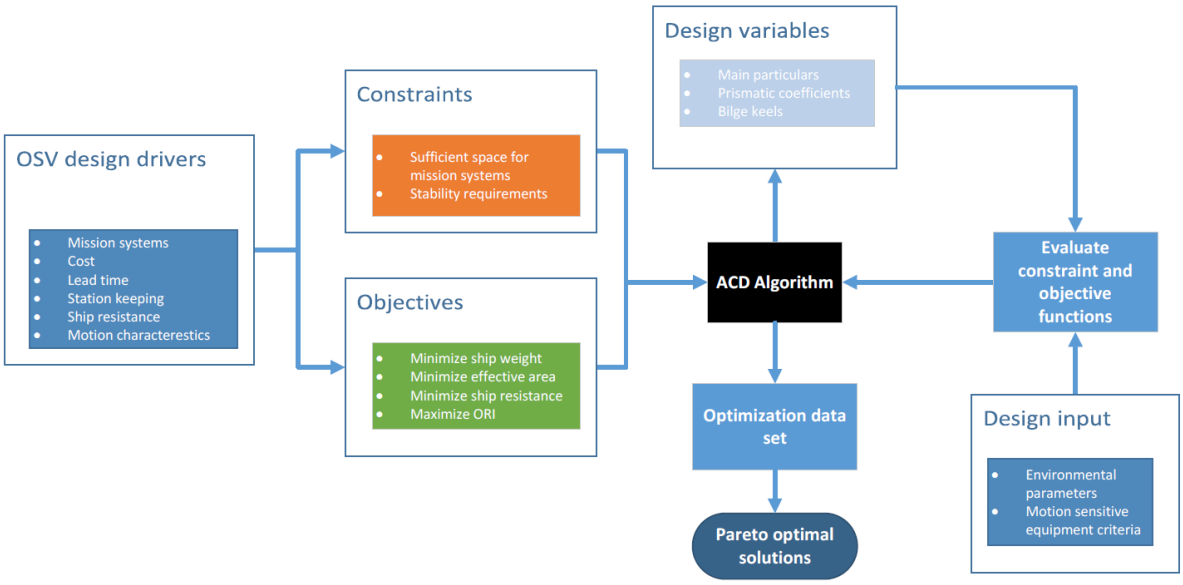

Figure 5.2: OSV design framework based on analysis per design driver

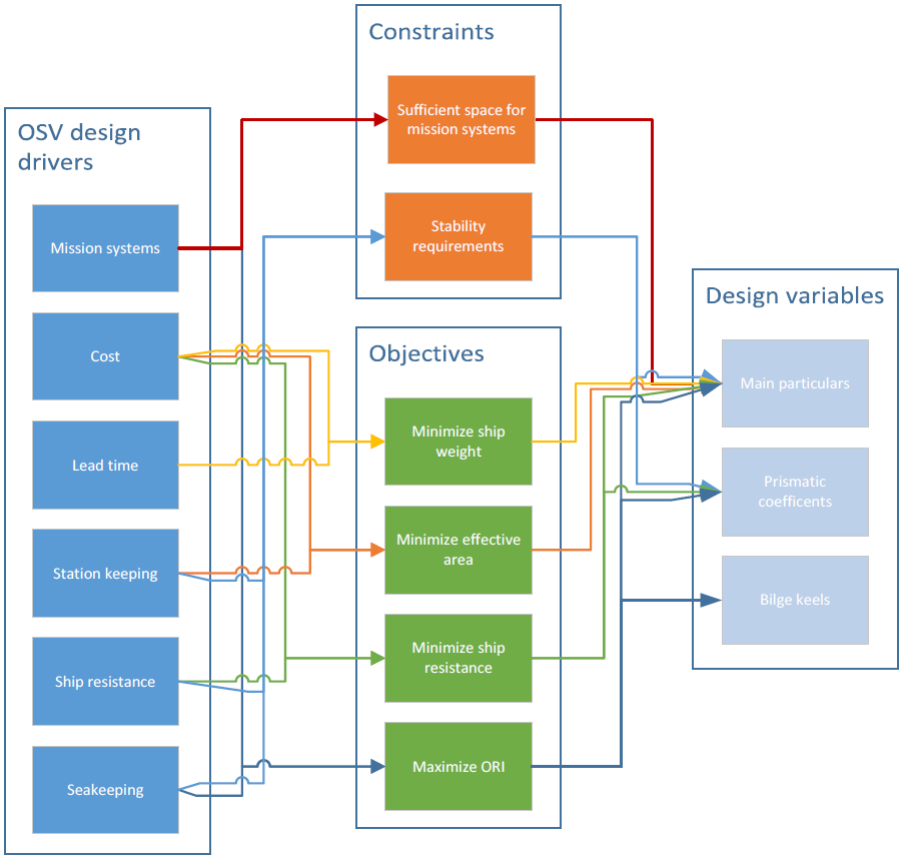

Figure 5.3: Relationships between OSV design drivers, objectives, constraints and design variables

5.3. Conclusion and summary

This chapter takes a first step towards answering the research sub-question *'What are the requirements for a concept design framework involving ship motion characteristics?'*. Section 5.1 showed a concept design method using C-Job's ACD method may form a method to effectively incorporate motion char-

acteristics early in the design of OSVs. To do so, the development of a bespoke parametric OSV model is required. This model consists of certain objectives, constraints, design variables, and evaluation requirements that need to be incorporated. Based on an analysis of ship motions and design drivers, the resulting framework is summarized and visualized in figure 5.2.

With the requirements for the framework known, the design variables need to be parametrically modeled. For some of these variables, many methods of parametric modeling exist. As such, these methods will be considered in the next chapter, chapter 6.

6

Parametric modelling

The purpose of this chapter is to review and compare various methods to accurately reflect a parametric ship comprising the design variables determined previously (see sub-section 5.2.4). In doing so, this chapter takes a first step towards answering the research sub-question *'How is a concept design framework incorporating motion characteristics developed in practice?*.

6.1. Parametric modelling methods

In this section, methods will be discussed for developing a parametric representation of a ship, based on the design variables elaborated in chapter 5. To ensure optimization efficiency, the ship should be parameterized in the minimal number of variables required. As such, different techniques of parameterizing a ship whereby the hull shape and bilge keels are discussed.

6.1.1. Hull shape (including main particulars and prismatic coefficients

As determined in chapter 5, the main particulars and prismatic coefficients heavily influence ship motion behavior. The finer hull shape can be of large influence on the ship resistance. The parametric model should be able to vary to influence the main particulars and prismatic coefficients to influence seakeeping. To fully influence ship resistance, the finer hull shape should be able to be adjusted by the framework. Parametric hull shape representation has been a subject of intensive academic study and many methods are available. Methods that have been used in determining optimal hull designs are: Testing a predetermined set of varying hull shapes ([69]), free-form deformation of a particular hull shape ([82], [25]), shape blending of different hull shapes ([86], [81]) and representing a hull by splines controlled by variable points ([85], [58], [15] [38], [75], [43]). In the text below, each of these methods will briefly be discussed.

- **Predetermined set of varying hull shapes**

  A relatively easy method of varying the hull shape is by creating a set of varying hull shapes. Each hull shape can be evaluated separately.

  özum et al. ([69]) demonstrated this by creating a set of hull forms manually. Each hull form varied in length, B/D ratio, the center of buoyancy, and prismatic coefficient. A base hull shape was firstly changed in length, with the B/D ratio fixed and vice versa in fixed increments. Secondly, the longitudinal CoB and prismatic coefficient were changed. The shape of the sections remains the same as in the parent hull, but are moved in the longitudinal direction, hereby, both the center of buoyancy and the prismatic coefficient are varied. The final result is a set of hull shapes with varying parameters. This pre-determined set was analysed for powering and seakeeping and subsequently allowed for manual identification of optimal performing hull shapes. An optimization algorithm may also select the optimal hull shape. Creating a set of hull shapes is laborious and the design space can be fairly constrained by the limits of the hull predetermined hull shapes. Additionally, the actual optimal design may lay between two predetermined designs.

- **Free-form deformation method**

The free-form deformation method is a technique developed to perform relatively simple deformations on solid 3D objects. It was first described by Sederberg et al. ([82]) in 1986. The method bounds a geometric object by a box with control points. By moving one of the control points, the bounded shape is transformed. An example of transforming a sphere by this method is shown in figure 6.1.

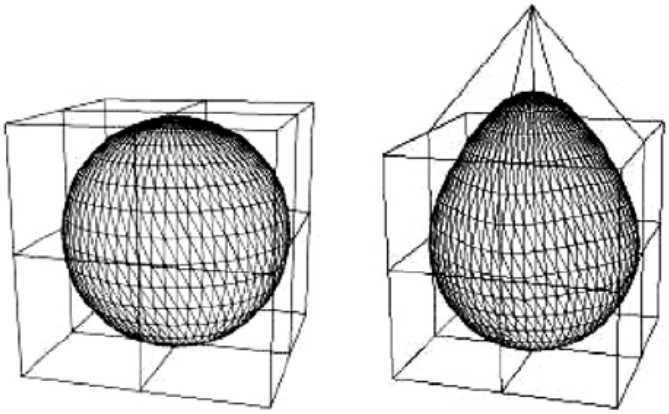

Figure 6.1: Free-Form-Deformation of a sphere [64]

Within the spaces within the bounded box, the location of the surface of geometry is described by a vector. Moving the control point transforms the space within the bounding box. The relative location of the geometry within the space is preserved. Consequently, the geometry is transformed by transforming the surrounding space.

De Winter et al. ([25]) applied the free-form deformation method to optimize the sizing of a ship hull. Hereby, a bounding box surrounding the hull was changed by control points, thereby 'stretching' the hull in length and width. The draft if the vessel was determined based on hydro-statics. The method allowed for easy deformation of the hull shape to change the main particulars, yet lacked any method of adjusting the finer geometry. As such, the relative hull shape remained the same, yet the prismatic coefficient could not be changed. A workaround to this is by creating multiple bounding boxes, thereby being able to transform specific parts of the hull. This allows for the ability to change the hull shape so that the prismatic coefficients can be adjusted, though the finer shape of the hull remains unchanged.

- **Shape blending**

  A shape blending method to transform hull shapes was first introduced by Tahara et al. ([86]) to optimize the hull of a surface combatant. In Tahara's method, the hull geometry is represented by Bezier curves. Different hull designs with corresponding Bezier curves were created. By interpolating the Bezier curves, a 'blend' of the predefined hull shapes was created.

  Scholcz et al. ([81]) applied a hull blending technique to parameterize the ship hull. Hereby, three different hull shapes were 'blended' to form a single hull shape. Each hull shape varied in length, breadth, draft, and other aspects. These three different hulls are shown in figure 6.2.

  The hulls were defined by the control points of a B-spline surface. The B-splines of the different shapes were blended by linear interpolation. The 'weight' of the interpolation was controlled by a design vector.

  Hong et al. ([47]) showed this method could also be too specific for parts of the hull, such as the bulbous bow.

  A drawback of this method is that the design space is limited by the extremes of the parent hull shapes. Additionally, the hull shapes may not vary wildly from each other to ensure feasible hull designs.

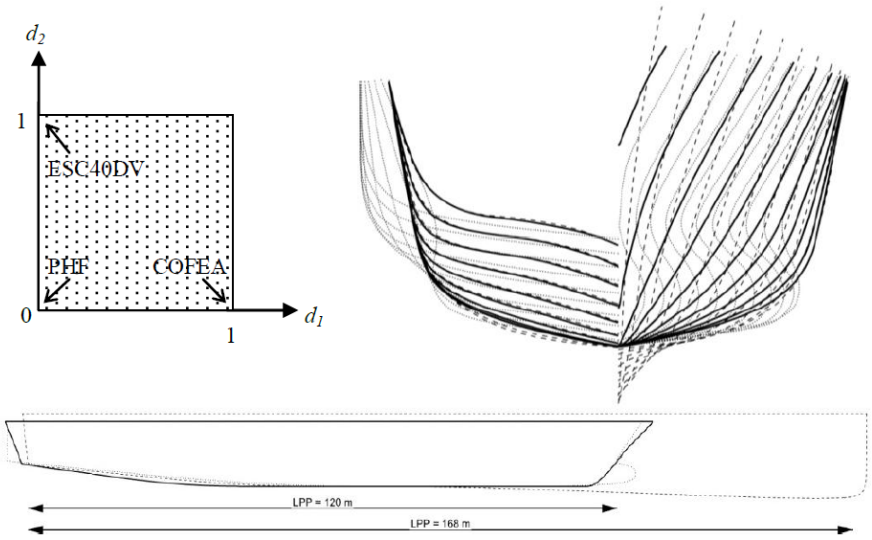

Figure 6.2: Design space (left), body plans (right) and center plane buttocks (bottom) of basis designs: solid line = PHF hull, dotted line = COFEA hull, dashed line = ESV40DV hull [81]

- **Splines**

  Within CAD design, splines are used both for curves and surfaces. A spline is a function comprised of polynomial functions, each joined at the other end. Consequently, a smooth curved line can be represented by a set of polynomials.

  A particularly widely used method in hull design involving splines is the Lackenby transform. Lackenby ([58]) illustrated that by shifting various spline shapes longitudinally, which define the hull shape, the prismatic coefficient and longitudinal center of buoyancy can easily be changed. The method still ensures smooth hull shape. Figure 6.3 compares the variation of LCB with both generic hull deformation and Lackenby transform. The generic method shows lots of fine adjustments to each defining hull line. The Lackenby method shows a longitudinal shift of the original hull shape, smooth lines, which can also shift the LCB.

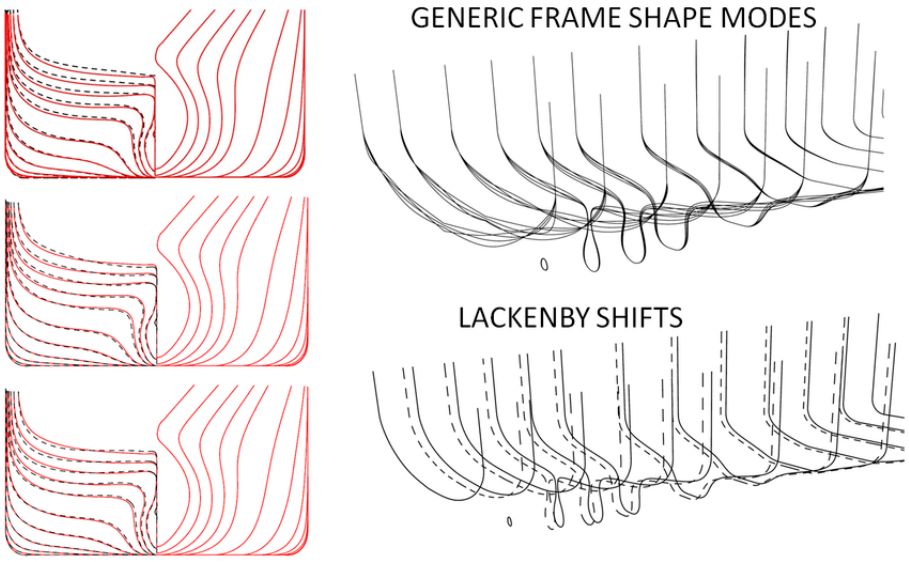

Figure 6.3: Typical example of generic aft ship section shape variations and Lackenby LCB shifts [81]

Splines and Lackenby transforms have extensively been applied in ship hull optimization studies. For example, Priftis et al. ([75]) optimized a parametric hull for, amongst other objectives, total ship resistance. The main particular formed variables. Finer areas in the front and aft end of the ship were modified by Lackenby transform. The finer geometry in the aft and front areas of the vessel was influenced by modifying B-splines. This combination of the Lackenby transform for the global geometry of the hull, and direct B-spline modification showed a good balance between simplicity of the parametric model and finer control in areas of large influence to ship resistance.

Concluding the review of hull form parametric modeling methods, a trade-off exists between fidelity of the method and amount of design variables. The aim is to change the main particulars and prismatic coefficient of the hull shape with sufficient freedom but minimal variables. The usage of splines, specifically the Lackenby transform method, provides adequate fidelity and minimal control points. As such, the Lackenby transform method should be adequate to parameterize the hull shape, thereby changing the main particulars and prismatic coefficients. If it is not possible to implement a Lackenby transform in the framework, the free-form deformation should prove a second best option. The free-form deformation method can be applied in such a way that the prismatic coefficients can be adjusted, although the finer hull shape still remains mostly unchanged.

6.1.2. Bilge keels

As discussed in chapter 4, appendages significantly influence ship motion behavior. Specifically, bilge keels (see figure 4.4) are widely used to improve the roll motion behavior. Consequently, chapter 5 stressed the need to incorporate these appendages in the design framework. As such, the appendages need to be parametrically represented in some form. Modelling bilge keels requires computationally expensive simulation methods, thus an empirical method will have to be used. Specifically, the 'Ikeda method' has been widely used by industry and shown to be in good agreement with experiments ([52], [84]).

In 1978, Ikeda et. al. published five papers describing methods for estimating the roll damping term of a ship hull, and bilge keels ([53], [54], [49], [50], [51]). Nowadays, the Ikeda method is the most widely used method for estimating roll damping effects. Throughout the years, many efforts have been made by the industry to continuously improve the accuracy of Ikeda's empirical method. Currently, Ikeda's method offers adequate accuracy for engineering applications [84]. This method not only offers the required accuracy to optimize seakeeping of a ship hull including appendages but also lends itself to parametric modeling.

The International Towing Tank Convention (ITTC) has published a detailed procedure guide for applying Ikeda's method [68]. The core concepts will be discussed here. Ikeda's method discretizes the roll damping moment into five components. Namely, wave, lift, frictional, eddy, and appendage components comprise the roll damping moment M_ϕ,

$$M_\phi = M_{\phi\mathrm{W}} + M_{\phi\mathrm{L}} + M_{\phi\mathrm{F}} + M_{\phi\mathrm{E}} + M_{\phi\mathrm{APP}} \tag{6.1}$$

The wave and lift components ($M_{\phi\mathrm{W}}$ and $M_{\phi\mathrm{L}}$) are linear components proportional to the roll angular velocity. The frictional, eddy and appendage components ($M_{\phi\mathrm{F}}$, $M_{\phi\mathrm{E}}$ and $M_{\phi\mathrm{APP}}$) are nonlinear components. The nonlinear components are assumed to proportional to the square of the roll angular velocity. This allows for representing the roll damping coefficient, B_ϕ, in linear form,

$$B_\phi = B_{\phi\ \mathrm{W}} + B_{\phi\ \mathrm{L}} + B_{\phi\ \mathrm{F}} + B_{\phi\mathrm{E}} + B_{\phi\mathrm{APP}} \tag{6.2}$$

Each term is separately calculated by an empirical method. Depending on the type of vessel, that is, displacement hull, hard chine hull, multi-hull, different empirical components are to be applied. As each component is considered separately, the method lends itself to parameterized. Ikeda showed this by specifically describing a routine to optimize the size of the bilge keel, depending on other hull parameters [52]. Consequently, the bilge keel and its effect on the roll coefficient, can be described as a function of the hull shape.

6.2. Conclusion and recommendations

This chapter briefly touched upon parameterizing a ship based on the design variables concluded in chapter 5. Thereby, this chapter made the first step in answering the research sub-question *'How is a*

concept design framework incorporating motion characteristics developed in practice?'.

The main particulars and prismatic coefficients, which define a particular hull shape, can be parameterized by the 'Lackenby shift' method. This method has been widely used in industry, has sufficient fidelity to effectively affect seakeeping and ship resistance. The free-form deformation method forms another suitable candidate, primarily for optimizing seakeeping. The method lacks the ability to adjust the finer hull shape, though the ship resistance can still be significantly influenced by changing forward and prismatic coefficients.

The bilge keels can be parameterized by the 'Ikeda method' ([52], [84]). This method has been widely used in industry and has shown good agreement with experimental results.

With this investigation on parameterizing the ship completed, the foundations for a holistic OSV concept design framework are known. As such, the next chapter will focus on a plan-of-approach to develop the design framework.

7

Seakeeping optimization framework

This chapter provides an answer to the research question *How is a concept design framework incorporating motion characteristics developed?*. To do so, it describes the methodology of the seakeeping optimization framework. Section 7.1 gives a general description and a global overview of the framework. The specific components of the framework are further deliberated in 7.3. Finally, a conclusion and summary is given in section 7.4.

7.1. General framework description

Chapters 1 - 5 saw a decomposition of the design problem that lead to a proposal for the design framework. Chapter 6 provided methods to parametrically reflect a ship. Based on these findings, a design framework has been developed, which is depicted in figure 7.1.

The framework has been developed in NAPA software and comprises five parts. A brief overview describing the function of each part is given below. Calculation methods used in the framework are further deliberated in subsection 7.3.

1. **Input**

   This part of the framework defines the input to the optimization. A base hull shape that is to be transformed is defined. Additionally, parameters defining the area of operation, initial bilge keel dimensions, area of operation, motion-sensitive equipment, and loading conditions are defined.

2. **Variables**

   In this part of the framework, the design variables are presented. The variables define the hull shape, thereby parametrically representing the ship.

3. **Calculation**

   This part of the framework performs all necessary calculations, following the predefined objectives and constraint functions. Specifically, the variables form input to a free-form deformation (FFD) method. The FFD method transforms the base hull shape to an iteration-specific hull shape. Additionally, the variables are used to calculate new bilge keel dimensions. The hull shape forms input to calculations for ship resistance, lightship weight, station keeping force, initial stability, and ship motion response. The latter is further supplemented by a roll damping value based on the bilge keel dimensions.

4. **Result viewer**

   This section provides the output of the calculation. These results are either used by the optimization to determine the variables for a new iteration or presented to the naval architect.

5. **Optimization manager**

   This section manages the optimization. A user can select certain experiment settings, and execute the optimization.

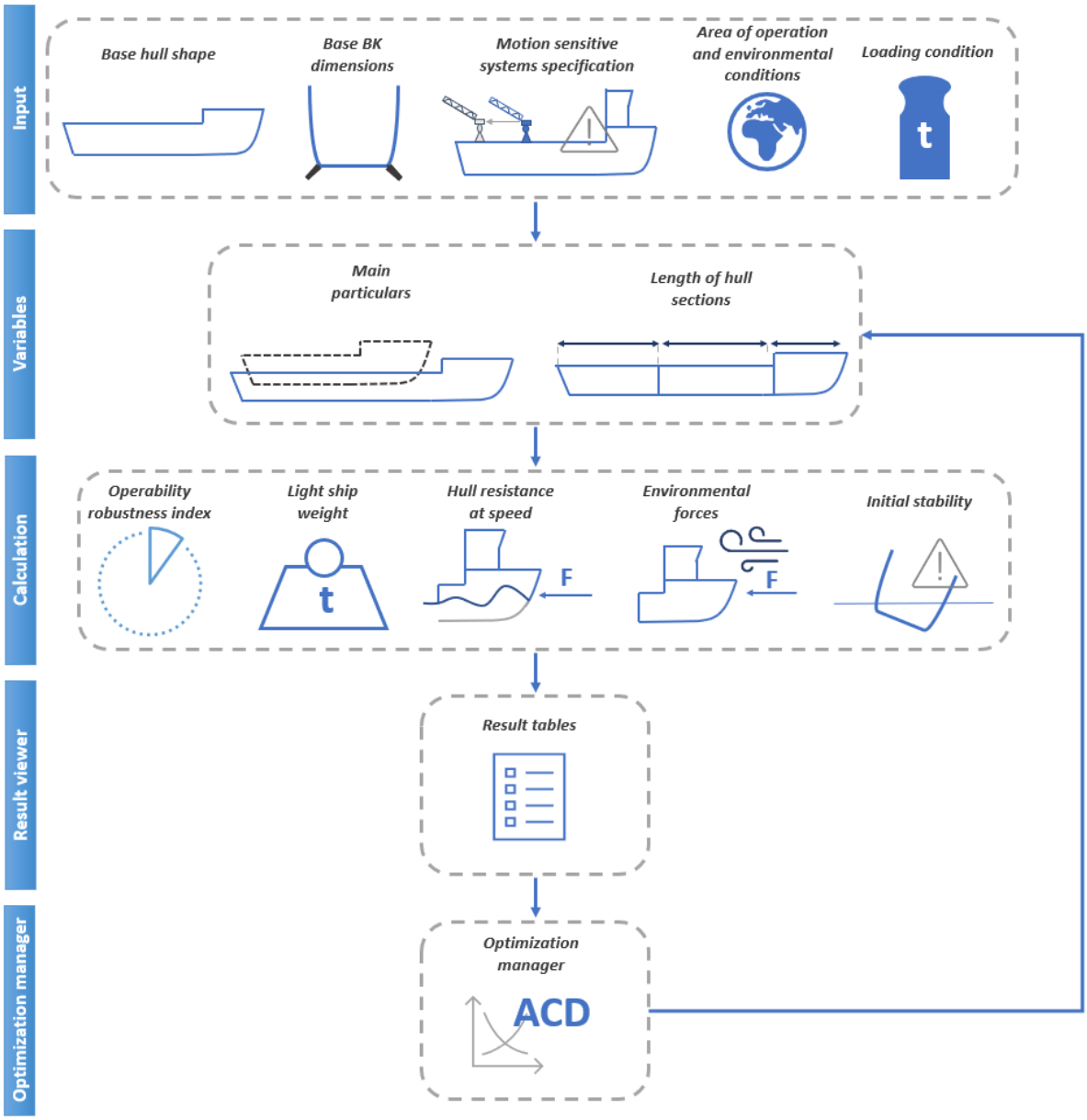

Figure 7.1: Seakeeping optimisation framework in NAPA. Arrows indicate the followed process

To better illustrate how a NAPA manager application functions, a brief explanation of the NAPA software is given in the next section.

7.2. NAPA software

The NAPA (Naval Architecture PAckage) software is a collection of design tools developed to aid in the design of vessels. The software provides methods for hull form design, hydrodynamics, hydrostatics, and stability-analysis, and much more, available in predefined NAPA 'manager' applications [9]. The framework has been implemented as a custom NAPA 'manager' application. Specifically, it comprises custom programmed macro's, databases, and table structures. Figure 7.2 shows an example of a manager application.

During optimization, the calculation steps are automated. A manual calculation, for a specific set of variables, can also be carried out. To better illustrate how a NAPA manager application functions, a brief explanation is given in the next section.

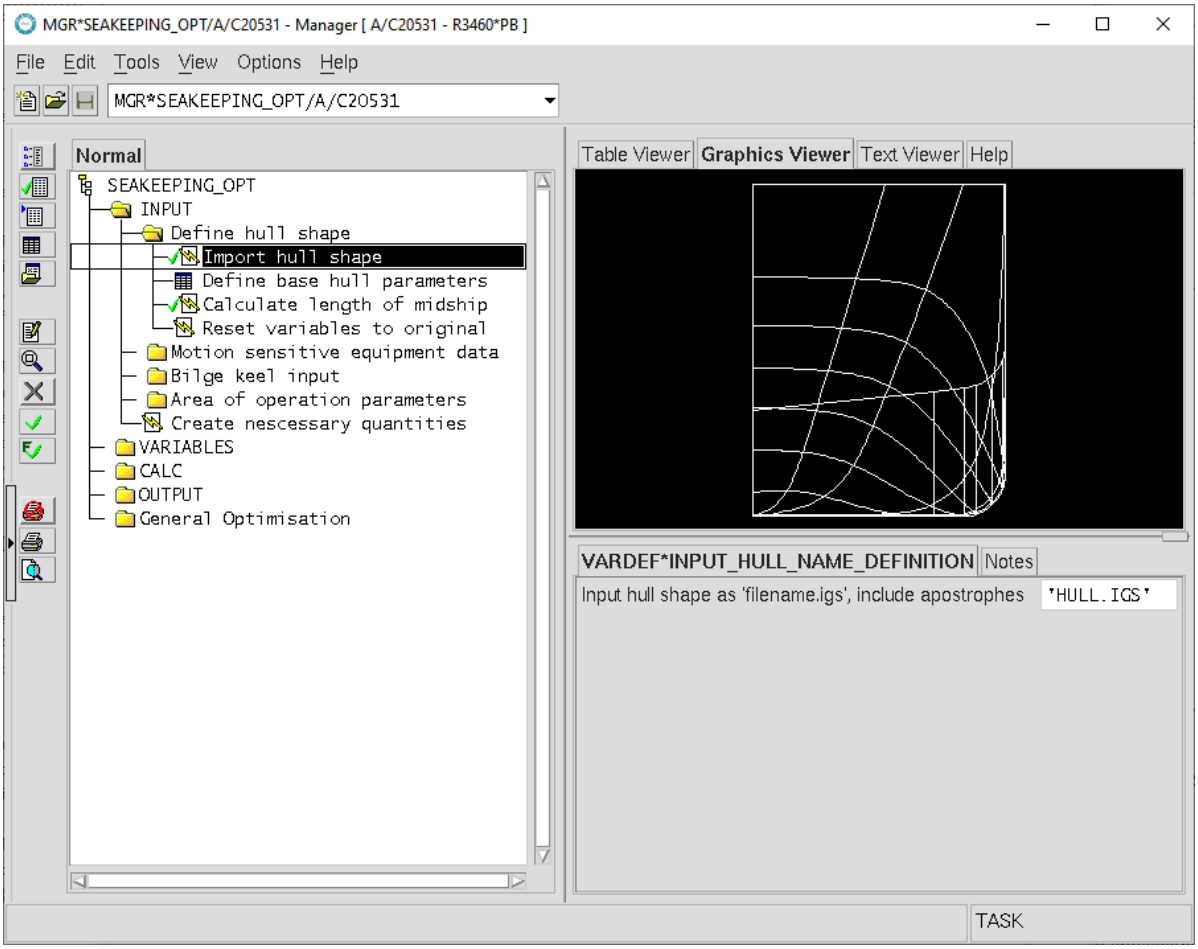

Figure 7.2: NAPA manager application for seakeeping optimization

7.3. Detailed framework description

This section explains the framework as presented in figure 7.1. Specifically, the process carried out by either the naval architect or optimization and the used calculation methods is described per part in detail.

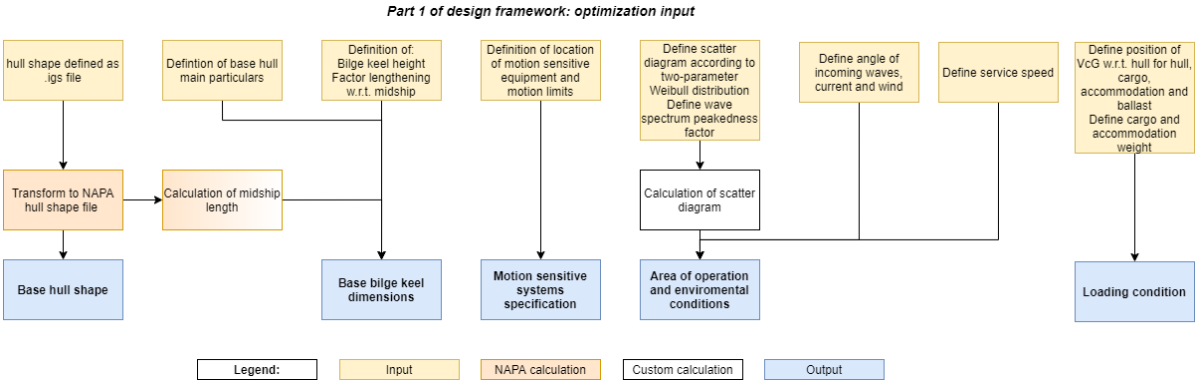

Figure 7.3: Framework methodology for defining input

7.3.1. Input

The method for defining optimization input is visualized in figure 7.3. A description of each specific input item is given below:

- **Base hull shape**

  This application imports a hull shape to be used as the basis for the optimization. The hull shape is defined as a .igs file, which may be defined using software such as Rhinoceros 3D. The to-be-imported file is stored local file on the computer. The file is automatically transformed into a NAPA geometry file. Additionally, calculations are carried to determine the start and end of the aft-, mid- and forwardship of the hull. The start and end of the midship correlate with the coordinates where the crossectional area of the hull is constant and the largest, as the midship has the largest transverse area.

  When importing, calculations are carried out computing the base location of the aft, midship and forward sections of the hull. The user further defines the base length, beam, draught, and depth. These parameters form input to the coordinates of the bounding boxes used for the FFD method. The user can reset the variables of the calculation to these base parameters to revert back to the base vessel.

- **Bilge keel (BK) dimensions**

  The influence of a bilge keel is calculated according to Ikeda's method. To do so, a bilge keel height, moment arm, and bilge keel length are required [52]. The latter two are calculated automatically (see subsection 7.3.3), yet, a bilge keel height needs to be defined as it is determined by the bilge radius. In this item, the height and extension of the length of the bilge keel (with respect to the length of the midship) are defined.

- **Motion sensitive systems specification**

  This item defines the motion limits and location of motion sensitive equipment. The location forms the input to the calculation of motion response on the location of the equipment (local RAOs). The motion limits form input to the ORI calculation.

- **Area of operation**

  In this section parameters reflecting the area of operation and environment are defined. To calculate the ORI, ocean data such as the wave spectrum and scatter diagram are required. Both are calculated following guidelines from DNV-GL [90]. Specifically, a Pierson-Moskowitz (PM) spectrum model and a two-parameter Weibull distribution for the scatter diagram are used. The framework automatically calculates the wave spectrums and scatter diagram based on the input parameters. See appendix C for the full calculation procedure. Both the wave spectrums and scatter diagram provide input to the calculation of the ORI.

- **Loading condition**

  In this item, the operational loading condition is established. Specifically, the weight and VcG w.r.t. deck of the deck load and accommodation and the VcG of the hull and ballast w.r.t. the ship depth are defined. These parameters form input to the lightship weight in the initial stability calculation.

7.3.2. Variables

In this section, the framework variables are defined. During an optimization run, these values are changed by the algorithm per iteration. If needed, a user can also input variables manually. Variables defining the main particulars and length of hull sections are defined. Thereby, the global dimensions and front, aft, and global prismatic coefficients are varied. The method for defining variables input is described in figure 7.4. A description of each specific variable item is given on the next page.

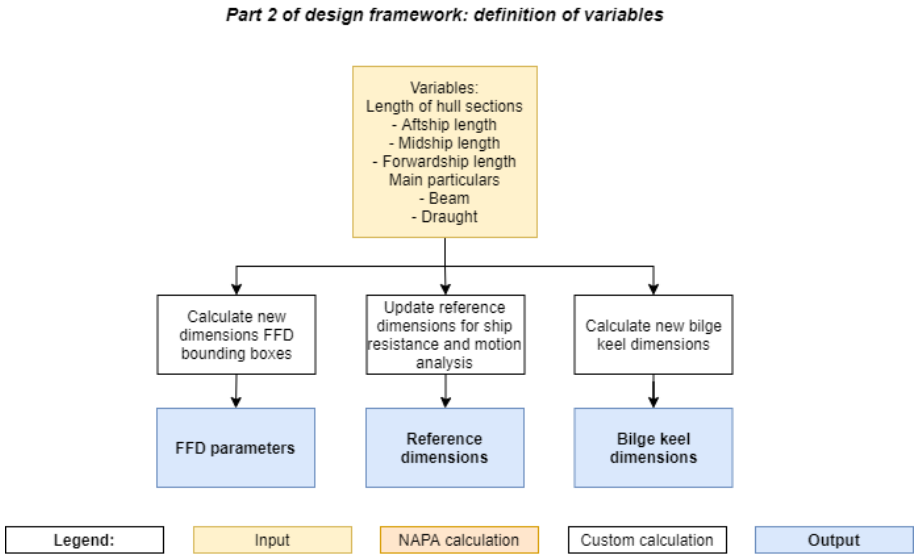

Figure 7.4: Framework variables

- **Main particulars**

  The beam and draught are changed individually. The total length of the vessel is changed by varying the length of specific sections of the hull. Thereby, the length is defined as,

$$L_{tot} = L_{afts} + L_{mids} + L_{fwds} \tag{7.1}$$

  Where L_{afts}, L_{mids}, and L_{fwds} are the aft-, mid- and forward-section length of the hull.

- **Length of hull sections**

  In this item, the aft-, mid- and forward-section length of the hull is varied, which are summed to determine the total length of the ship.

The variable length and beam form input to the FFD-calculation. The variable main particulars form input to vessel reference dimensions, which are called upon for the ship resistance calculation and motion analysis. Based on the variables, the bilge keel moment arm and length are calculated, whereby,

$$RBILGE = \sqrt{VcB^2 + (0,5B)^2} \tag{7.2}$$

and,

$$LBILGE = L_{mids} \cdot \eta_{LBILGE} \tag{7.3}$$

Where $RBILGE$ is the moment arm, $LBILGE$ the length of the bilge keel. On some vessels, the bilge keel length may be slightly longer than the midship length to further increase roll damping. To account for this, a lengthening factor, $\eta_{L-bilge}$, can be defined.

The variables further form input to the calculation, which is discussed in the next subsection.

7.3.3. Calculation

The calculation process is visualized in figure 7.5.

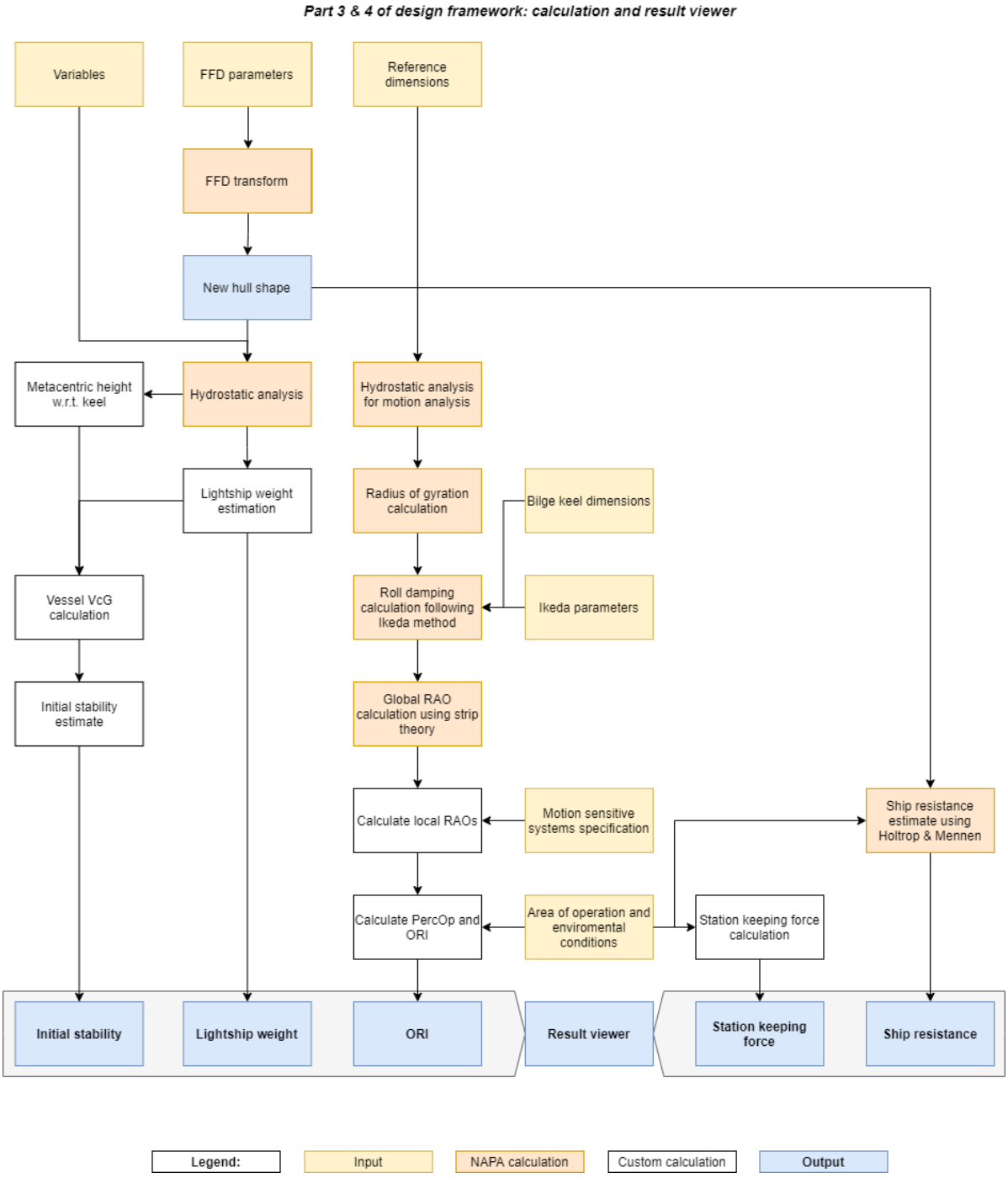

Figure 7.5: Framework calculation process

A description of the output items (highlighted in blue in figure 7.5) are given below:

- **New hull shape**

  The calculation for all objective and constraint scores begins by transforming the parent hull shape. This is done so by the FFD-method (described earlier in section 6.1.1). For example, to lengthen the forward section of the hull, the forward bounding box is stretched. As the hull shape may be composed of weighted spline shapes (see subsection 6.1.1), whereby weight 'points' are

outside the hull. To ensure these weights are shifted with the hull shape transform, the bounding boxes exceed the dimensions of the base vessel. The variables defining the hull shape are automatically transformed to new coordinates for the bounding boxes. For instance, new longitudinal coordinates of the forward bounding box are calculated by,

$$\Delta L_{fwds} = (\frac{L_{fwds,n}}{L_{fwds,b}} - 1) \cdot L_{fwds,b} \tag{7.4}$$

In which ΔL_{fwds} is the change in length of the forward points of the bounding box, $L_{fwds,n}$ the new forwardship length defined by the variables, $L_{fwds,b}$ the base forward ship length, $L_{fwds,b}$ the base bounding box length.

An example of a hull shape in which the forward section is lengthened is shown in figure 7.6.

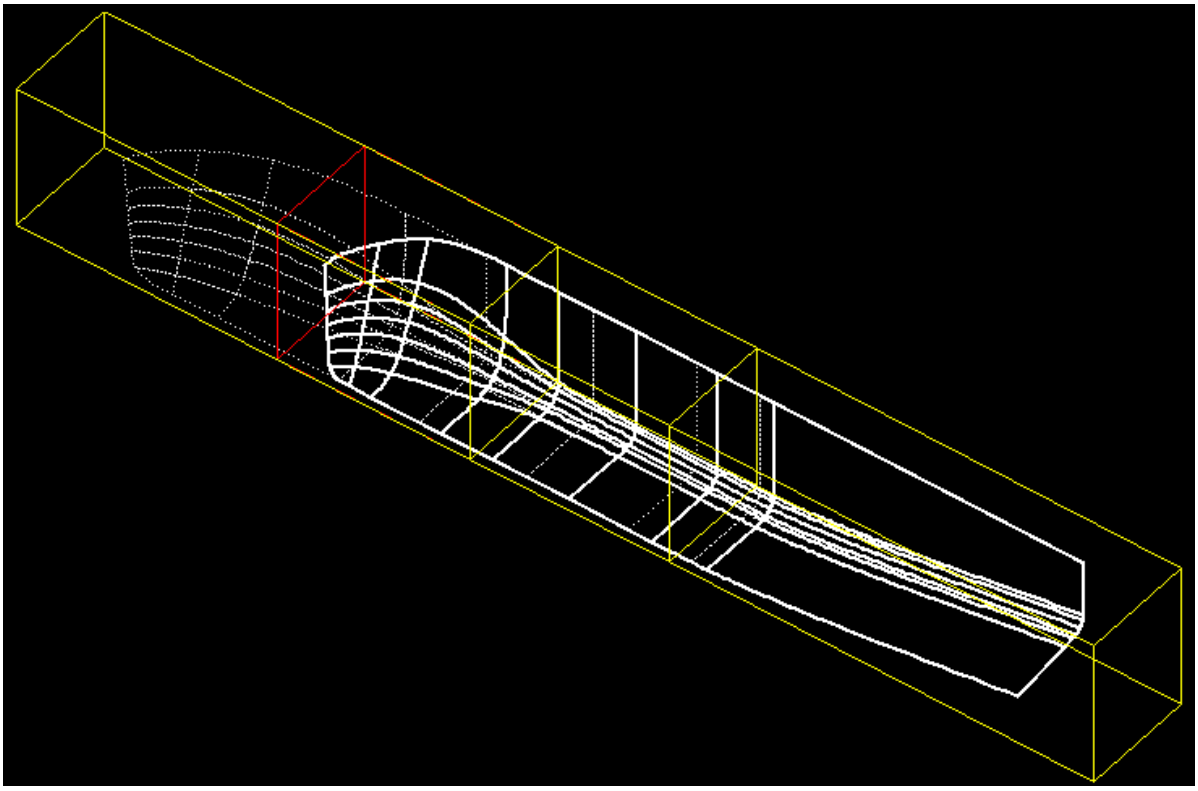

Figure 7.6: Example of an FFD transform in the framework. The red lines indicate a shortened bounding box for the forward section of the ship, resulting in a shorter (forward-) ship, blunter fore-end, and increased forward prismatic coefficient.

The new hull shape is stored in the runtime, and forms input to the remaining calculations.

- **Lightship weight**

  This item estimates the lightship weight of the iteration.

  To calculate the lightship weight, the hull shape is estimated by the quadricubic number [89],

$$m_{ls} = \eta_{ls-contingency} \cdot k \cdot N_{qc} \tag{7.5}$$

  Where m_ls is the lightship weight, k is a parameter determined based on a regression analysis of similar vessels from C-Job's RefWeb database [1]. $\eta_{ls-contingency}$ is a contigency factor, as there is still uncertainty involved (especially during concept desing). N_{qc} is the quadricubic number which is calculated by,

[1] C-Job's RefWeb database is C-Job RefWeb is a maritime reference tool that contains 170 000+ reference vessels with 100+ database fields per vessel. The tool provides information for various regression analyses for a specific vessel type.

$$N_{qc} = L^{4/3} \cdot B \cdot D^{1/2} \cdot \left(1 + \frac{3}{4}Cb\right)^{1/2} \tag{7.6}$$

Equation 7.6 shows the differing influences of length, beam, draught, and block coefficient. Marsich et al. found this relationship to be more accurate as to a simple product formulation, as for instance length exponentially increases lightship weight due to a required increased bending stiffness and so forth. This formulation was shown to provide good accuracy by multiple studies [45].

Importantly, it should be considered this method provides enough accuracy for relative differences between different hull configurations.

- **Initial stability**

  In this section, the initial stability in the form of transverse metacentric height (GM_T) is calculated. An estimate for KG is made by the following equation,

$$KG = \frac{KG_{ss}m_{ss} + KG_{dl}m_{dl} + KG_h m_h + KG_b m_b}{\sum m_i} \tag{7.7}$$

  In which the ss denotes the superstructure, dl the deck load, h the hull, and b the ballast.

  The values for the superstructure and deck load form input to the calculation. The mass of the hull and the weight of the ballast is calculated by,

$$m_h = m_{ls} - m_{ss} - m_{dl} \tag{7.8}$$

  and,

$$m_b = m_{disp} - m_{ls} - m_{dl} \tag{7.9}$$

  The displacement weight, m_{disp}, is calculated by NAPA's own hydrostatic calculation package for the iteration draught. The vertical center of gravity of both the hull and ballast are estimated based on a factor defined by the user.

  By subtracting KG from KM_T, an initial estimate for GM_T is obtained,

$$GM_T = KM_t - KG \tag{7.10}$$

  In which, KM_T is calculated by NAPA's own hydrostatic calculation package. It should be noted this method serves to determine the initial stability to determine which designs are feasible, and which are not. Final initial stability calculations require a much higher fidelity of the mass (distribution) of the vessel. Determining this mass distribution requires, amongst others, information about the specific compartments onboard, a more refined lightship weight estimate, the placement and weight of machinery, and more. This information may not be available during early concept design and is also bound to change by changing the main particulars of the hull. Hence, the simplified method discussed above is used.

- **Station keeping force**

  To provide an indication of the station keeping capabilities the environmental forces enacted on the vessel are calculated. This is done so according to the recommendations by the TU Delft offshore hydromechanics reader [55]. Hereby, the wind forces are defined as,

$$C_{Xw} = a_0 + \sum_{n=1}^{5} a_n \sin\left(n \cdot \alpha_{rw}\right) \tag{7.11}$$

  and,

$$C_{Yw} = \sum_{n=1}^{5} b_n \sin(n \cdot \alpha_{rw}) \tag{7.12}$$

For the longitudinal and traverse wind loads respectively. α_{rw} is the angle between the forward direction of the ship, and the direction of the wind. The coefficients a_n, b_n and c_n are provided in the Offshore Hydromechanics reader.

Current forces are estimated by,

$$X_c = \frac{0.075}{\left(\log_{10}(Rn) - 2\right)^2} \cdot \frac{1}{2}\rho V_c^2 \cdot \cos\alpha_c \cdot |\cos\alpha_c| \cdot L \cdot (B + 2T) \tag{7.13}$$

in which,

$$Rn = \frac{V_c \cdot |\cos\alpha_c| \cdot L}{v} \tag{7.14}$$

and,

$$C_{Yc}(\alpha_c) = \sum_{n=1}^{5} b_n \cdot \sin(n \cdot \alpha_c) \tag{7.15}$$

Where X_c and C_{Yc} are the longitudinal and traverse current forces, respectively. It can be seen, due to the relative slenderness in the longitudinal direction and relatively slow current speeds, that longitudinal current force is mostly due to skin friction. In this equation, V_c and α_c are the current speed and angle respectively. L is the length of the ship, rho is the density of water, and mu is the kinematic viscosity coefficient. The coefficients b_n are available in the TU Delft offshore hydromechanics reader [55].

The wave loads are determined by according to simplifications for second-order wave drift forces,

$$\bar{F} = \frac{-1}{16} \cdot \rho g \cdot H_{1/3}^2 \cdot L \cdot \cos^2\beta \tag{7.16}$$

Whereby $H_{1/3}$ is the significant wave height and β the incoming angle of waves. The total magnitude of the station keeping force is determined by,

$$F_{sk} = \sqrt{(\bar{F}\cos\alpha + X_c + C_{Xw})^2 + (\bar{F}\sin\alpha + C_{Yc} + C_{Yw})^2} \tag{7.17}$$

It should be noted that this metric is calculated by an empirical formula and mostly provides a relative comparison of the station keeping capabilities for different iterations.

- **Ship resistance**

  In this item, the ship resistance at service speed is calculated. Use is made of the NAPA Resistance and Propulsion manager application. This application provides a multitude of widely used empirical methods. Of these methods, Holtrop & Mennen is found to obtain accurate results for a wide range of vessels [46], and a calculation package is available in NAPA. It should be noted that during the optimization, accuracy boundaries such as the L/B and B/T ratio ranges may be exceeded. At these extremities, Holtrop & Mennen is still able to calculate the ship resistance with limited accuracy. In these regions, the ship resistance calculation provides more of a relative comparison for between different variable combinations.

- **Operability Robustness Index**

  The operability robustness index (ORI) forms a robust criterion to measure seakeeping performance. The ORI is based on the vessel RAOs, area of operation, and motion limits. RAOs are first calculated by NAPA's seakeeping application, which contains a strip theory formulation. As an input, a vessel loading condition is defined following the design iteration's draught and GM_T. Additionally, the radius of gyration is calculated as a factor of the length and width of the iteration. This factor is defined by the user and can be based on reference vessels. The roll damping factor is determined following Ikeda's method [52], which requires the length, height, and moment arm of the bilge keel. These dimensions are automatically scaled based on the iteration-specific ship dimensions. The RAO is defined as,

$$H_j(\omega;\beta) = \frac{s_j(\omega;\beta)}{\zeta(\omega)} \tag{7.18}$$

  Where $H_j(\omega;\beta)$ is the RAO per DoF j, $s_j(\omega;\beta)$ the vessel response output signal which is partially dependant on wave frequency ω and wave angle β, and $\zeta(\omega)$ the wave excitation input signal. Once the RAOs have been calculated, the vessel response spectrum is calculated,

$$S_j\,(\omega;\beta;T_Z) = \left|H_j(\omega;\beta)\right|^2 S_\zeta\,(\omega;T_Z) \tag{7.19}$$

  Whereby $S_\zeta(\omega;T_Z;H_s)$ is the wave spectrum (see appendix D for the full procedure of obtaining the wave spectrum). The area enclosed by the spectrum forms a measure of variance (spread of vessel response), also known as the spectral moment m_n,

$$m_n\,(n;\beta;T_Z) = \int_0^\infty \omega^n \cdot S_j\,(\omega) \cdot d\omega \tag{7.20}$$

  Depending on the value of n, the zeroth, first or second spectral moment is calculated. These represent the variance of response for motion, velocity, and acceleration, respectively. The root of this variance gives the standard deviation, σ_j,

$$\sigma_j\,(n;\beta;T_Z) = \sqrt{m_n\,(n;\beta;T_Z)} \tag{7.21}$$

  Which forms input to the tolerable significant wave height, $H_{s,tol}\left(n;\beta;T_Z;\sigma_{j,tol}\right)$ for a specific peak period, together with a particular motion limit $\sigma_{j,tol}$,

$$H_{s,tol}\left(n;\beta;T_Z;\sigma_{j,tol}\right) = \sigma_{j,tol}\frac{H_s}{\sigma_j\,(n;\beta;T_Z)} \tag{7.22}$$

  The percentage operability is then calculated by comparing the evaluation of the scatter diagram. Specifically, evaluated is the percentage of the occurring waves do not exceed the tolerable significant wave height. Hence, the total percentage operability is determined by,

$$PercOp\left(n;\beta;\sigma_{j,tol}\right) = \frac{\sum f_{T_Z|H_s}(T_z \mid H_s \le H_{s,tol}\left(n;\beta;T_Z;\sigma_{j,tol}\right))}{\sum f_{T_Z|H_s}(T_Z \mid H_S)} \tag{7.23}$$

  As the percentage operability is determined for a range of motion limits up until the maximum motion limit (where the limit is $\sigma_{j,tol,max}$). The resultant data provides a curve showing percentage operability as a function of the motion limit. Gutsch et al. only considered the ORI for a single motion, with constants n and β [42]. Considering $PercOp\left(\sigma_{j,tol}\right)$, the ORI is calculated by integrating and normalizing the area under the curve,

$$ORI = \frac{\int_0^{max(PercOp)} PercOp\left(\sigma_{j,tol}\right) d\,(PercOp)}{max(PercOp) \cdot 100} \tag{7.24}$$

  The total process of calculating the ORI for and individual motion limit is shown in figure 7.7.

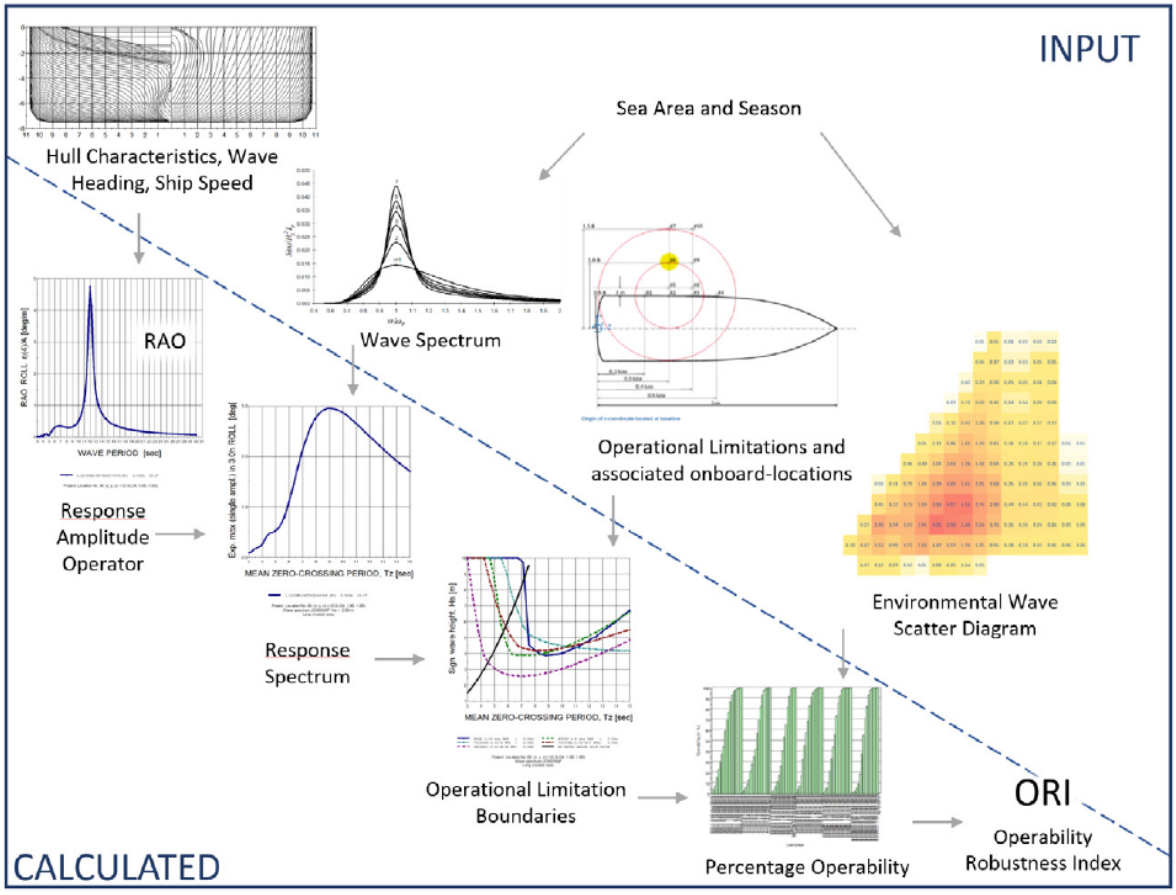

Figure 7.7: Individual calculation steps for operability analysis [42]

The procedure above describes the calculation of tolerable significant wave height for an individual motion limit. Gutsch et al. only considered a single limit in their research. However, to efficiently consider seakeeping, all limits should be considered. To do so, a modification is made to the calculation of the tolerable wave height, $H_{s,tol}$. Equation 7.22 is evaluated for a range of motion limits of a specific DoF and type of motion. For example, for a maximum heave acceleration limit of $\ddot{z}_{limit}$ of $1[m/s^2]$, percentage operability is evaluated for limits $\ddot{z}_{limit}$ of $0.1, 0.2, 0.3, ..., 1.0[m/s^2]$. The amount of steps in which the limit is varied is constant for each motion limit. For each 'step', or percentage of the motion limits ($\%_{limit}$) the most stringent motion limit is critical and limiting to the operability of the ship. The critical motion limit results in the lowest tolerable wave height. Hence the calculation of ORI is expanded by evaluating for each step,

$$H_{s,tol}\left(\%_{limit}, \beta; T_Z\right) = min(n; H_{s,tol}\left(\beta; T_Z; \sigma_{j,tol}\right)) \tag{7.25}$$

Thereby considering each motion limit. Once the tolerable wave height per limit step is known, the corresponding $PercOp(\beta; \%_{limit})$ is calculated by equation 7.23. Finally, the ORI is evaluated by,

$$ORI(\beta) = \int_0^{100\%} PercOp(\beta; \%_{limit}) d(PercOp) \tag{7.26}$$

When all calculations are carried out, the results are written to the result tables. These are viewed under the next item in the framework, the result viewer.

- **Result viewer or output**

  In this item, the results of a particular iteration can be viewed. Additionally, resultant design attributes such as displacement, block coefficient, and so forth can be seen.

7.3.4. Optimization manager

This item initializes and runs the optimization. The corresponding process is defined in figure 7.8

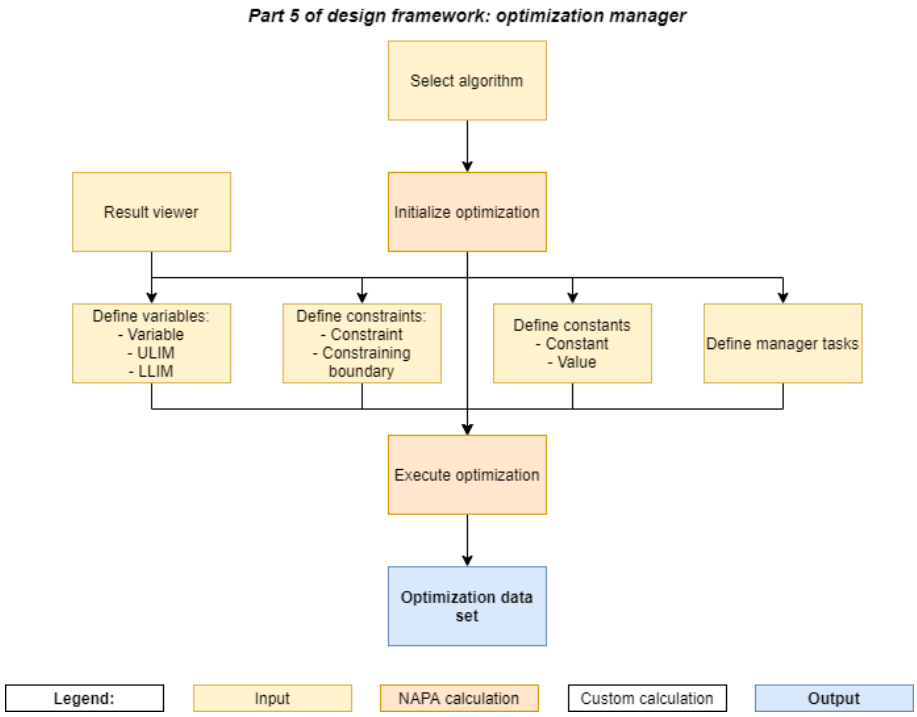

Figure 7.8: Framework optimization manager

The optimization comprises the following components:

- **Algorithm selection**

  The user can select a multitude of optimization algorithms, such as a conventional genetic algorithm. C-Job developed algorithms in-house, which can find the Pareto-frontier very efficiently compared to conventional algorithms [25]. One such algorithm was developed by de Winter et al. and is named 'SAMO-COBRA', wich stands for Self-Adaptive Multi-objective Constrained Optimization By using Radial Basis Function Approximations [26]. A very efficient algorithm, capable of dealing with multiple variables, multiple constraints, multiple objectives simultaneously [2].

  The SAMO-COBRA algorithm attempts to find the Pareto-frontier of the design problem in a limited amount of function evaluations. To do so, it maximizes the 'hypervolume' between the 'reference point' and the Pareto-frontier. The algorithm does so by minimizing the optimization objectives. The product of the distance between the 'reference point' and the objective scores forms the hypervolume. Undesired values are reflected by the reference point. The SAMO-COBRA algorithm finds variables and subsequent objective scores removed from these values until no feasible solutions are found. This can be a certain maximum for lightship weight, or a maximum ship resistance value. Visualization of two different hypervolumes is given in figure 7.9.

  After a certain number of iterations, this hypervolume is maximized and the extremities of the Pareto frontier are found. Once the Pareto-frontier has been found, the hypervolume score converges to an asymptote. New design solutions will only fall on the frontier or behind. As such,

[2] This section provides a simple explanation of the algorithm. A more detailed and elaborated explanation can be found in a paper by de Winter et al., as well as a comparison with other optimization algorithms. This paper is provided in appendix D.

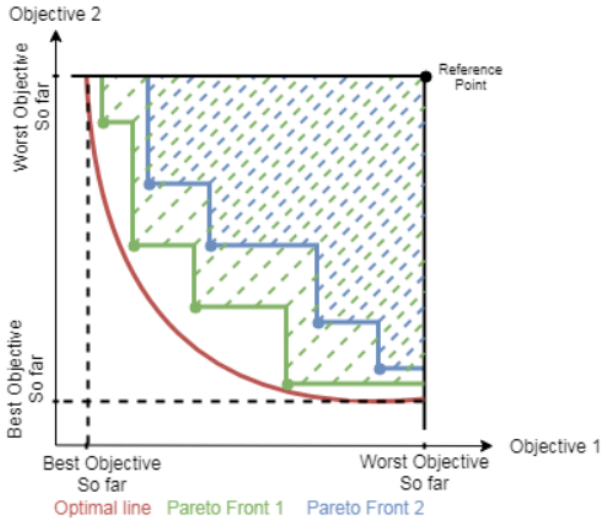

Figure 7.9: Hypervolume for two Pareto-fronts [28]

after a certain number of iterations, the hypervolume only improves marginally as the frontier with optimal solutions has been found.

- **Initialization**

  To apply the SAMO-COBRA algorithm to the optimization, the optimization is first initialized - whereby the necessary tables are defined. Certain input to the optimization is defined. These are:

- **Define variables**

  Experiment variables are defined, including lower and upper limits, starting point, and step size (if required by the algorithm). By defining these limits for the global dimensions of the vessel, sufficient space for onboard equipment can be ensured.

- **Define objectives**

  The objectives are selected, including a reference point. The reference point indicates undesired values, which SAMO-COBRA steers the design away from. The objectives are selected from the result viewer.

- **Define constraints**

  Constraints, that is, values for certain attributes that are not to be exceeded, are defined. The constrained are selected from the result viewer.

  The algorithm learns what combination of variables exceeds a defined constraint value. It thereby learns what variable combinations are not feasible, and steers away from these combinations.

- **Define constants**

  If required, certain variables can be set as constants.

- **Define manager tasks**

  This item defines the manager tasks that are to be run by the algorithm. Thereby, the experiment can be set up to involve specific tasks which may differ depending on the optimization problem.

Once the optimization is established, it is executed. Before executing, the user selects the number of iterations, as well as the initial randomly selected sample size. This sample size provides the algorithm with initial data, used for further calculating the location of the Pareto-frontier. Once the optimization is completed, an optimization data set is created which can be further processed by the user.

7.4. Conclusion and summary

This chapter describes the methodology of the design framework, thereby answering the research sub-question *How is a concept design framework incorporating motion characteristics developed?*. The focus of the framework was on being able to do an in-dept evaluation of the seakeeping performance of a vessel with the limited information that is available during concept design. Additionally, objectives were developed to give an adequate representation of a performance in the other design drivers governing OSV design. To verify whether the framework does indeed give a (sufficiently) accurate assessment of the performance of any specific OSV, but also if it is able to optimize the corresponding variables to maximize performance, a verification of the framework is done in the next chapter.

8

Model verification

This chapter's aim is to verify the framework. In doing so, part of the research question *'How can the new framework be verified and validated?'* is answered. To do so, section 8.1 verifies and analyses the accuracy of each of the KPI's. Section 8.2 performs a sensitivity study on the influence of variables and input. In section 8.3, the optimization if verified. Lastly, the chapter ends with a summary and discussion in section 8.4.

8.1. Verification of KPI's

8.1.1. Verification and accuracy of seakeeping assessment

This subsection analyzes the accuracy of- and verifies the seakeeping assessment. The particular seakeeping assessment process in the framework is described by figure 7.1. Firstly, the accuracy of the calculation method for RAOs is compared to that of a method that is typically more accurate. Specifically, the results from NAPA's strip theory code have been benchmarked against that of AQWA, which is a panel method. The results are shown in figure 8.1.

In figure 8.1, the RAOs of both AQWA and NAPA generally show good agreement with each other. However, strip theory does underestimate the roll natural frequency peak. Hence, the effect of a roll limit may be underestimated. Regardless, C-Job Naval Architects commented the peak is sufficiently high to form input to adequate seakeeping assessment.

To verify whether framework solutions actually maximize seakeeping performance, an optimization with a large design space has been run. Input settings as depicted in table 8.1 where used, which are based on the US Wind Feeder case study. Other input parameters are further deliberated in appendix E. The following objective and constraint functions were applied:

$$\begin{aligned} Objectives: \\ max(ORI) \\ min(LSW) \\ min(SR) \\ Constraints: \\ GM_t > 2.0[m] \\ L_{pp} > 90.0[m] \end{aligned} \tag{8.1}$$

For calculation of the different objectives and constraints, refer to 7.3.3. The resultant solutions are plotted in figure 8.2.

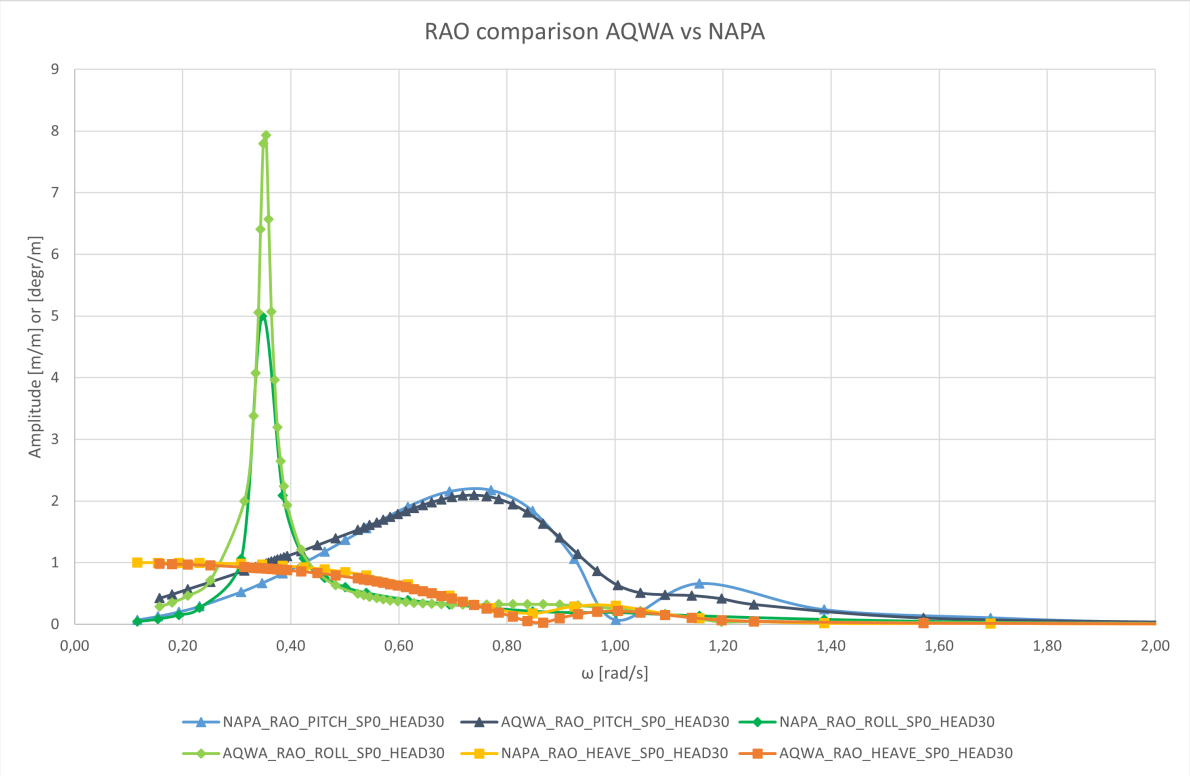

Figure 8.1: Comparsion of RAOs between NAPA and AQWA

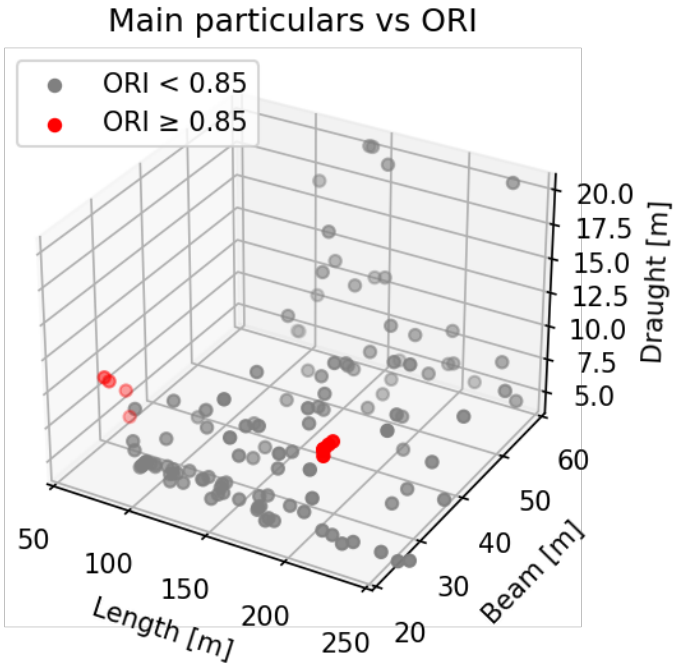

Figure 8.2: Main particulars versus ORI for optimization using input settings as depicted in 8.1

Figure 8.2 shows that both smaller and larger vessels lead to a high ORI value (highlighted in red). To better understand why, both a 'small' and 'large' design solution are compared to the base vessel. Additionally, the natural roll frequency has been computed for each result by the following equation,

Optimization settings

Input

Input	*Symbol*	*Setting/specification/value*	*Unit*
Area	-	23.0, North Atlantic Ocean, East Coast USA	-
Hull shape	-	US Wind Feeder concept	-
Angle incoming waves	α_{RAO}	30.0	°
Motion sensitive equipment	-	Ampelmann platform, near CoB from US Wind Feeder concept (see table)	-
Loading condition	-	Maximum loading condition US Wind Feeder (see table 8.7)	-

Variables

Variables	*Symbol*	*Lower limit*	*Upper limit*	*Unit*
Aftship length	L_{afts}	30.0	100.0	m
Midship length	L_{mids}	10.0	100.0	m
Forwardship length	L_{fwds}	30.0	100.0	m
Beam	B	17.0	60.0	m
Draught	T	4.5	15.0	m

Constraints

Constraints	*Symbol*	*Lower limit*	*Upper limit*	*Unit*
Metacentric height	GM_T	2.0	-	m
Total length	L_{tot}	60.0	-	%

Objectives

Objectives	*Symbol*	*Unit*
ORI	ORI	–
lightship weight	LSW	t
Ship resistance	SR	kN

Algorithm settings

Item	*Setting*	*Unit*
Algorithm	SAMOCOBRA	–
Maximum iterations	300	#

Table 8.1: Primary optimization settings, other settings available in appendix E

$$\omega_{n,roll} = \frac{\sqrt{\mathrm{gGM_t}}}{K_{xx}} \tag{8.2}$$

Where g is gravitational acceleration, GM_T the transverse metacentric height, and K_{xx} the roll radius of gyration. K_{xx} is calculated by $K_{xx} = 0.4875B$, based on the weight distribution of the current US Wind Feeder concept.

The RAOs of each of the three vessels are shown in table 8.2, which shows that both the small and large design solutions feature an higher ORI compared to the base vessel. To verify this outcome, the individual RAOs for heave, pitch and roll have been computed by the framework's strip theory code and compared to the ocean statistics for area 23. The results are shown in figure 8.3.

Figure 8.3 shows that the three vessels feature substantially different RAOs. The results show that the heave resonance peak of the base vessel falls within the range of typical waves of area 23. Both the smaller and larger optimized vessels minimized this heave motion response. Due to the increased draught of both vessels, there is an increase in added mass, dampening the peak heave motion. Additionally, the roll peak of the base vessel is quite far outside the range of typical waves. The resonance peaks coincide by the natural roll frequency calculation (see table 8.2). The smaller optimized vessel features a peak closer to the frequency of occurring waves, resulting in more roll motion response and

Comparison optimization results for seakeeping for different size vessels					
Variable	*Symbol*	*Value*	*Value*	*Value*	*Unit*
Vessel	-	**Base vessel**	**Optimized small vessel**	**Optimized large vessel**	-
Aftship length	L_{afts}	46.00	67.38	100.00	m
Midship length	L_{mids}	23.80	55.30	100.00	m
Forwardship length	L_{fwds}	34.80	30.00	30.00	m
Total length	L_{tot}	103.80	115.30	230.00	m
Beam	B	23.80	20.79	33.09	m
Draught	T	5.50	10.00	10.79	m
Metacentric height	GM_T	2.18	2.01	9.70	%
Operability	$PercOp$	99.8	100.0	100.0	%
ORI	ORI	0.817	0.857	0.841	–
Roll frequency	$\omega_{n.roll}$	0.40	0.44	0.60	rad/s

Table 8.2: Variables and subsequent ORI for different type of vessels. other input parameters as provided in table 8.1

a higher roll peak. Due to a smaller beam, the roll damping is slightly lower. Unexpectedly, the vessel features a higher ORI, thus better seakeeping behavior for the given limits. This leads to the conclusion that the roll limit is not critical for the Ampelmann limits. The large optimized vessel shows a much lower overall RAO response compared to the smaller vessels, even in the resonance peaks. This indicates substantial damping components for the larger optimized vessel. Hence, the vessel is comparatively less excited by any encountered waves, leading to a high ORI value.

To conclude, the higher ORI values of the optimized vessels are explainable by the inspection of the individual RAOs. It is concluded that the framework is able to vary dimensions of the vessel to influence RAOs for optimal seakeeping behavior for the given motion limits.

8.1.2. Verification of other objective and constraint functions

- **Accuracy of ship resistance calculation**

  The ship resistance at service speed is estimated using Holltrop & Mennen (see section 7.3.3). This method has been widely used by industry, and generally shows good agreement for vessels within the described range of applicable main particulars. This range is [14],

$$\begin{aligned} Fr &\leq 0.45 \\ 0.55 \leq C_B &\leq 0.85 \\ 3.9 \leq \frac{L}{B} &\leq 9.5 \end{aligned} \tag{8.3}$$

  Table 8.3 compares the dimensions of the US Wind Feeder, the vessel used a reference OSV, to the boundaries of Holltrop & Mennen. The comparison shows that the vessel is close to exceeding the L/B constraint. Though the current concept does not exceed the constraint, there is a possibility the constraint may be violated during an optimization run. For extreme design configurations, the measure for ship resistance becomes more relative as opposed to an absolute KPI.

- **Accuracy of lightship weight estimation**

  The lightship KPI is calculated according to equations 7.5 and 7.6. To verify the accuracy of the method, a comparison is done between the results of regression analysis, and a detailed LSW estimate done for the US Wind Feeder by C-Job naval architects. This detailed LSW estimate comprises a weight estimate per ship item, such as powerplant, equipment, and so forth.

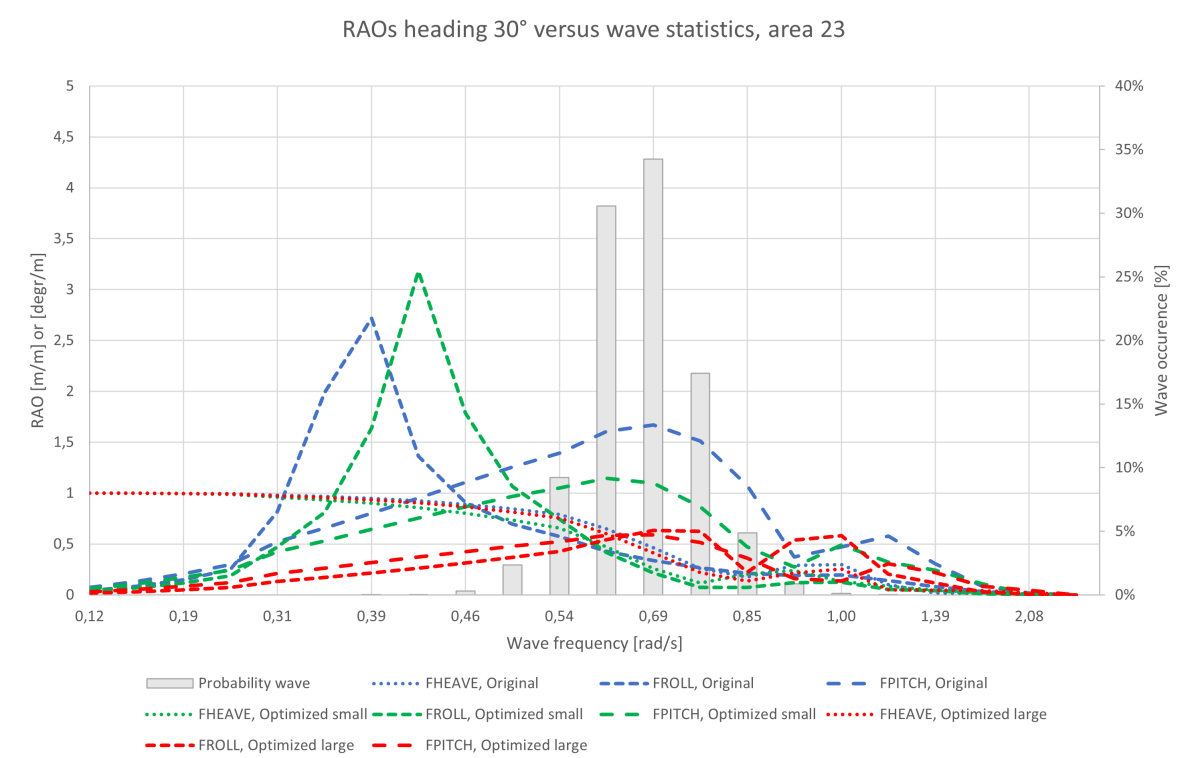

Figure 8.3: RAO's versus wave statistics

Boundaries H&M compared to the US Wind Feeder					
Variable	*Symbol*	*Value*	*Value*	*Value*	*Unit*
Vessel or boundary	-	**US Wind Feeder**	**Lower H&M boundary boundary**	**Upper H&M boundary boundary**	-
Total length	L_{tot}	103.80			m
Beam	B	23.80			m
Length over beam	L/B	4.36	3.90	9.50	–
Vessel speed	V_S	10.00			kn
Froude number	Fr	0.16		0.45	–
Block coefficient	C_B	0.73	0.55	0.85	–

Table 8.3: Comparison main particulars US Wind Feeder concept and boundaries for Holltrop & Mennen [14]

.

A regression analysis is performed for a selection of platform supply vessels from C-Job's RefWeb database [1]. As the offshore wind market leads to a development in new types of vessels, reference vessels may not be available. For example, there exist no reference vessels for the US Wind Feeder concept. For application on the US Wind Feeder, PSV's and general cargo vessels have been found to approximately match the characteristics from the US Wind Feeder, given the typical length, depth, width, service speed and deck. The results of the regression analysis, performed in Excel, are shown in figure 8.4, thereby finding the factor k in equation 7.5.

[1] C-Job's RefWeb database is C-Job RefWeb is a maritime reference tool that contains 170 000+ reference vessels with 100+ database fields per vessel. The tool provides information for various regression analyses for a specific vessel type.

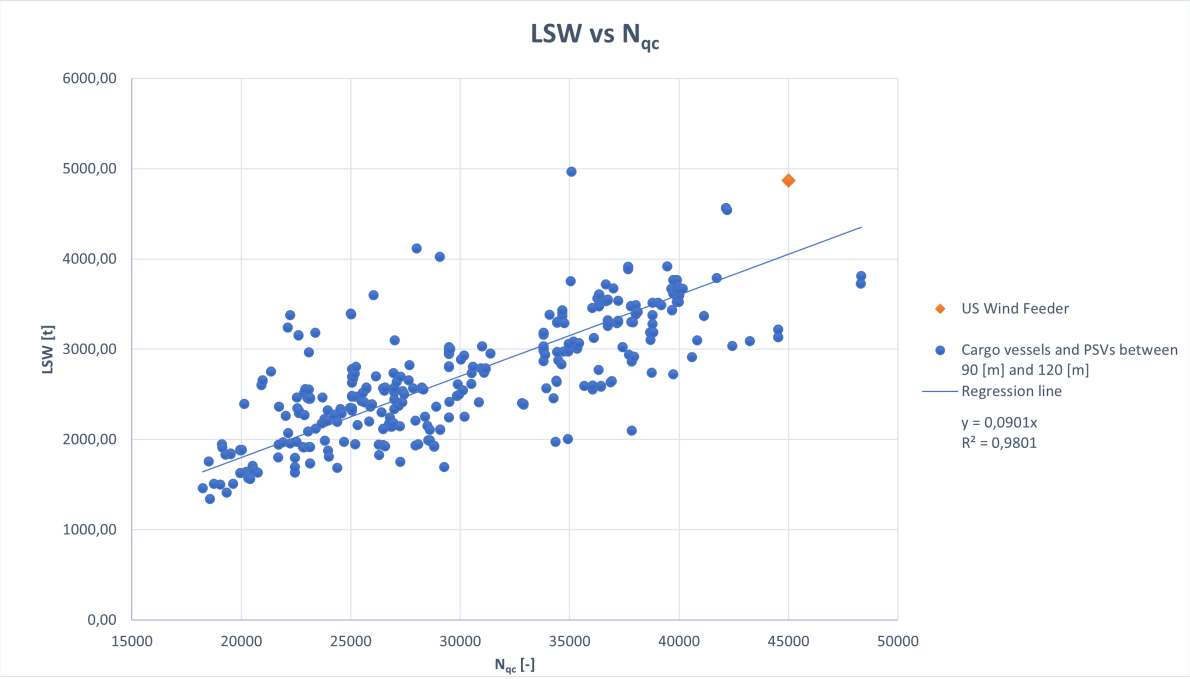

Figure 8.4: Results of regression analysis on cargo vessels and PSVs

Figure 8.4 shows a visual fit of the linear regression line, and the reference vessels. This is further proven by the high R^2 value of 0.9801. Additionally, it should be noted that the majority of and cargo vessels are comparatively shorter and slenderer compared to the wind feeder concept. Subsequently, the lightship weight is underestimated as shown in the table 8.4.

Comparison weight estimation methods				
Variable	*Symbol*	*Value*	*Value*	*Unit*
Type of calculation	-	**Framework estimate**	**High fidelity weight group estimate**	-
Quadricubic number	N_{qc}	45264		–
lightship weight	LSW	4078	4426	t
lightship weight with 10% contingency	LSW_c	4486	4869	t
Difference w.r.t. high fidelity estimate	-	7.86		%

Table 8.4: Differences in current concept LSW and estimated LSW for US Wind Feeder

Table 8.4, shows an approximate $7,9\%$ difference between the current US Wind Feeder concept weight and the estimated weight. As no wind feeders have been built yet, the actual weight of the vessel will only be certain once the vessel is built. A lightweight estimate should fall within an accuracy boundary whereby any deviations of the final weight do not heavily influence ship performance. Typically, C-Job considers a 10%, to be sufficiently accurate during concept design. As such, the framework's lightship weight estimate is adequate.

Regardless of accuracy, equations 7.5 and 7.6 appropriate reflect the influences of length, beam, draught and block coefficient in the weight estimate. Thereby, the method is able to differentiate between design configurations for *relative* weight differences, even if the estimate is not fully accurate.

- **Accuracy of station keeping force**

  The station keeping force has been calculated according to empirical formulas (see equations 7.11, 7.12, 7.13, 7.14, 7.15, 7.16 and 7.17). Therefore, certain inaccuracies are expected. The method has been validated against large container vessels with a high block coefficient. Due to the latter property, shared with the US Wind Feeder, the decision has been made to use this method. Due to the probable uncertainty, the required station keeping force KPI should be evaluated as a *relative* measure. Thereby, it does not give an absolute indication of station keeping capabilities, but forms a measure to differentiate between framework solutions.

- **Accuracy of initial stability calculation**

  Based on the estimated lightship weight and defined operational loading condition, the vessel's VcG is calculated, as seen by equation 7.7. The estimated VcG forms the input to the initial stability, following equation 7.10. Under the assumption that the deck load and superstructure do not change in weight and VcG with respect to the deck, these values remain constant throughout the optimization. The VcG of the hull and ballast is estimated as a factor of the vessel's depth. These factors are determined based on vessels with an intact stability booklet in C-Job's project database. Specifically, C-Job naval architects recommended using the current concept US Wind Feeder, DEME Orion, and Atlantic Dawn for input. The weight distribution information for the Wind Feeder concept is accurate to a degree they may use as input. The DEME Orion and Atlantic Dawn feature a similar configuration in terms of deck and equipment layout, as both feature an open deck designed to carry heavy cargo (similar to wind turbine components). The results are shown in table 8.5.

Comparison location of weight components

Variable	*Symbol*	*Value*	*Value*	*Value*	*Value*	*Unit*
Vessel	-	**DEME Orion**	**Wind Feeder concept**	**Atlantic Dawn**	**Average**	-
Depth	D	16.80	9.20	6.86	-	m
VcG hull	VcG_{hull}	12.04	5.16	5.00	-	m
Factor w.r.t. depth	-	0.72	0.79	0.79	0.75	m
VcG ballast	$VcG_{ballast}$	7.84	4.00	2.52	-	m
Factor w.r.t. depth	-	0.47	0.44	0.37	0.42	m

Table 8.5: Factor depth with respect to center of gravity for hull- and ballast weight for various vessels

Table 8.5, shows that the VcG of the hull occurs typically at a factor of around 0.75 of the depth of the vessel. Additionally, the VcG is typically located and approximately a factor 4.23. The maximum difference between the average factor and that of the vessels is approximately 10%, hence some uncertainty is present. The calculated GM_t is not definitive and mostly forms an indication for the stability, and subsequent feasibility of the vessel. As such, the GM_T constraint should be high enough to provide flexibility for changing hydrostatic attributes in later design stages.

8.2. Sensitivity study

8.2.1. Influence of variables on KPI's

To validate whether the model behaves as is expected, the sensitivity of each KPI with relation to the different parameters is analyzed. To do so, an optimization has been run with 400 iterations, to fully explore the design space. The input settings from table 8.1 have been used. The optimization has been run for a large initial sample, where variables are selected randomly. As such, no correlation between individual variables is present. A correlation matrix based on the results has been created using Python. A correlation matrix shows the correlation between each of the variables and KPI's. To be specific the correlation value has been computed for each item by,

$$r_{xy} = \frac{\sum_{i=1}^{n} (x_i - \bar{x})(y_i - \bar{y})}{\sqrt{\sum_{i=1}^{n} (x_i - \bar{x})^2} \sqrt{\sum_{i=1}^{n} (y_i - \bar{y})^2}} \tag{8.4}$$

Which produces the Pearson correlation coefficient [74]. The result is a value between -1 and 1. -1 indicates a perfect negative linear correlation, 0 indicates no linear correlation, and 1 indicates a perfect positive linear correlation between two variables. Thereby, it should be noted that this method fails to appropriately weigh non-linear relationships. Hence, the values mostly indicate how strong a certain trend is between different values. The results are visualized in figure 8.5 (see next page). In figure 8.5, AFTSHIPL, MIDSHIPL and FWDSHIPL represent the length of the aft-, mid- and forward-section of the hull. The BEAM and DRAUGHT represent the beam and draught respectively. GM is the initial transverse metacentric height, SKF is the station keeping force, RT is the ship resistance, ORI is the operability robustness index, and LSW is the lightship weight. To better explain some correlations, the block coefficient, CB, is also included. Due to only using an initial (random) sample no correlation exists between variables.

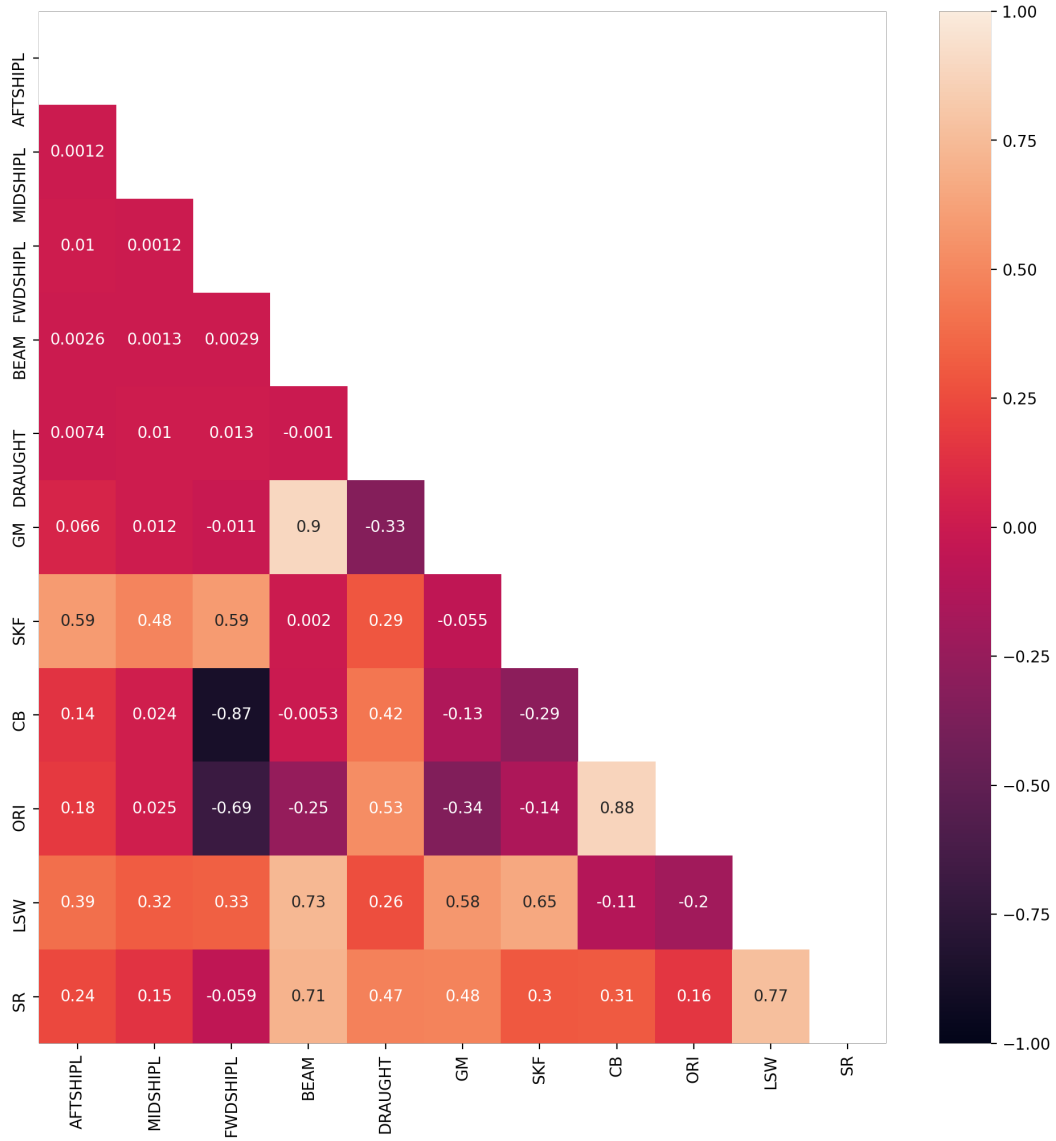

Figure 8.5: Correlation matrix for design framework, based on the results of a 400 design combinations with randomly generated variables

Focusing on the KPI's, the following correlations between variables are seen (in order from above to below in the correlation matrix):

- **GM** - Metacentric Height

  The correlation matrix shows that the length of the ship barely influences the GM_t. This is to be expected as the longitudinal properties (minimally) influence the elements in equations 7.10. The draught is seen to have a negative correlation with the GM_t. That is, when draught increases, GM_t decreases. Table 8.6 shows the results of varying the draught between $4.5m$ and $6.5m$, whilst keeping freeboard the same.

Influence of draught on GM_T					
Variable	*Symbol*	*Value*	*Value*	*Value*	*Unit*
Draught	T	**4.5**	**5.5**	**6.5**	m
Depth	T	**13.7**	**14.7**	**15.7**	m
Beam	B	23.8	23.8	23.8	m
Vertical center of gravity	VcG	11.4	10.5	10.0	m
Distance keel - metacentre	KM_t	14.0	12.7	11.9	m
Metacentric height	GM_t	2.6	2.2	1.9	m

Table 8.6: Influence of draught on parameters influencing GM_T

  Table 8.6 shows that the VcG and KM_T (the same freeboard height is maintained), both decrease with increasing draught. KM_T is shown to decrease quicker compared to the VcG at increasing draught and depth, resulting in the difference, GM_T, becoming smaller. Hence there is a negative correlation between draught and GM_T, as reflected by the correlation matrix.

  There is a positive correlation between the beam and GM_T, that is, an increasing beam leads to an increase in GM_T. This is to be expected, as a wide ship leads to a high KM_T, as the transverse waterplane area increases substantially.

- **SKF** - Station Keeping Force

  The required station keeping force increases with the increased length of the hull sections. This is to be expected, as increasing the length increases the area on which wind, wave, and current forces can take effect. An increase in the beam is shown to have a minimal effect increasing the station keeping force. This indicates majority of required station keeping force is due to the length and depth of the vessel at an incoming wave, current, and wind angle of $30°$.

  An increase in depth is seen to increase the station keeping force. This is to be expected, due to an increase in current forces.

- **RT** - Ship Resistance

  A positive correlation is seen between aft- and midship length and ship resistance. A negative correlation exists between the forwardship length and ship resistance. When the forwardship length is increased a finer front end is created, improving form resistance. Increasing the aft- and midship length creates a fuller hull shape, thereby having the opposite effect. This behaviour is confirmed by comparing the relation between dimensional parameters and block coefficient, where the same correlations persist. When considering all length parameters together, the correlation between length and ship resistance is positive, since an increase in length is paired with an increase in hull surface and thus frictional resistance.

  An increase in beam shows an increase in ship resistance, as it increases both form and frictional resistance resistance, which also holds for an increase in draught.

- **ORI** - Operability Robustness Index

  The length is seen to have a substantial effect on ORI [2]. Decreasing the forwardship length increases the block coefficient of the vessel, increasing the (added-)mass terms, thereby dampening motions. The opposite relation is seen for the aftship length. An increase in draught is also

[2]The correlations between dimensions and ORI are partially defined by the operational conditions. The optimization has been run for bow waves, yet for beam waves, the correlations may be different, especially for length.

shown to increase the ORI due to an increase in mass terms. An increase in beam shows an increase in ORI, mostly due to a decrease in GM_T. Furthermore, a lower GM_T typically leads to an increase in ORI, confirming the findings in section 8.1.1.

Concluding the findings above, the ORI shows opposite behaviour to that of ship resistance, indicating a trade-off between both KPIs.

- **LSW** - Lightship Weight

  As expected, an increase in all (dimensional) variables lead to an increase in LSW. This correlation is in line with the estimation method for LSW, following equation 7.6. To verify the magnitude of correlations, a discussion on the differences in lightship weight for the results of the case study is performed in section 9.3.3.

8.2.2. Influence of input parameters

In this section, the effect of input parameters is analyzed. As describes by chapter 7, the hull shape, bilge keel dimensions, location of motion sensitive systems, area of operation and operational loading condition form input to the optimization. In particular, chapter 4 stressed the need to consider the area of operation, as well as the location of motion sensitive equipment as critical input for an effective seakeeping optimization framework. As such, both input parameters have been varied, and the results analyzed.

- **Influence of hull shape**

  Different hull shapes form input to the optimization. These hulls can have a large influence on seakeeping performance, as discussed in chapter 4. Specifically, finer hull (V-shaped) shapes have lower ship resistance, but less displacement and cargo carrying capacity compared to fuller hull shapes (U-shaped). Additionally, finer hull shapes typically have worse seakeeping performance. An optimization has been run using the same settings as shown in 8.1, though varying the hull shapes.

  Three hull shapes have been used, that of a container vessel which has been optimized for ship resistance and features a bulbous bow, a hull shape of an trailing suction hopper dredger (TSHD) vessel, which maximizes cargo carrying capacity and is a typical U-shape, and a special V-shaped hull from a research vessel. These hull shapes are shown in figure 8.6. The optimization results are shown in figure 8.7.

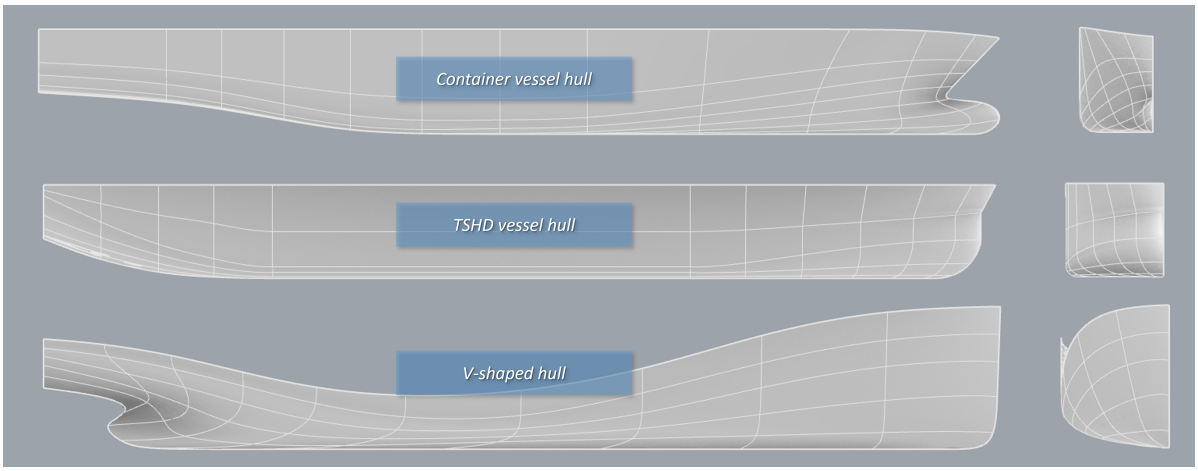

Figure 8.6: Hull shapes used for comparison study

Figure 8.7 shows that the container vessel is able to obtain the best seakeeping performance as well as the best ship resistance. Research has shown a bulbous bow is effective at reducing vertical motions, due to the increase in added mass without an increase of water-plane area [93] [3]. The low ship resistance is obtained due to the fine entry angle and bulbous bow in comparison

[3] It should be noted that the implemented strip theory in NAPA is able to consider a bulbous bow, regardless of strip-theory-inherent simplifications [19].

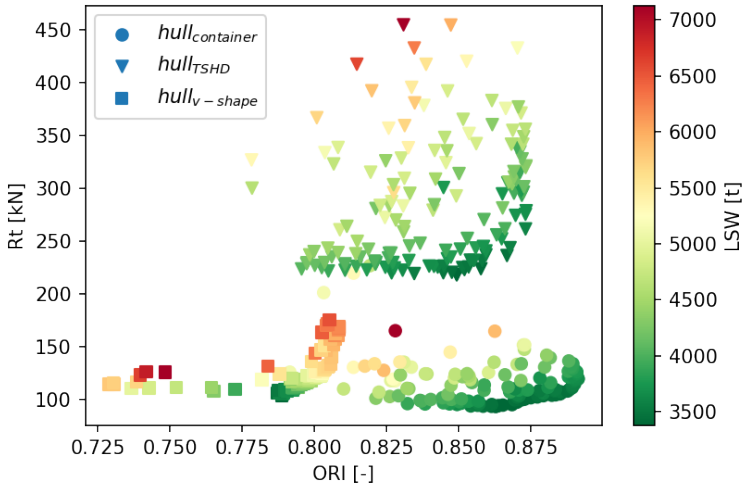

Figure 8.7: Resultant KPI scores for three different hull shapes

to the other hull shapes. Following in attainable ORI values, the TSHD hull shape provides a very stable, almost barge-like ship hull, resulting in good seakeeping results due to the high block coefficient en subsequent increase in (added-) mass, damping terms. Due to the fullness of the hull, attainable ship resistance is by far the largest. The v-shaped hull follows the container vessel in ship resistance, which is to be expected due to the fine hull shape. The attainable ORI values are low in comparison to the other vessels. This hull shape is of a special research vessel, and the design was bound by many constraints. Hence, the hull shape may be sub-optimal for seakeeping. Considering the different results, the influence of the hull shape is clear, stressing the need to start the optimization with a suitable base hull shape.

- **Influence of loading conditions**

  As seen by equations 7.7, 7.8, 7.9 and 7.10, the loading condition forms direct input to the required amount of ballast. Subsequently, the loading conditions influence the vertical center of gravity of the vessel and the resultant metacentric height. Additionally, influencing the draught whilst maintaining the same beam was found to have a limited influence on GM_t. Regardless, GM_T heavily influences the resultant ORI. The framework is able to optimize for a single loading condition. To study the effects of changing loading conditions, the US Wind Feeder concept's loading condition has been varied. The loading conditions and subsequent results are shown in table 8.7. The results show that a lighter loading condition leads to a higher GM_T due to the overall lowered VcG of the vessel. The influence on the ORI is clearly seen, as the higher GM_T increases the motion response of the vessel.

- **Influence of angle of incoming waves**

  To verify the effect of changing the incoming angle of waves, an optimization run has been carried out for both an incoming angle of $30[°]$ (bow waves) and $90[°]$ (beam waves). Except for changing the angle of incoming waves, the input settings as listed in table 8.1 have been used. Figure 8.8 shows the Pareto-optimal solutions of both runs as a parallel coordinate plot. Specifically, shown is which combination of variables results in a certain ORI value. Both plots have been color-coded based on the resultant ORI value.

  Figure 8.8 shows that the maximum attainable ORI differs substantially. The maximum attainable ORI for 30[°] incoming waves is approximately $0.83[-]$, whereas for 90[°] incoming waves it is limited to $0.73[-]$. Typically, beam waves cause excessive roll motions and have a significant effect on seakeeping performance [59]. The framework increased the midship length, to maximize bilge keel length and roll damping, to counteract the roll motions. Thereby, it is shown that the framework recognizes different variables leading to optimal seakeeping behavior, depending on the incoming wave angle.

Effect of different loading conditions				
Variable	*Symbol*	*Value*	*Value*	*Unit*
Loading condition	-	**US Wind Feeder. full transit load**	**US Wind Feeder. last item to be lifted onboard**	-
Weight deck load	M_{dl}	2184	760	t
VcG w.r.t. deck	VcG_{dl}	14.8	5.17	m
Length	L_{tot}	103.8	103.8	m
Beam	B	23.8	23.8	m
Draught	T	5.5	5.5	m
Metacentric height	GM_T	2.2	5.7	m
Percentage operability	$PercOp$	99.6	99.5	%
ORI	ORI	0.817	0.806	–

Table 8.7: Influence of loading conditions on subsequent GM_T and ORI values

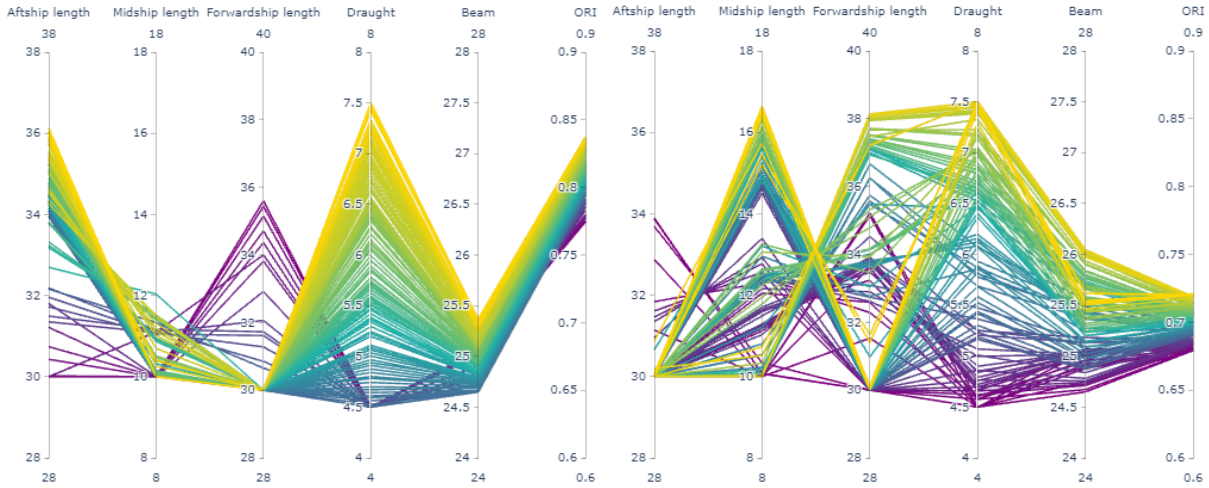

(a) 30[°] incoming waves (b) 90[°] incoming waves

Figure 8.8: Comparison of influence of angle of incoming waves (with respect to forward direction of ship)

- **Influence of bilge keels**

  The literature review indicated a need to incorporate bilge keels in the optimization. To verify the effect of bilge keels and validate the need, two optimization runs have been carried out, with and without bilge keels respectively.

  The verification study has been based on a W2W-vessel, the 'Bibby WaveMaster 1', which is equipped with a motion compensated gangway. In figure 8.9, this vessel is depicted.

  Based on this vessel, motion limits as depicted in table 8.8 have been deducted. An optimization run with bilge keels has been carried out, whereby the Ikeda method has been applied to determine the critical roll damping factor ([52], [84]). This method has been tuned as such that the critical damping factor falls between 4% and 10% depending on the bilge keel dimensions, which has been found to be a realistic result by literature [39].

  For the optimization run without bilge keels, a damping factor is still present due to the damping effects inherent to the hull. According to the SNAME Principles of Naval Architecture ([59]), the resonance magnification factor for roll is $10[°/m]$ or more for a bare hull or $7[°/m]$ for a ship equipped with bilge keels. A (constant) critical damping factor has been tuned to approximately match the height of this resonance peak for a bare hull. The resulting constant critical damping factor is 1%.

Figure 8.9: W2W-vessel 'Bibby WaveMaster 1', with motion compensated gangway in operation [1]

Motion limit case for roll damping verification					
Variables	*Symbol*	*Value*			*Unit*
Motion limit case	–	**Motion compensated gangway**			–
Longitudinal location w.r.t. CoB	X	-20			m
Transverse location w.r.t. CoB	Y	10			m
Height w.r.t. CoB	Z	20			m
Type of motion	–	Motion	Velocity	Acceleration	–
Surge	x	20	20	20	m,m/s,m/s^2
Sway	y	20	20	20	m,m/s,m/s^2
Heave	z	1	1	1	m,m/s,m/s^2
Roll	ϕ	2	1.5	1	$°$,$°/s$,$°/s^2$
Pitch	θ	2	1.5	1	$°$,$°/s$,$°/s^2$
Yaw	ψ	20	20	20	$°$,$°/s$,$°/s^2$

Table 8.8: Motion limit input for roll damping verification

Both optimizations have been run with the same input settings as seen in table 8.1, with the exception of angle of incoming waves, set to beam waves, motion sensitive equipment and maximum draught, which has been set to $8[m]$ to resemble the Bibby WaveMaster 1, as well as the vessels area of operation, which is the North Sea. It should be noted that the ship resistance prediction method has not been adjusted for the influence of bilge keels for the two optimization runs. The resulting Pareto-optimal solutions of both optimization runs are plotted in figure 8.10.

Figure 8.10 shows two Pareto-frontiers occurring for both vessels. The 'upper' Pareto-front, indicated by the highest ship resistance, shows both the results with and without bilge keels obtaining mostly a similar ORI value. The 'lower' Pareto-front clearly shows the optimization with bilge keels being able to attain a higher ORI. Further inspection shows that both Pareto-frontiers are the result of design combinations with either high or low draught. Two examples for both optimizations are shown in table 8.9.

Table 8.9 shows that for both the results with deep draught and shallow draught, the solutions with bilge keels perform slightly better. This is seen by a minor improvement in the ORI value. However, given the major improvement in roll damping value, the increase in ORI is expected to be higher. Upon closer inspection of the roll RAOs, it becomes clear why the improvements in ORI are relatively minor compared to the substantial increase in critical roll damping. See figure 8.11, for the different roll RAOs, as well as the wave statistics of the North Sea.

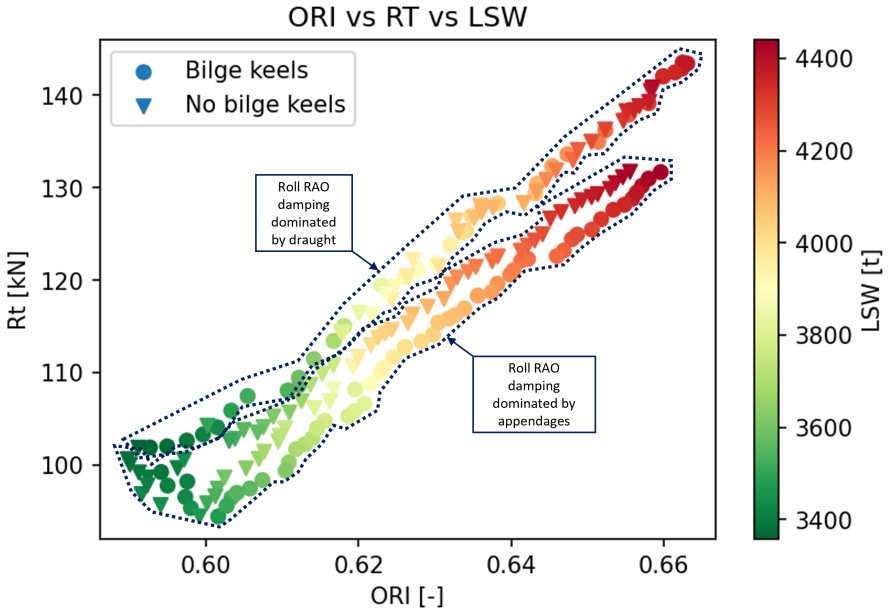

Figure 8.10: Comparison bilge keels and no bilge keels optimization results

Pareto-optimal solutions with, and without bilge keels						
Variables	*Symbol*	*Value*	*Value*	*Value*	*Value*	*Unit*
Pareto-optimal solution	–	**With bilge keels shallow draught**	**Without bilge keels shallow draught**	**With bilge keels deep draught**	**Without bilge keels deep draught**	–
Draught	D	4.50	4.50	8.00	8.00	m
Length aftship	L_{afts}	30.0	30.0	30.0	30.0	m
Length midship	L_{mids}	10.0	10.0	29.8	24.4	m
Length forwardship	L_{fwds}	50.0	50.0	30.2	35.6	m
Beam	B	25.3	25.3	25.2	25.7	m
Metacentric height	GM_T	2.00	2.00	2.00	2.08	m
Critical roll damping	RLD	5.69	1	6.20	1	%
ORI	ORI	0.602	0.599	0.663	0.659	–
Lightship weight	LSW	3470	3470	4380	4410	t
Ship resistance	R_T	94.4	94.4	143	141	kN

Table 8.9: Comparison of Pareto-optimal solutions with, and without bilge keels

Figure 8.11 shows both solutions without bilge keels have a significant influence on the roll peak value. Thereby, the shallow vessel is shown the have the highest roll peak value, which is to be expected due to the lower damping effects associated with a decreased draught. The addition of bilge keels significantly reduces the peak due to increased damping, which is expected (see also section 4.4.2). The vessel with a higher draught has a lower roll peak value, although only slightly. The damping of the roll RAOs is dominated by the increased added mass effect of the deeper draught. When compared to the North Sea wave statistics, the roll peaks lie substantially out of the range of occurring waves. However, it is observed that the vessels without bilge keels have a slightly higher RAO value in this frequency range ($0.46 - 1.00[rad/s]$). Hence, a slight reduction in ORI is present for these vessels.

In table 8.9, it is also seen that the framework steered towards an increase in midship length, thereby increasing the bilge keel length and subsequent roll damping value, for the vessel with bilge keels and a deep draught.

It is concluded that bilge keels do in fact allow better motion behavior. However, depending on the area of operation (and subsequent wave statistics), as well as the natural roll frequency, the benefits may only be minor. Regardless, the framework is able to effectively incorporate the effects of bilge keels.

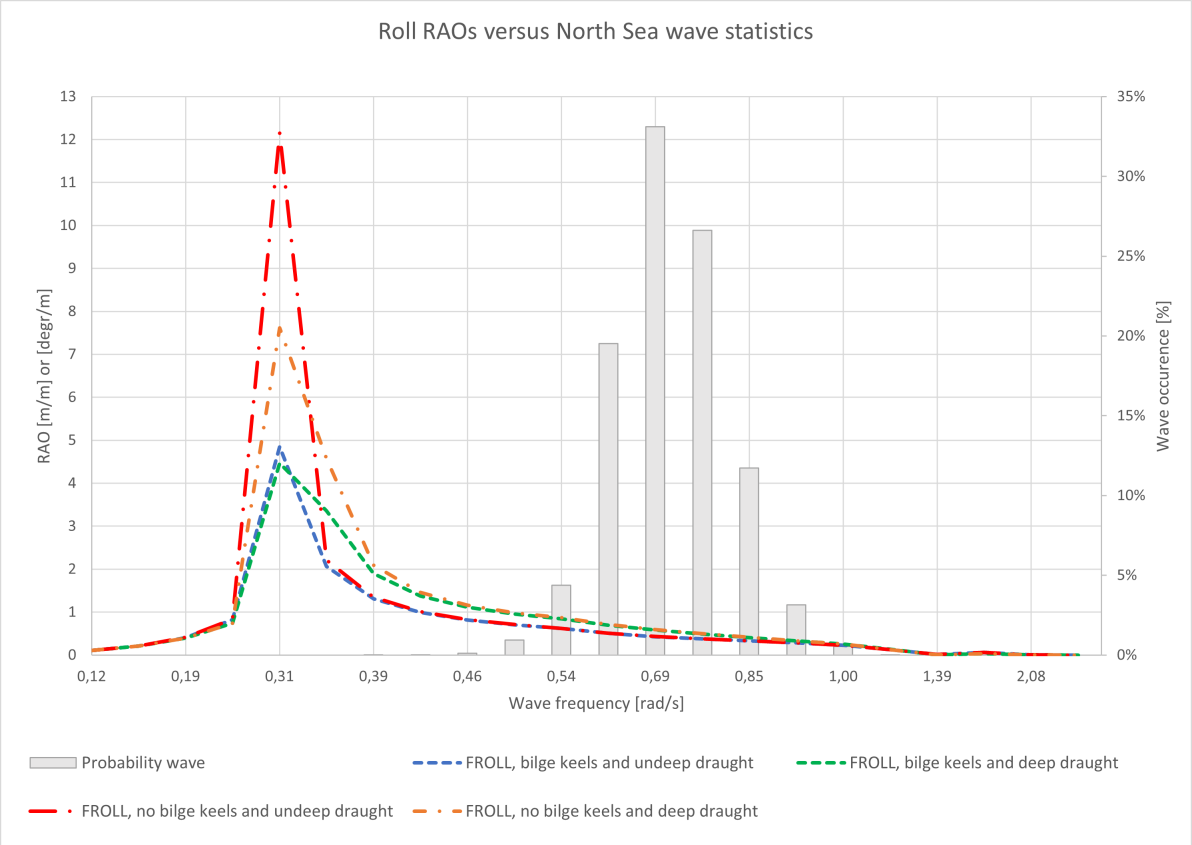

Figure 8.11: Comparison of roll RAOs for vessels with, and without bilge keels (see also table 8.9)

- **Motion sensitive equipment criteria**

  The motion limits directly influence the final ORI value. This is proven by calculating two motion limit cases for the base US Wind Feeder vessel. A calculation for the motion limits as given in the prior section, that is, to test the bilge keels, have been compared to the result for motion limits of the Ampelmann platform. The incoming wave angle α_{RAO}, has been set to $90[°]$. The ORI for the Ampelmann platform is $0.655[-]$. The percentage operability is 0.972%. The ORI for the roll limits is $0.781[-]$, with a percentage operability of 0.971%. In part, this is due the motion 'failure mode' of both motion limit cases being different. These are plotted in figures 8.12 and 8.13.

  Both figures show the motion failure mode per percentage of motion limit and wave peak period. The ORI is calculated by integrating from 0% of the motion limit, till the full limit, at 100%. Hence, for each wave peak period and per percentage, it is determined which limit fails. Comparing both plots shows significantly different motion failure mode behavior. For the Ampelmann platform, the failure mode varies between sway and roll. As expected, the roll limits lead to failure modes surrounding roll. Hence, the ORI for the Ampelmann platform is mostly based on heave and sway RAOs, whereas, for the roll limit, the ORI is determined by the roll RAO. In an optimization case, this may lead to different optimal vessel designs.

- **Area of operation**

  The area of operation is defined using wave statistics, which change per area (see appendix C). An optimization has been run for area 4 (Norwegian Sea), 23 (North Atlantic) and 28 (East China Sea). These areas differ in the peak period as seen by figure 8.14.

  These areas differentiate in input to the scatter diagram and wave spectrum which are calculated according to the procedure in appendix C. Other than the area, the same input settings have been used as shown in table 8.1. Each optimization has been run for 200 iterations. The Pareto-optimal solutions are shown in figure 8.15.

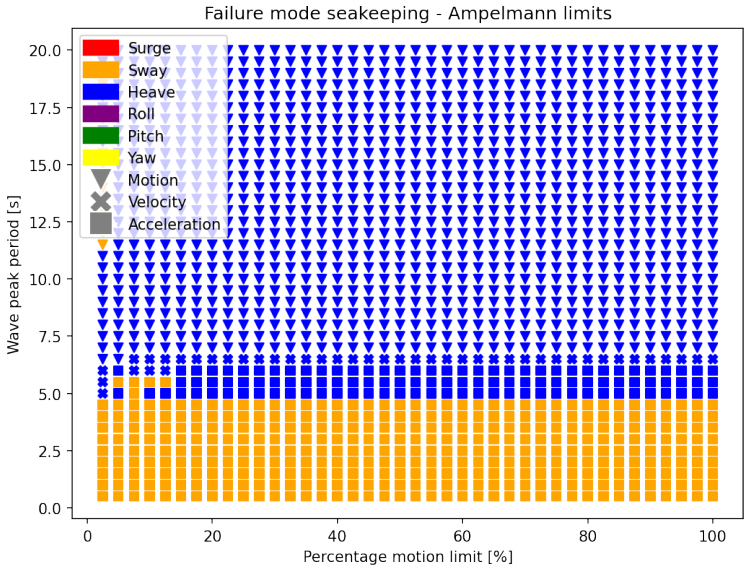

Figure 8.12: Motion failure modes for US Wind Feeder Ampelmann motion limits

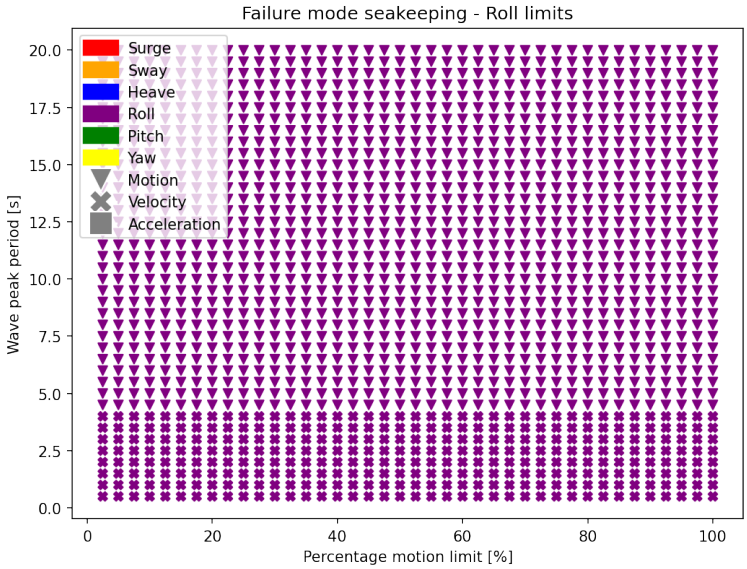

Figure 8.13: Motion failure modes for US Wind Feeder with only roll motion limits

Figure 8.15 shows that the different areas lead to substantially different ORI values. Specifically, it is shown that area 4 shows the lowest values for the ORI, area 28 the highest, with area 23 in-between. When compared to the probability of waves occurring at a certain peak period, the conclusion is made that a high average peak period (and subsequent low wave frequency) leads to a lower ORI value and subsequent lower seakeeping performance. The best performing vessels of each area are shown in table 8.10. It should be noted that the maximum possible length following the input settings (see table 8.1) may fall in a range leading to sub-optimal ORI values. Figure 8.2 sees vessels with high ORI values occur at specific lengths. The upper range of this length may not be achieved on the given boundaries, thus only smaller optimal results are shown in the Pareto-front. Subsequently, there may be vessel variable combinations able to attain a high ORI for area 4 or 23, that are not shown on the Pareto-front of the optimizations.

Table 8.10 shows that the optimization steers towards vessels with the shortest length possible. When considering the findings in section 8.1.1, and figure 8.3, the conclusion is made the optimization steers vessel RAOs outside the range of typical wave periods. Area 4 is characterized

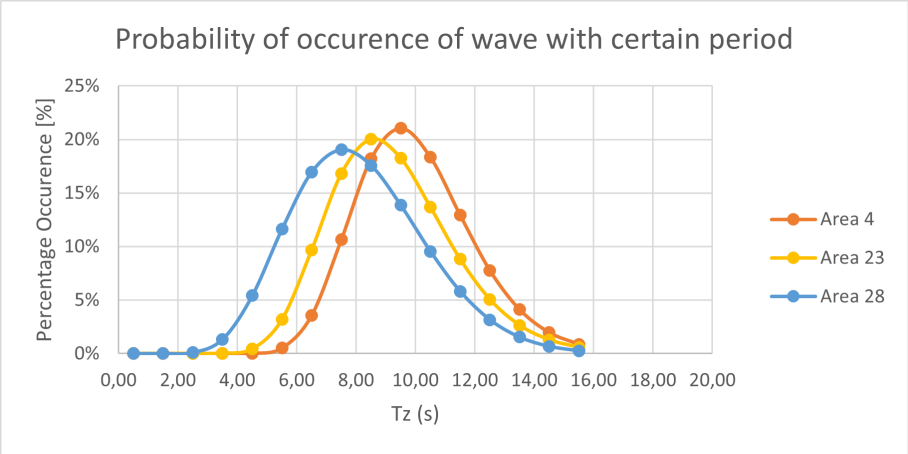

Figure 8.14: Probability of occurrence of waves of certain peak period in different areas [90]

.

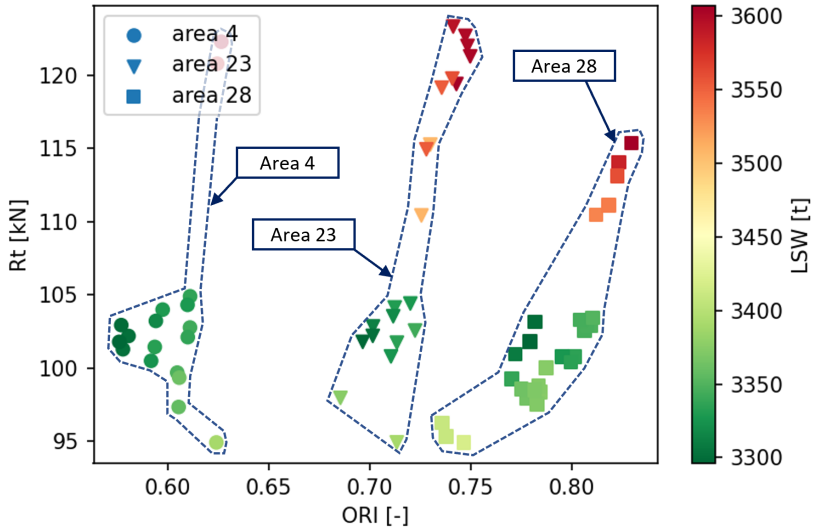

Figure 8.15: Pareto-frontier for optimization runs in different oceanic areas

Optimal results for different areas					
Variable	*Symbol*	*Value*	*Value*	*Value*	*Unit*
Area	-	**4**	**23**	**28**	-
Aftship length	L_{afts}	30.0	31.3	30.0	m
Midship length	L_{mids}	24.9	22.3	23.0	m
Forwardship length	L_{fwds}	35.1	36.4	37.0	m
Beam	B	22.8	22.8	23.07	m
Draught	T	6.5	6.5	5.89	m
Metacentric height	GM_T	2.0	2.0	2.0	m
Percentage operability	$PercOp$	88.4	95.2	98.3	%
ORI	ORI	0.63	0.75	0.83	–

Table 8.10: Optimization results for different oceanic areas

by waves with comparatively high wave periods and low wave frequencies. Figure 8.3 showed that for smaller vessels, the framework 'steers' RAO's to have a low natural frequency. For area

4, this frequency peak may still partially coincide with the frequency of the encountered waves, resulting in more motion excitation and a lower ORI.

8.3. Verification of optimization

8.3.1. General verification

In general, the optimization runs as expected. An individual iteration takes approximately 10 seconds to be completed on a desktop with an Intel Xeon Processor E3-1245 v3 quad-core processor with $16[GB]$ of working memory. Once the algorithm obtains data, the run-time is increased due to data processing of an increasing data set. 200 iterations take approximately one and a half hours to complete. 300 iterations take approximately three and a half hours. Additionally, certain verifications of convergence have been carried out. These will be discussed in the section.

8.3.2. Verification of convergence

- **Results with same initial sample**

  The optimization has been running twice for an identical optimization case. Both optimizations show the same progression and result.

- **Convergence check by Hypervolume**

  To determine the number of iterations required, the optimization has been run with 400 iterations using the optimization input as shown in table 8.1. The subsequent progression of the hypervolume is plotted in figure 8.16.

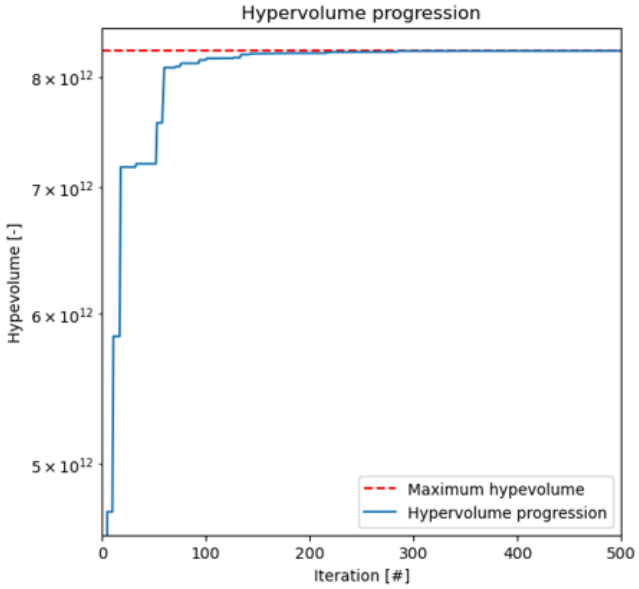

Figure 8.16: Hypervolume progression throughout optimization run

Figure 8.16 shows that the hypervolume converges to an asymptote after approximately 300 iterations. Hence, for a full optimization study, 300 iterations should be sufficient to determine Pareto-frontier. It is also seen that after 200 iterations the hypervolume is nearing the asymptote, hence for quick optimization 200 iterations is adequate. In a constrained design space, the Pareto-frontier may be found even more quickly, as the possible design combinations are simply more limited.

- **Results with different initial samples**

  The SAMO-COBRA optimization algorithm finds design solutions converging to the Pareto-frontier. To do so, any optimization is begun with the initial sample size. This sample size is a set of design variables chosen based on a random number sequence, and provides the algorithm with a data set to 'learn'. The set of variables is chosen based on a 'seed' of random numbers. If global optimal solutions are found, each optimization run should result in the same Pareto-frontier, regardless of the initial data set. To test the convergence of the optimization, the algorithm is run with three different seeds, each with a different random set of numbers. The resulting hypervolume progression is shown in figure 8.17.

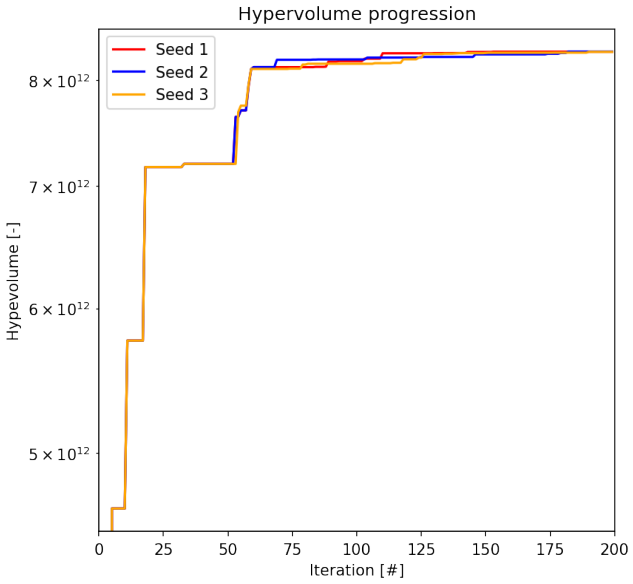

Figure 8.17: Comparison of hypervolume progression for runs with different seeds

Figure 8.17 convergence to roughly the same Pareto-frontier for each of the different seeds. Hence, it is concluded that the optimization is able to converge to a global optimum.

8.4. Summary and discussion of results

This chapter answers part of the research question *'How can the new framework be verified and validated?'*, verifying the framework as a result. Specifically, for the seakeeping assessment, the computation of RAOs was found to be sufficiently accurate. The resulting design solutions and corresponding seakeeping properties were found to be sensible. The estimation of lightship weight and initial stability was found to be reasonable, considering the typical uncertainty during concept design. The ship resistance estimation method, Holltrop & Mennen, is sufficiently accurate for conventional hull shapes that fall within its application range. For extreme OSV designs with a small L/B, the method becomes inaccurate and provides more of a relative measure between different designs. The station keeping force estimate is based on empirical methods and provides a relative measure to differentiate between vessels.

A sensitivity study shows the expected correlations between variables and KPI's. Additionally, the effect of design input is as expected. The optimization shows convergence regardless of the initial sample size characteristics. Hence, the optimization framework has a good ability to find Pareto-frontiers. Additionally, it has been found that approximately 300 iterations are needed to find the full Pareto-frontier of any design study.

To conclude, the optimization framework shows a good ability to find optimal design solutions during concept design. Typically uncertainty during concept design still applies and should be considered during application.

To demonstrate the application of the model, and validate the framework, a case study is performed in the next chapter.

9

Model validation

This chapter applies the framework to a case study, following a real-world design problem. Thereby, this chapter aims to validate the model and answer part of the research question *'How can the new framework be verified and validated?'*. Furthermore, the case study serves to determine whether the framework forms an effective design tool for concept design. Additionally, this chapter provides an initial answer to the primary research question *'How can concept design framework involving seakeeping improve the design of OSVs?'*.

The vessel used for the cases study is the 'US Wind Feeder', which will be introduced in section 9.1. The optimization set-up is discussed in section 9.2. The results are discussed in section 9.3. Finally, the chapter is ended with a brief conclusion and summary in section 9.4.

9.1. Case study vessel introduction and design philosophy

Figure 9.1: US Wind Feeder concept design by C-Job [10]

The 'US Wind Feeder' is a vessel designed to support the construction and logistics of offshore wind farms in the United States. Specifically, the vessel allows for non-American wind turbine installation vessels (WTIV) to construct wind farms in compliance with the Jones Act [10]. Traditionally, a WTIV

would transport the components and then do the installation of the turbines. The Jones Act prohibits any foreign-built, foreign-owned, or foreign-flagged vessel from engaging in coastwise trade within the United States, such as the 'trade' of wind-turbine components [22]. Additionally, requiring the WTIV to sail between port and installation site for each turbine is considered an inefficient use of the vessel.

With the feeder concept, the turbine components are brought to the installation site by the feeder's vessel. With two or more vessels per project, this allows the WTIV to focus on the installation of the turbines and ensures operations can continue at all times.

The specialized 'wind feeder' OSV is designed with maximum operability in mind, whilst being relatively compact to minimize construction and operational costs. To maximize operability, the vessel features a motion compensated platform design by Ampelmann. The compensator is positioned close to the vessel's center where it compensates vessel motions to allow for continued operations – even in adverse weather conditions – throughout the year. The primary design driver for this vessel is seakeeping. The design directive is to maximize operability, thereby realizing a continuous supply of turbine components to the WTIV. The second design driver is costs- both CAPEX and OPEX. The vessel is part of a new business case proposing that maximizing WTIV's installation capability minimizes the building costs of a wind farm. Subsequently, the vessel's CAPEX -linked with the lightship weight - is a critical component. Additionally, the CAPEX is interlinked with seakeeping performance. The Ampelmann platform forms a significant portion of the CAPEX - around 20% in the current concept - to realize high operability. Better seakeeping capabilities, lead to lesser requirements for the Ampelmann, improving its CAPEX. The ship's resistance is of lesser concern, as the wind farm site is close to shore. The station-keeping force does not form an objective, but rather input to dimensioning the DP system.

Based on the vessel's design philosophy, input to the optimization has been determined, which is given in the next section.

9.2. Optimization input

The optimization input has been determined together with C-Job naval architects. An overview of the most important input parameters is given in E.3. Other input parameters are further deliberated in appendix E. The two loading conditions have further been deliberated in table 8.5 in chapter 8. Three motion limit cases have been applied. Motion limit case 1 concerns the motion compensated Ampelmann platform. Motion limit case 2 concerns the risk of a turbine blade tip touching the water, which imposes a heave limit. Motion limit case 3 concerns a maximum amount of blade accelerations, which the turbine blade can sustain. An overview is given in figure 9.2. The corresponding exact limits and location are given in table 9.2.

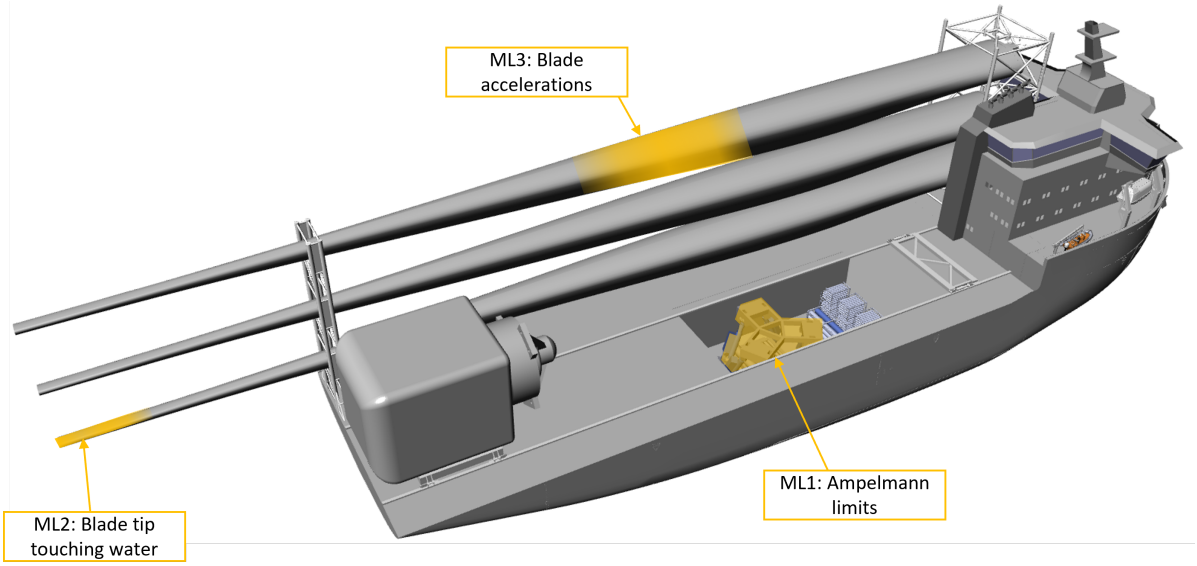

Figure 9.2: Motion limit cases of US Wind Feeder

Performance in three objectives has been optimized. Specifically, the ORI, lightship weight, and ship

resistance. The station keeping force of each iteration is recorded, though not optimized on, as it does not form a primary objective for this vessel. Additionally, minimizing the number of objectives reduces computing time. To calculate the RAOs, a radius is generated for roll, K_{xx}. This K_{xx} is calculated by $K_{xx} = 0.4875B$, based on current concept weight distribution of the US Wind Feeder. The GM_T was required to be at least $2.0[m]$ to ensure stability and feasibility. Fitting the turbine blades required a minimum length of $90[m]$. Hence, the objective and constraint functions applied where:

$$\begin{aligned} &Objectives: \\ &max(ORI) \\ &min(LSW) \\ &min(SR) \\ &Constraints: \\ &GM_T > 2[m] \\ &L_{PP} > 90[m] \end{aligned} \tag{9.1}$$

Optimization settings

Input

Input	*Symbol*	*Setting/specification/value*	*Unit*
Area	-	23, North Atlantic Ocean, East Coast USA	-
Hull shape	-	US Wind Feeder concept	-
Angle incoming waves	α_{RAO}	30.0	°
Motion sensitive equipment	-	Case 1: Ampelmann platform, near CoB Case 2: Lifting operation Case 3: End of blade tip	-
Loading condition	-	Condition 1: Maximum loading condition Condition 2: Lifting last item	-

Variables

Variables	*Symbol*	*Lower limit*	*Upper limit*	*Unit*
Aftship length	L_{afts}	30.0	50.0	m
Midship length	L_{mids}	10.0	40.0	m
Forwardship length	L_{fwds}	30.0	50.0	m
Beam	B	17.0	28.0	m
Draught	T	4.5	7.5	m

Constraints

Constraints	*Symbol*	*Lower limit*	*Upper limit*	*Unit*
Metacentric height	GM_T	2.0	-	m
Total length	L_{tot}	90.0	-	%

Objectives

Objectives	*Symbol*	*Unit*
ORI	ORI	–
lightship weight	LSW	t
Ship resistance	SR	kN

Algorithm settings

Item	*Setting*	*Unit*
Algorithm	SAMOCOBRA	–
Maximum iterations	300	#

Table 9.1: Optimization settings

Results of optimization for US Wind Feeder concept - critical condition							
Variables	*Symbol*	*Motion limit case*					*Unit*
Solution	–	**Ampelmann platform**			**Blade tip**	**Blade accelerations**	–
Longitudinal location	X	-10.402			-70	-11	m
Transverse location	Y	-2.5			10	10	m
Height	Z	6.3			7	10	m
Type of motion	-	Motion	Velocity	Acceleration	Motion	Acceleration	-
Surge	x	1.17	0.9	0.69	-	3.92	m,m/s,m/s^2
Sway	y	1.17	0.9	0.69	-	7.55	m,m/s,m/s^2
Heave	z	1.25	1	0.89	6.7	17.36	m,m/s,m/s^2
Roll	ϕ	5	4	3	-	-	$°$,$°/s$,$°/s^2$
Pitch	θ	5	4	3	-	-	$°$,$°/s$,$°/s^2$
Yaw	ψ	20	20	20	-	-	$°$,$°/s$,$°/s^2$

Table 9.2: Motion limit cases for US Wind Feeder optimization

Six optimizations for 300 iterations have been run, for each combination of motion criteria and loading condition. Each optimization took approximately three and a half hours to complete on a desktop with an Intel Xeon Processor E3-1245 v3 quad-core processor with $16[GB]$ of working memory. The results are shown in the next section.

9.3. Results

9.3.1. General results

Six optimization runs have been completed, each varying in either motion limit case or loading condition. The Pareto-frontier has been found for all optimization runs as seen by the progression in hypervolumes in figure 9.3, which all converge to an asymptote.

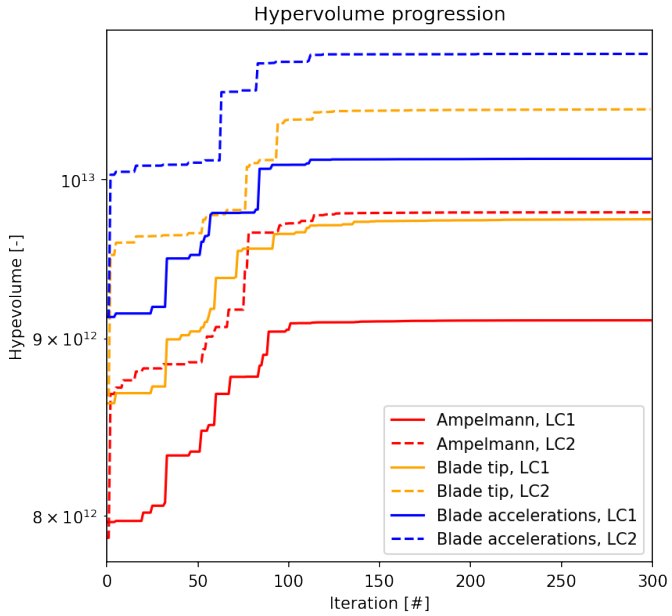

Figure 9.3: Hypervolume progression for six case study optimization runs

Figure 9.3 shows that each optimization case leads to a different converged asymptote. As described in subsection 7.3.4, a higher hypervolume implies higher attainable objective scores. Hence, Ampelmann limits in combination with loading condition one impose the largest impact on attainable performance. This is further confirmed when comparing the obtained Pareto-frontiers the different motion limit cases and loading conditions, which are plotted in figure 9.4.

Figure 9.4 shows that the motion limits based on the blade accelerations allow for an ORI value that almost always exceeds $0.95[-]$. Blade tip motion limits form a more limiting criterion, though the limits

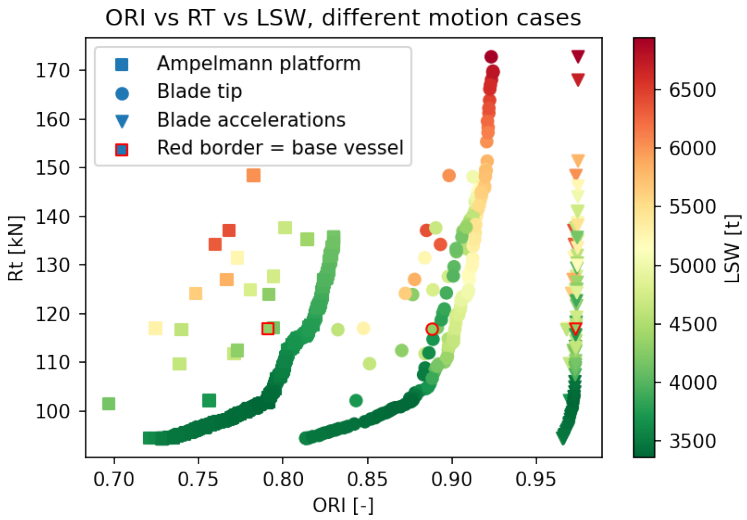

Figure 9.4: Optimization results for different motion limit cases

surrounding the Ampelmann platform appear to be the most stringent. All three results show broadly similar trends in ship resistance versus lightship weight on the Pareto-frontier, as well as the maximum attainable lightship weight. Hence, the motion limits influence the attainable ORI value, whereby for the US Wind Feeder, the limits surrounding the Ampelmann platform are most critical. Therefore, the case study will be continued optimizing for the Ampelmann motion limits.

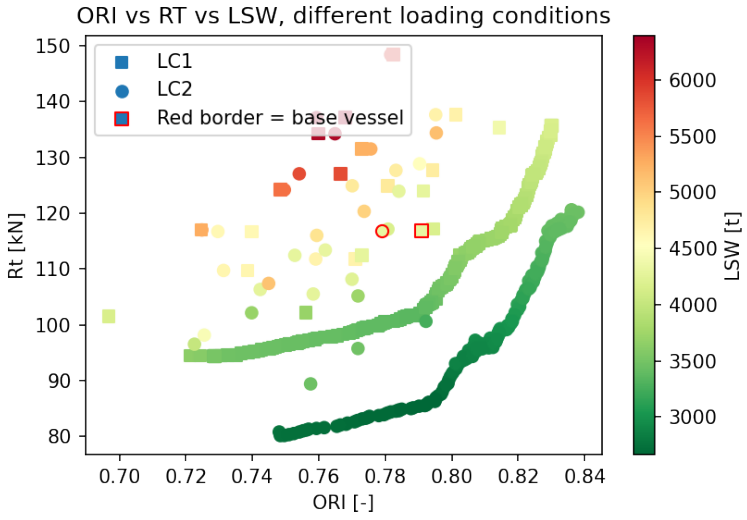

Figure 9.5: Optimization results for different loading conditions, with Ampelmann motion limits.

The effect of the two loading conditions (LC1 and LC2) becomes apparent when comparing the corresponding Pareto-frontiers in figure 9.5. Figure 9.5 shows LC2 allows for lower ship resistance and slightly lower lightship weight, whilst maintaining the same ORI value compared to that of LC1. Interestingly, it is also seen that the base vessel will have a lower ORI value for LC2 than for LC1, which contrasts the differences in both Pareto-frontiers. To explain these results, the primary effect of changing loading conditions should be considered. The loading condition significantly influences the vertical center of gravity of the vessel. LC1 features a high deck load at relatively high VcG. If the draught is kept the same throughout the lifting operation, KM_T remains the same, whilst the ship's VcG lowers and GM_T (see equation 7.10) increases. The sensitivity study in chapter 9, and thereby the correlation matrix depicted in figure 8.5, showed that a high GM_T typically corresponds with a lower

ORI. This explains why the base vessel has a lower ORI value for LC2. Additionally, the sensitivity study also showed that increasing the beam increases the GM_T, as KM_T is increased. Since LC2 has a lower VcG, KM_T may also be lower whilst still achieving the minimum GM_T constraint in the optimization. Hence, slenderer vessels are able to achieve the GM_T constraint. The correlation matrix (figure 8.5) saw a positive correlation between beam and ship resistance, hence the slenderer ships have a lower ship resistance and the Pareto-frontier is shifted. These findings are further confirmed by comparing the main particulars versus GM_T for both optimizations.

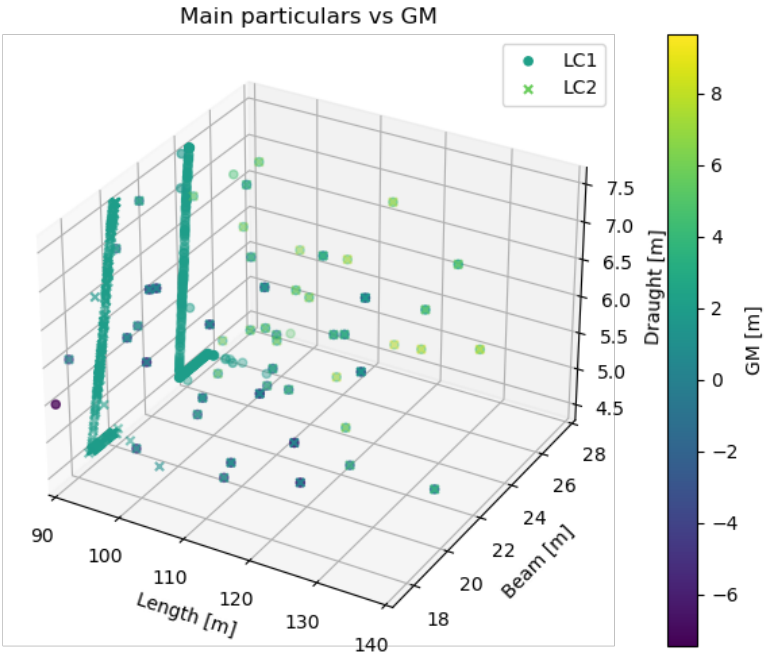

Figure 9.6: Main particulars versus GM_T for LC1 and LC2

In figure 9.6, it is observed that the GM_T constraint of $2[m]$ is satisfied for vessels at least 23 meters wide for LC1. For LC2, the GM_T constraint is satisfied by vessels around 19 meters wide. Critically, it should be considered that slenderer vessels do not satisfy the initial stability constraint for LC1. Hence, LC1 is the critical loading condition. Together with the motion limits of the Ampelmann platform, this forms the critical vessel condition. In the next section, the results for this vessel condition will be further deliberated.

9.3.2. Analysis on critical vessel condition

To determine what variables lead to feasible solutions and high objective scores, a parallel coordinate plot is plotted. The parallel coordinate plot shows show the objective and constraint scores of a certain set of variables. In figure 9.7, the parallel coordinate plot of the results of the US Wind Feeder in critical condition is shown. In this plot, variable combinations have been scaled according to the ORI value. In the list below, correlations between the KPI's and variables are discussed.

1. **Correlations between ORI value and variables**
   The resulting ORI value is seen to span anywhere between $0,75[-]$ and $0,85[-]$. All associated percentage operability values are quite high. A long aft ship and short forwardship, together with a high draught show to result in an ORI value. The higher ORI values are typically obtained for a shorter midship length, though high ORI values also exist for combinations with a long midship length. Some combinations with a longer aft ship also show to attain high ORI values. The overall length is shown to be between $90[m]$ and $105[m]$, indicating shorter vessels are able to attain a high ORI. The beam is adjusted to result in an initial GM_T of two, which allows for a high ORI value. Additionally, a higher block coefficient (C_B) corresponds to a high ORI value.
2. **Correlations between initial stability and variables**

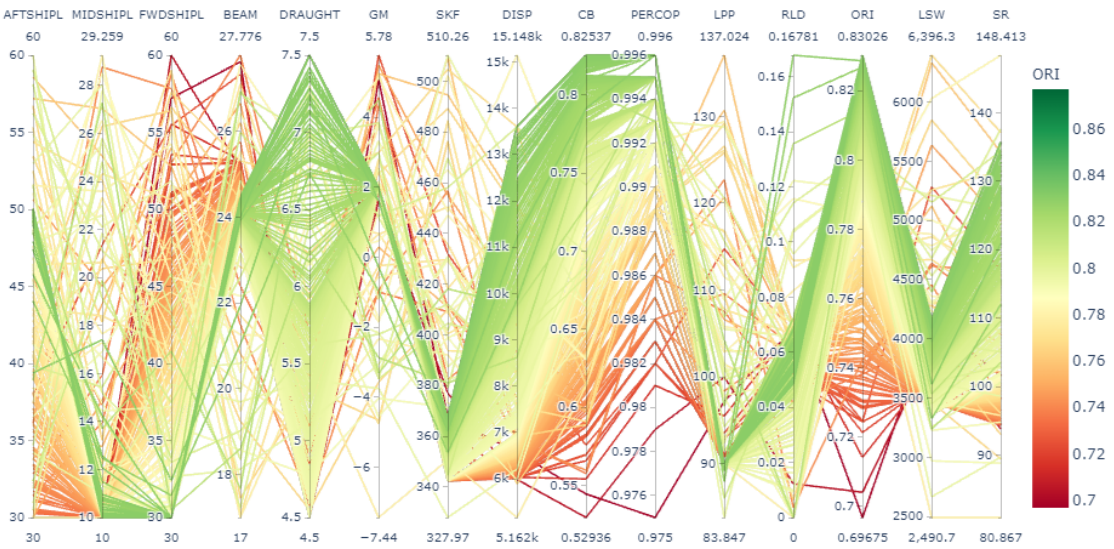

Figure 9.7: Parallel coordinate plot for US Wind Feeder case, LC1 and Ampelmann motion limits

It is clearly seen the optimization steers variable combinations towards a GM_T of $2[m]$, as this allows for a high ORI score. Consequently, this results in an inverse relationship between the draught and the beam. A slenderer beam requires the draught to be higher to satisfy the GM_T constraint, and vice versa.

3. **Correlations between lightship weight and variables**
   A direct and positive correlation exists between length, beam, draught, and block coefficient (see equation 7.6). This is seen in the parallel coordinate plot. Additionally, most of the results have an LSW between $3500[t]$ and $4300[t]$, which is likely due to the relative shortness of Pareto-optimal vessels. The vessels with a higher ORI are seen to have a higher lightship weight, due to having a higher draught and block coefficient, hence a trade-off exists between ship resistance and draught.
4. **Correlations between ship resistance and variables**
   The ship resistance is seen to vary between $95[kN]$ and $130[kN]$ for most results. A shorter aftship and longer forwardship lead to a lower ship Resistance. The draught is seen to have an inverse relationship with ship resistance. Vessels with a deeper draught may be slenderer whilst satisfying the GM_T, though it is not seen to result in a lower ship resistance. The adverse effects of a higher draught supersede the positive effects of a lower beam on ship resistance. The vessels with a higher ORI are seen to have a higher ship resistance, due to having a higher draught and block coefficient, hence a trade-off exists between ship resistance and ORI.
5. **Correlations between station keeping force and variables**
   The station keeping force is seen to vary between $350[kN]$ and $370[kN]$ for most results. The longer the length- and the higher the draught, the higher the station keeping force. An increase in the beam is shown to increase the station-keeping force. This is to be expected given the finding in chapter 7.

In general, the results for the objectives (including station keeping force) can be summarized to fall somewhere in the range as shown in table 9.3. The results show the range of attainable KPI values for the final concept. Rather the strength of the framework is to provide insight into the combination of variables resulting in 'optimal solutions', solutions that maximize performance into one objective for a certain value for another objective. These results are shown in a detailed Pareto-front in the next subsection. Additionally, these attainable values are compared to the current US Wind Feeder concept of C-Job.

Attainable objective values for US Wind Feeder concept				
Variables	*Symbol*	*Lower value*	*Upper value*	*Unit*
Operability robustness index	ORI	0.75	0.85	–
Lightship weight	LSW	3500	4300	t
Ship resistance	SR	95.0	130	kN
Station keeping force	SKF	350	370	kN

Table 9.3: Attainable objective values for US Wind Feeder concept

9.3.3. Comparison with base vessel

In figure 9.8, a detailed Pareto-front of the optimization case is depicted.

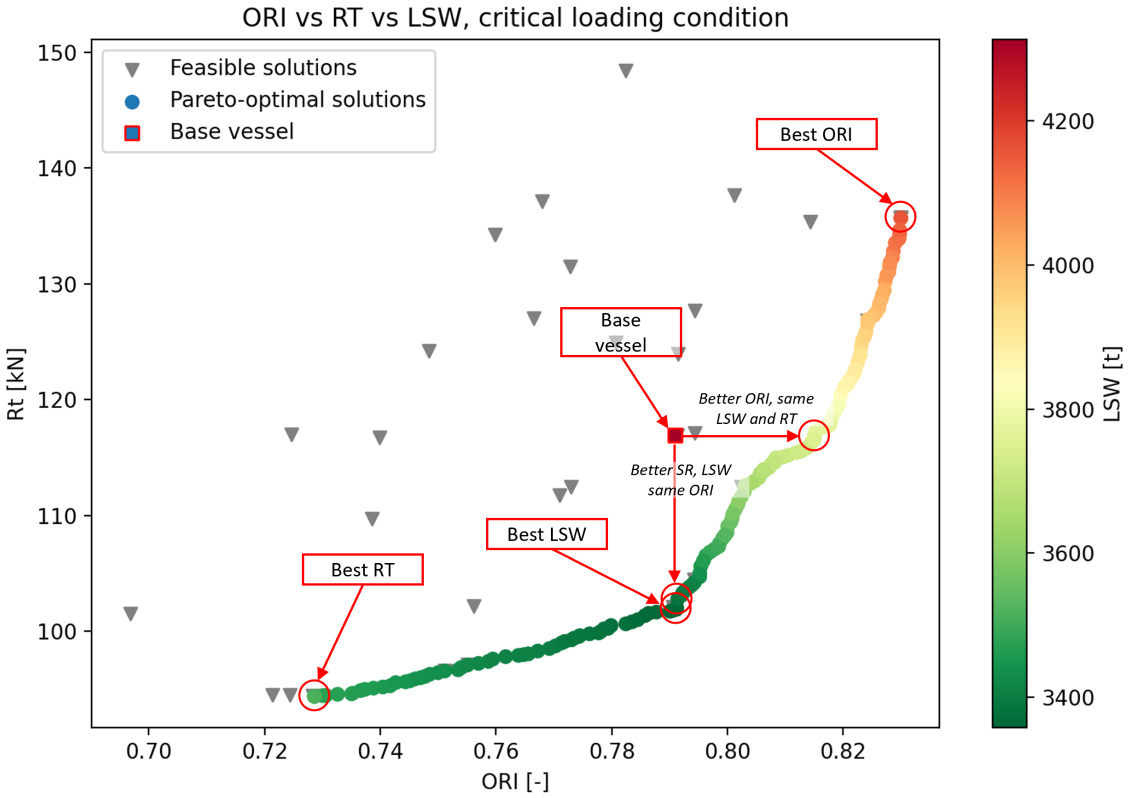

Figure 9.8: Detailed Pareto-frontier of case study, LC1 and Ampelmann motion limits

The Pareto-frontier can clearly be identified. When compared with the current concept design, annotated as 'base design', some significant improvements can be made. Firstly, all Pareto-optimal solutions show an improvement over the base design in lightship weight. Additionally, some Pareto-solutions show improvements in both ORI, ship resistance and lightship weight. Specifically, the solution with the same ORI but improving the ship resistance and lightship weight has been highlighted, as well as the solution with a similar ship resistance but improved ORI and lightship weight. The extremes of the Pareto-frontier are also annotated. The corresponding variables and KPI scores of these design solutions are further shown in table 9.4. To gain further insight into why a certain design combination leads to certain objective scores, the block coefficient is also shown. The percentage operability is given for each combination to provide a more tangible metric compared to the ORI parameter. Additionally, the percentage difference between the critical KPIs - ORI, lightship weight, and ship resistance, is also shown. The potential improvements are discussed per critical objective, as well as the subsequent trade-offs.

Results of optimization for US Wind Feeder concept - critical condition								
Variables	*Symbol*	*Value*	*Value*	*Value*	*Value*	*Value*	*Value*	*Unit*
Solution	–	**Base vessel**	**Same RT. better ORI and LSW**	**Same ORI. better RT and LSW**	**Best ORI**	**Best LSW**	**Best RT**	–
Aftship length	L_{afts}	46.00	50.00	49.25	49.80	50.00	30.00	m
Midship length	L_{mids}	23.00	10.00	10.4	10.20	10.00	10.00	m
Forwardship length	L_{fwds}	34.50	30.00	30.35	30.00	30.00	50.835	m
Beam	B	23.80	23.99	23.6	24.22	23.48	25.26	m
Draught	T	5.50	5.98	4.5	7.50	4.50	4.50	m
Block coefficient	C_B	0.72	0.78	0.72	0.83	0.73	0.58	–
Metacentric height	GM_T	2.18	2.00	2.00	2.00	2.00	2.00	m
Stationkeeping force	SKF	398.78	354.70	342.38	367.44	342.38	342.36	kN
Operability robustness index	ORI	0.791	0.815	0.791	0.830	0.791	0.729	–
Difference ORI w.r.t. base vessel	-	-	3.03	0.00	3.55	0.00	-7.84	%
Percentage Operability	$PercOp$	99.2	99.4	99.2	99.6	99.2	98.3	%
Lightship weight	LSW	4310	3760	3450	3880	3360	3510	t
Difference LSW w.r.t. base vessel	-	-	-12.76	-21.14	-9.98	-22.04	-18.56	%
Ship resistance	R_T	116.93	116.90	101.79	135.69	101.91	96.36	kN
Difference R_T w.r.t. base vessel	-	-	-0.03	-12.95	16.04	-12.85	-17.49	%

Table 9.4: Overview of specific results of optimization for US Wind Feeder case study

Below, improvements in objectives are further elaborated.

- **Improvements in ORI**

  The ORI shows to be improved up to 3.6%, depending on the combination of variables. The ORI is improved over the base vessel by increasing the aftship length, draught, and subsequently the block coefficient, thereby keeping GM_T at $2.0[m]$. The design solution with the highest ORI also shows a minor improvement in operability, namely 99.6% over 99.2% This does show that the base vessel should already allow for good year-round operability. The solutions offering the lowest lightship weight and ship resistance do so by minimizing draught. The vessel with the best ORI has an estimated lightship weight 16.0% than that of the base vessel. The vessel with the lowest ship resistance shows a decrease of -7.8% in ORI. Hence, a trade-off exists between lightship weight and ship resistance.

- **Improvements in lightship weight**

  The Pareto-optimal design solutions allow for a reduction in lightship weight between 12.8% and 22.0%. The framework results showed that shorter vessels (length = $90[m]$) are able to attain good seakeeping performance. Due to the shorter length, the lightship weight is also substantially decreased (see section 7.3.3 and equation 7.6). It should be noted that this substantial reduction is due to the length having a significant impact on the lightship weight due its relation in the quadricubic number formula. Possibly, the quadricubic number method overestimated the impact of length on lightship weight. Furthermore, the lightest solutions are characterized by a minimal draught and low block coefficient, further reducing the different terms in equation 7.6. Thereby, the lightship weight depends on variables similarly to the ship resistance, yet a trade-off exists between lightship weight and ORI.

- **Improvements in ship resistance**

  The Pareto-optimal design solutions allow for a reduction in ship resistance of up to 17.49%. These solutions achieve a lower ship resistance due to a shorter length, and subsequently lower frictional ship resistance. Additionally, it is that a reduction in block coefficient and draught, a typical indication of a finer hull shape, further reduces ship resistance. The opposite holds true for the ORI, as the vessel with the highest ORI value shows a reduction in ship resistance compared to the base vessel. Hence, on the Pareto-front, a trade-off occurs between ship resistance and seakeeping.

The findings discussed above clearly show how the framework is able to efficiently explore the design space to find optimal design solutions. In doing so, and thereby providing the Pareto-front, the

naval architect is provided with tons of useful design information. The base design, created with much deliberation by expert Naval Architects, shows the difficulty of designing a concept that maximizes performance in either one objective. This lead to an over-dimensioned vessel design in an effort to guarantee seakeeping performance.

9.3.4. Improvements regarding design philosophy

The improvements in individual objectives contribute to the vessel's design philosophy in multiple ways. Regardless of ORI, all vessels show percentage operability between may be overestimated due an overestimation in roll damping (see section 8.1), it does show that the Ampelmann has been designed with *maximum* operability in mind. By optimizing on the ORI parameter, *robustness* in seakeeping performance is maximized. Vessels with a high ORI value show the potential to be fitted with smaller Ampelmann platforms whilst maintaining high operability. In an effort to further rationalize the decrease in ORI, the limits of the motion compensated platform have been scaled on the vessel with the highest ORI. Thereby, the limits have been scaled to achieve the same ORI or percentage operability as the base vessel. The limits have been scaled linearly. These results are shown in table 9.5.

Results of optimization for US Wind Feeder concept - critical condition					
Variables	*Symbol*	*Value*	*Value*	*Value*	*Unit*
Solution	–	**Base vessel**	**Same ORI**	**Same PercOp**	–
Percentage scaling motion limits	–	–	80%	86%	%
Operability robustness index	ORI	0.791	0.791	0.803	–
Percentage Operability	$PercOp$	99.2	98.8	99.2	%

Table 9.5: Allowable reduction in motion limits of vessel (see table 9.2) with best seakeeping performance (see table 9.4) whilst maintaining either ORI or percentage operability

In table 9.5, it is shown the motion limits can be reduced by 80% whilst maintaining the ORI value, or 86% whilst maintaining the percentage operability. By reducing the tolerable motion limits, the Ampelmann can be downsized, as well as supporting hydraulic equipment. Thereby, both the CAPEX and the OPEX of the motion compensated equipment are reduced. It should be noted that it is difficult to estimate exactly how much this reduction in CAPEX or OPEX is, without input from Ampelmann. However, it does show that the CAPEX of the vessel is minimized at minimal expense to the operability of the vessel. Furthermore, the framework demonstrates that smaller vessels can indeed achieve high operability. The framework presents options with minimal draught or beam while satisfying stability constraints, showing the vessel combinations with minimal lightship weight possible and ship resistance with minimal expense to seakeeping performance.

Although ship resistance, nor station keeping force is a critical design driver in this specific use case, the results do allow Naval Architects, or a client, to evaluate the exact trade-off between the related OPEX, and CAPEX. By presenting this information to the Naval Architect and the client, the design philosophy can be further refined.

For this case study, a specific design solution has not been chosen to be 'better than the base vessel. This requires further investigation together with the client, Ampelmann and C-Job. Yet the objective scores of the Pareto-optimal solutions clearly show that the performance of the base vessel can be improved.

9.4. Conclusion and summary

Validating the framework tested its functionality and added value for concept design. Thereby, the main research question, *How can a new concept design framework incorporating seakeeping improve the design of offshore service vessels?*, is answered. The framework proved capable of evaluating and optimizing a substantial number of OSV designs in a short amount of time. It is able to find the best performing OSVs, maximizing performance regarding specific design drivers, while ensuring feasibility by stability requirements. The final result is a set of designs on a Pareto-front maximizing the performance in each objective and the design problem's trade-offs. Thereby, the framework provides naval architects with the information required to make an optimal design direction.

This notion is further proven by the comparison study with the US Wind Feeder concept. The framework was able to find significant improvements in the design compared to the base vessel. Specifically, the base vessel was shown to be over-dimensioned for its purpose. Smaller vessels, which maintain or improve on seakeeping performance, showed a possible reduction in lightship weight of 21%, and the ship resistance reduced up to 13%. These improvements translate to a direct reduction in CAPEX and OPEX. The seakeeping performance can be improved allowing for more stringent motion limits of up to 14%, thereby reducing the CAPEX and OPEX of the Ampelmann platform.

The conclusions are further discussed from a more general perspective in chapter 10.

10

Discussion, recommendations and conclusion

This chapter draws to a final conclusion of this thesis. To do so, section 10.1 discusses the answers to each sub-research question and the main research question. The contributions to academia and science are elaborated in section 10.2. Recommendations are given in 10.3. Based on the (discussion of-) answers, contributions and recommendations, a final conclusion of this thesis is drawn in section 10.4. Finally, this chapter, and the thesis, are ended with a brief personal reflection in section 10.5.

10.1. Discussion

10.1.1. Research sub-questions

1. **Why is motion behavior an important characteristic of offshore service vessels?**

   This thesis is the product of a need by the industry to improve concept design methods for OSVs, specifically to effectively incorporate seakeeping. Many new types of OSVs define their function by having motion compensated equipment and/or cranes. These systems are subject to motion limits, hence motion behavior heavily dictates the performance of these vessels. Specifically, both factors determine the operability of a vessel- how often a vessel is to operate in a certain area over a certain time frame. Thereby, the seakeeping is directly linked with the operational effectiveness of many OSVs.

   The case study showed another dimension to the importance of seakeeping. Motion compensated equipment can be designed to allow for high operability, even on vessels with sub-optimal motion behavior. The drawback thereby is that the motion sensitive equipment significantly increases purchase costs and required operating costs. By improving on seakeeping performance, more sensitive systems may still function with high operability. Thereby, the demands on hydraulic systems, CAPEX, and OPEX decrease.

   Based on these findings, it can be concluded that vessel seakeeping is an important characteristic for OSVs, and even forms a critical design driver for specific vessel types, whereby the performance is highly dependant on the performance of motion sensitive equipment.

2. **What is the state-of-the-art of concept design frameworks?**

   The increase in computing power has allowed for new novel concept design methods enabling naval architects to develop higher performing vessel designs. Some of these methods serve to better evaluate a vessel design against certain missions. Other methods serve to efficiently explore a design space in a short amount of time and are often called 'Holistic' design methods. An example of the latter is C-Job's ACD method. ACD shows potential to be developed into an effective design method whereby seakeeping is considered.

3. **What are the main design drivers of offshore service vessels?**

Based on the experience of naval architects at C-Job, primary design drivers for offshore service vessels are:

- Required mission systems
- Motion characteristics
- Cost
- Lead time
- Station keeping
- Ship resistance

These design drivers are specific to C-Job, though they are considered to be important for all OSVs. For very specific OSVs, such as ice-breaker vessels, the most critical design drivers may be different. It should be considered that implementing the aforementioned design drivers into a framework allows for application in more general OSVs. For very specific OSVs other design drivers may be applicable or governing.

4. **What is the current state-of-the-art in design optimization for ship motion characteristics?**

   Some concept design methods have been developed which involve seakeeping, but with significant simplifications to the parametric model and seakeeping evaluation method. These methods served mostly to globally determine good design solutions, but not synthesize a particular optimal vessel design. For instance, these methods lack the ability to evaluate a specific hull shape on percentage operability (- or ORI). To effectively consider seakeeping for a to-be-designed vessel, the design method needs sufficiently high fidelity, both in the evaluation method as in parametric model. No academically published method considered both to such an extent.

5. **What are the requirements for a concept design framework involving seakeeping?**

   Based on the findings in research questions one and three, requirements for an effective concept design framework have been determined. Design drivers have been translated to optimization objectives. Variable requirements have been determined to establish a design framework with adequate fidelity. Additionally, experiment input and feasibility constraints have been determined. The resultant requirements of the design framework were:

   - **Framework components**
     - *Input*
       - Area of operation
       - Specification of motion sensitive equipment
     - *Variables*
       - Hull shape
     - *Objectives*
       - Operability Robustness Index (ORI)
         The ORI is a robust measure for seakeeping performance. It considers the area of operation, vessel motion criteria, and motion behavior.
       - Lightship weight
         A direct relationship exists between lightship weight and building costs as well as building complexity. Hence, it forms a good KPI during concept design to evaluate these design drivers.
       - Ship resistance
         The ship resistance is a direct KPI for the fuel costs of the vessel.
       - Station keeping force
         The station keeping force forms a KPI to indicate the DP capability of the vessel.
     - *Constraints*
       - Initial stability
         The initial stability is an important measure for the feasibility of a concept design, hence it is required as a constraint in the framework.

    - ◊ Global dimensions
      The global dimensions of the vessel can be constraint within a boundary to ensure sufficient space for mission systems.
  - *Optimization algorithm*
    To complete the holistic design framework, an optimization algorithm should be employed.
- **Specific framework requirements**
  - Bilge keels
    Bilge keels form an effective measure at reducing roll motions. The effectiveness of a bilge keel is partially dependant on the hull shape. As such, bilge keels should be considered in the framework.
  - Loading conditions
    The loading condition forms a significant factor in the feasibility of a vessel, more specifically the ability to satisfy an initial stability constraint. Hence, loading conditions should be implemented in the framework.

6. **How is a concept design framework incorporating motion characteristics developed?**

   The ACD method comprises an efficient optimization algorithm and a design environment in the software NAPA. The design environment enables the development of a design framework in which a parametric vessel is evaluated on various objectives and constraints. Based on the aforementioned requirements, a design framework has been developed. This framework takes the following form:

   Critically, the hull shape variable is decomposed into varying the main particulars and length of hull sections of a base hull shape. Though not allowing for finer modification of a hull shape, it does allow for finding optimal configurations of a base hull design/philosophy. This method allows for sufficient concept design fidelity for more conventional OSV hull shapes.

7. **How can the new framework be verified and validated?**

   To answer this question, multiple tests have been carried out. Each element in the final framework has been verified by either a sensitivity study or benchmarked. The framework has been validated by application on a C-Job OSV concept that is currently in development. The validation study saw the framework effectively explore the design space, indicate trade-offs in the design, and propose design solutions over the base concept.

10.1.2. Main research question

Answering the research sub-questions built an answer to the main research question,

How can concept design framework involving seakeeping improve the design of OSVs?

A bespoke design framework has been developed to aid the naval architect during OSV concept design. The framework is able to quickly perform extensive seakeeping analyses on many variable combinations, thereby performing an optimization and finding the design problem's Pareto-frontier. In the validation and verification study, the added value of this framework became apparent during concept design. It is able to adjust global hull properties to find the optimal trade-off between seakeeping, station keeping, and lightship weight. By applying the ORI as seakeeping KPI, designs are created that are very robust in their seakeeping performance. This also allows for motion compensate equipment with more stringent limits, reducing the CAPEX and OPEX of such equipment, whilst maintaining high operability.

By achieving the above, the framework allows the naval architect to quickly gain insight into what variable combination is optimal for the OSV. Additionally, the framework also allows for evaluation of what the critical performance limiting factors are. Hence, the framework is to improve the design of OSVs in many facets. It is able to find the best designs given the constraints, and thereby limitations within the design space. In doing so, it offers naval architects insight into whether it is worth investigating if the design space can be further expanded.

The case study saw that the framework was able to find large improvements on a concept design created by C-Job's expert naval architect. Primarily due to being able to test many designs in a short

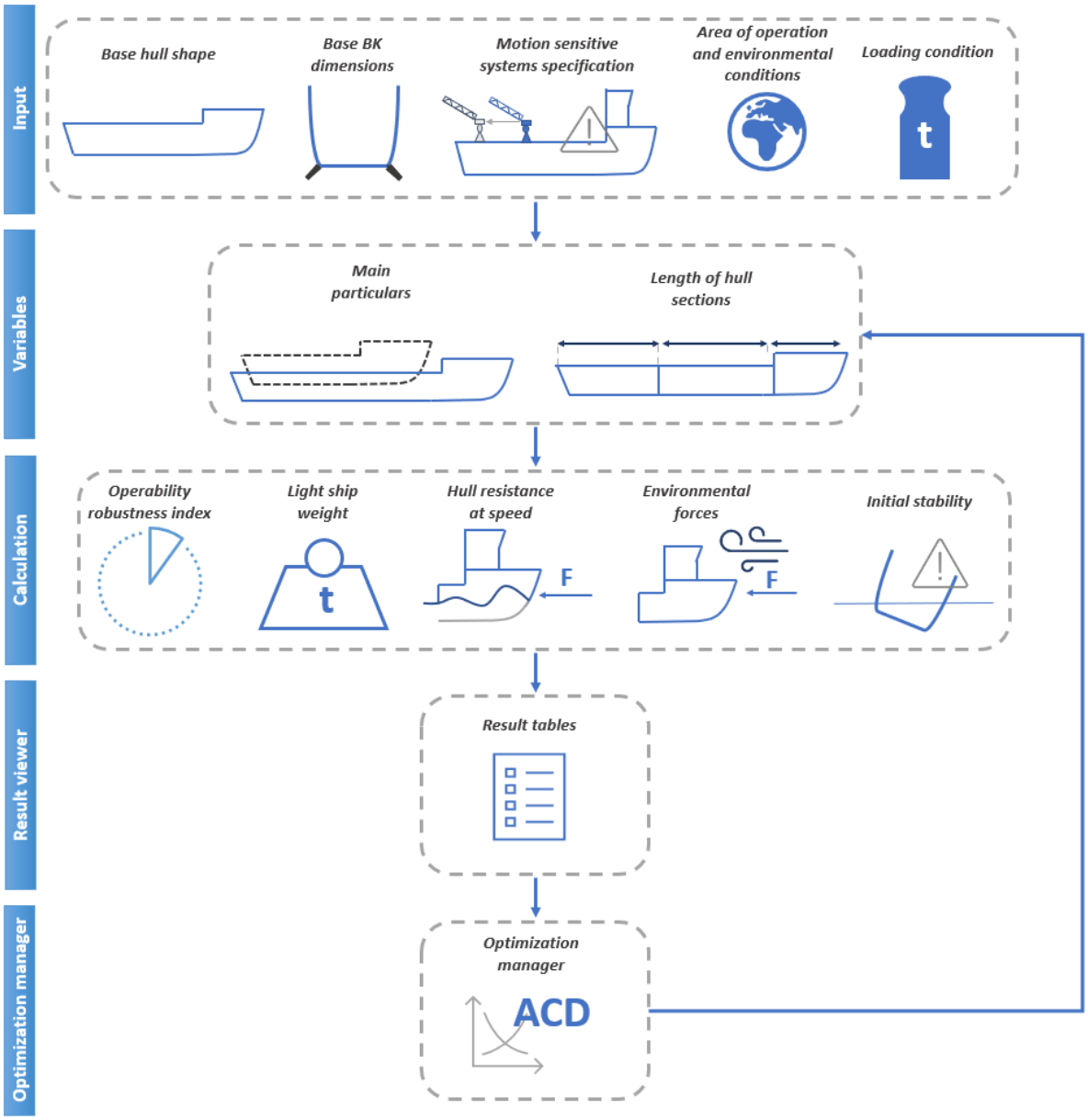

Figure 10.1: Seakeeping optimisation framework in NAPA. Arrows indicate the followed process

time, the framework was able to find these improvements. Potential improvements ranged from a 3% in ORI, 21% in lightship weight, and 13% in ship resistance, whilst not decreasing in performance on any KPI's compared to the base vessel. It should be note that the reduction in lightship weight is mostly due to the Pareto-optimal results being shorter than the base vessel, but may be overestimated in the used lightship estimation method (see section 7.3.3 and equation 7.6). The improvements in ORI allowed for a reduction in motion limits up to 20%, reducing the CAPEX and OPEX of the motion compensate equipment. To conclude, it can be stated that by being able to evaluate and actively steer variable combinations towards maximum performance, the framework is able to quickly find high-performance designs. Thereby, naval architects are given the opportunity to decide an optimal design direction during concept design.

10.2. Contributions

Multiple contributions are made to the maritime industry by this thesis. These are:

1. **Proof of concept 'holistic design methods'**

   This thesis showed another proof of concept for holistic design methods- or design synthesis models. Though academia showed many developments in this field, the application for commercial practices has been limited. This framework demonstrated a practical and applicable design framework and showed the added value of holistic design methods over classical design methodologies.

2. **Efficient and extensive consideration of vessel seakeeping during concept design**

   Varies studies saw an attempt at effective consideration of seakeeping during concept design. These studies resorted to simplifications regarding the seakeeping analysis. The methodology of the framework is able to consider seakeeping, with full consideration of RAOs, relevant scatter diagrams and wave spectra, and the hull shape.

3. **Dedicated framework for feasibility studies of new OSV concepts**

   Due to the growth in the offshore wind industry [23], many new OSVs are being developed. Amongst them are feeder vessels, W2W-vessels, and large floating WTIVs (contrary to jack-up WTIVs, which can only install turbines up until a certain size due to constraints in load on the jack-ups). These vessels are highly dependant on motion behavior for their performance, and proof of concepts still need to be done. This framework allows for easy yet advanced analysis of the motion performance and subsequent operability, even when design information is limited. Therefore, the framework lends itself well for feasibility studies on the capability of these vessels.

10.3. Recommendations

1. **Consider multiple operational conditions and motion limit cases at once**

   In the current state of the model, an individual optimization is run for a specific area of operation, loading condition, and motion limit case. In reality, as seen by the US wind feeder case study, multiple loading conditions exist, and multiple onboard pieces of equipment are subject to motion limits. In the case study, six cases were considered separately, with six optimization runs spanning three and a half hours each. By considering these conditions at once, the optimization time can be substantially reduced, as only one run has to be performed, improving the efficiency of the model. In the current framework, only absolute limits are considered. The motion limits cases can be further improved by considering relative motions to the wave surface, which would be more suitable for the operability assessment of a blade tip touching the water.

2. **Further refine hull shape variable**

   The hull shape is currently varied by transforming a base hull shape by the free form deformation method. This allows for varying the length of hull sections and beam. Under the notion that typical OSVs will have conventional hull shapes, this method suffices. However, the model is able to evaluate hull shapes on more intricate properties, such as entry angle, or bulbous bow. This brings forth the potential to optimize specific hull shapes on both seakeeping and ship resistance. Specifically, the Lackenby shift method discussed in section 6.1.1, offers finer adjustment of the hull shape, whilst still minimizing the amount of variables.

3. **Further verify lightship weight estimate**

   The results of the case study show that a reduction of 21% in lightship weight is possible (see table 9.4). This reduction is mostly achieved due to a reduction in length of the Pareto-optimal solutions when compared to the base vessel. The applied quadricubic number method (see section 7.3.3 and equation 7.6) may overestimate the influence of length on lightship weight for Wind Feeder-like vessels. A further verification study is recommended to identify whether the reduction in length does actually amount to such a substantial reduction in lightship weight. Possibly, an alternative method is better suited for lightship weight estimation of wind feeder vessels.

4. **Further refine area of operation parameters**

   Currently, the area of operation is considered in the form of a scatter diagram and wave spectrum. These are determined by statistical models following Global Wave Statistics and the recommendations by DNV-GL [30]. The scatter diagram underestimate extreme weather cases, as it is

based on the observation of ships (which attempt to avoid bad weather on oceans). The ability to consider measured wave scatter diagrams would further improve the accuracy of the seakeeping assessment.

5. **Implement CAPEX and OPEX calculation methods**

   The framework is able to determine the operability or yearly up-time, station keeping force, and ship resistance. This data can be used to perform an estimate on the OPEX of the vessel. The required station keeping force and ship resistance can further be developed into a powering requirement. Together with the estimate for lightship weight, an indication for CAPEX can be given. Subsequently, both the CAPEX and OPEX can be used by the naval architect and client to further deliberate the final optimal design.

6. **Implement uncertainty in framework**

   Currently, the method does not account for inaccuracies in the estimation method. Given some assumptions are made throughout the method, such as the estimation of VcG for multiple components, some uncertainty is present for the initial stability estimation. It is worthwhile to investigate the implications of this uncertainty to the Pareto-frontier. If this VcG shifts by 10%, what is the result for optimal hull shapes? How does the Pareto-frontier shift? Priftis et al. showed in figure 2.7 that trade-offs may become worse [27]. Implementing a method to account for uncertainty can further improve the applicability of the framework.

7. **Method to account for anti-roll tanks**

   The research into ship motions in chapter 4 saw the added benefit of anti-roll tanks. This method of motion compensating is often employed on OSVs. Given the complexity of involving these anti-roll tanks in motion analyses, it was decided not to include this in the thesis. To give a more accurate assessment of the seakeeping capabilities on suitable vessels, improvements can be made by involving anti-roll tank.

10.4. Conclusion

This thesis answered the need for new design methods following a development in the offshore wind industry and its supporting OSVs. To efficiently design these vessels, seakeeping should be considered upfront in the design process. This thesis produced a framework capable of doing so. The framework involves seakeeping and is able to find the Pareto-frontier of a specific ship design problem. Trade-offs between seakeeping performance and other KPIs are presented. This allows naval architects to determine the optimal design direction during concept design. Clients and naval architects can decide what trade-off in performance provides the ideal combination to achieve the ship's mission. Consequently, besides producing high-performance designs, the framework increases early design knowledge. Thereby, the overall design process becomes more efficient. The framework highlights the inefficiency of conventional design methods, where a naval architect is typically bound to just two or three iterations during the concept design stage due to time and cost constraints.

This framework demonstrated the potential of holistic design methods. Additionally, it demonstrated that the increase in computing power allows for new innovative design methods, not only in academia but also in a more practical applied setting. Though academia has developed such methods for a longer period [56], novel design methods have only started to gain traction by the industry in recent years. Critically, this design method should be considered as another method in the toolbox of a *21st century* naval architect. This thesis answered the need for new design methods following a development in the offshore wind industry and its supporting OSVs. To efficiently design these vessels, seakeeping should be considered upfront in the design process. This thesis produced a framework capable of doing so. The framework involves seakeeping and is able to find the Pareto-frontier of a specific ship design problem, presenting trade-offs between seakeeping performance and other KPIs. Thereby, it allows naval architects to determine the optimal design direction during concept design. Clients and naval architects can decide what trade-off between performance in different aspects provides the ideal combination to satisfy the ship's mission. Consequently, besides producing high-performance designs, the framework allows for a more efficient design process in the later design stages, due to the increase in design knowledge. Thereby, the framework highlights the inefficiency of conventional design methods,

where a naval architect is typically bound to just two or three iterations during the concept design stage due to time and cost constraints.

This framework demonstrated the potential of holistic design methods. Additionally, it demonstrated that the increase in computing power allows for new innovative design methods, not only in academia but also in a more practical applied setting. Although academia has developed such methods for a longer period [56], novel design methods have only started to gain traction by the industry in recent years. Critically, this design method should be considered as another method in the toolbox of a *21st century* naval architect.

10.5. Personal reflection

This thesis marks the final leg in completing my student career. Throughout my student years, I have certainly had my ups and downs. I enjoyed this thesis process, but rather I would like to reflect on what I have experienced in the past 10 years. Specifically, I would like to share three moments with you that have defined me to be the person that I am today. 10 years ago, I stood at a crossroads between 'HAVO' (higher general continued education) and 'VWO' (preparatory scientific education). Having skipped classes that amounted to a whopping 350 hours of missed education, the decision was clear, and certainly not one I had any say in. I had to drop a level in education and do a repeat of the year. This confrontation with my irresponsibility made one thing abundantly clear to me: **Nothing comes for free, you can set a high goal for yourself, but you need to be prepared to put in the hours**. You have the ability to shape your future, but you have to put in the hours. After finishing up HAVO, I enrolled in mechanical engineering at the university of applied sciences in Groningen. I certainly did not find my groove immediately and fell into a depression in the winter of my first year. This second reality check gave me my second critical lesson: **You need to take care of yourself, mentally and physically, as well as the people surrounding you**. Short term you may not feel like it, but dare yourself to move out of your comfort zone and think long-term! Taking this lesson to heart, I have been given incredible opportunities to intern on a ship, sailing in England and Germany, study for half a year in Prague, and working for two months at a shipyard in Vietnam! I am no more special than the next person, yet with hard work and determination, and having some guts to put in an application, I have found myself in places I could never imagine. However, unfortunately, there was another major lesson to be learned. At the end of my bachelor's, both my parents fell ill with cancer, within one year of each other. Though they are doing okay now, this gave me my last important lesson. Life is going to throw you curveballs, whether you want it or not. And often, it will happen at the worst possible times. **Adversity is part of life, and we all experience it. During difficult times, it is important to take things one day at a time and focus on what is good for you and the ones you care about.** Eventually, things will get better. Show an appreciation and understanding to the ones around you, and you will receive the same.

I am grateful for the above lessons, which have brought me understanding and compassion for others. Having finished my mechanical engineering bachelor's, I enrolled at the TU Delft for the study Marine Technology. After completing a tough bridging program, I experienced one of my fondest student years. During the 1st year of my master's, I could help other students make the transition from applied sciences to university as bridging program mentor. My 'life' lessons (I am very aware that this sounds cliché) culminated in me being able to help the students on a deeper level, something I have tremendously enjoyed.

To anyone reading this, I implore you to dare yourself to move out of your comfort zone. TU Delft is a great university, and its alumni have given me endless inspiration. I consider the beginning of this century to be marked by both the digital transformation as well as the energy transition. These subjects are starting to have a massive impact on the maritime industry- and will continue to do so. As such, we naval architects face a challenge but also an opportunity to make the world a better place. I encourage you to think about what you want to be your part in it because the world is at your doorstep!

Bibliography

[1] Bibby wavemaster 1 completes galloper charter. URL https://www.4coffshore.com/news/bibby-wavemaster-1-completes-galloper-charter-nid7372.html.

[2] Walk to work vessel kasteelborg put into service. URL https://www.wagenborg.com/news/walk-to-work-vessel-kasteelborg-put-into-service.

[3] Dof subsea vessel skandi skansen. URL http://www.dofsubsea.com/vessels/skandi-skansen/.

[4] Find your solution. URL https://www.ampelmann.nl/systems/.

[5]

[6] *System based design of offshore support vessels*, 2012.

[7] C-job projects: Ahtsv design by c-job. Jul 2017. URL https://C-Job.com/project/neptune-shipyards-ahtsv/.

[8] C-job explained: Ship design pyramid - c-job. sep 2017. URL https://C-Job.com/C-Job-explained-ship-design-pyramid/.

[9] Nov 2020. URL https://www.napa.fi/.

[10] Wind feeder vessel - solution for us offshore wind - c-job, Apr 2021. URL https://c-job.com/wind-feeder-vessel-solution-for-us-offshore-wind/.

[11] D Andrews. The sophistication of early stage design for complex vessels. *Special Edition IJME Part A June*, 2018.

[12] R Beck, A Reed, P Sclavounos, and B Hutchison. Modern computational methods for ships in a seaway. discussion. author's closure. *Transactions-Society of Naval Architects and Marine Engineers*, 109:1–51, 2001.

[13] W Beukelman and A Huijser. Variation of parameters determining seakeeping. *International Shipbuilding Progress*, 24(275):171–186, 1977.

[14] L Birk. *Fundamentals of Ship Hydrodynamics: Fluid Mechanics, Ship Resistance and Propulsion*. John Wiley & Sons, 2019.

[15] V Bolbot and A Papanikolaou. Parametric, multi-objective optimisation of ship's bow for the added resistance in waves. *Ship Technology Research*, 63(3):171–180, 2016.

[16] E Boulougouris, A Papanikolaou, G Zaraphonitis, and NTUA-SDL. Optimization of arrangements of ro-ro passenger ships with genetic algorithms. *Ship Technology Research*, 51(3):99–105, 2004.

[17] D Brown. Defining a warship. *Naval engineers journal*, 98(2):31–40, 1986.

[18] W Burger and A Corbet. Ship stabilizers: A handbook for merchant navy officers. Elsevier, 2014.

[19] Xiaochi Cai et al. Ship response estimation in early design stage. 2016.

[20] N Charisi, Hs Hopman, A Kana, N Papapanagiotou, and T Muller. Parametric modelling method based on knowledge based engineering: The lng bunkering vessel case. 2019.

[21] JP Coelingh, AJM Van Wijk, and AAM Holtslag. Analysis of wind speed observations on the north sea coast. *Journal of Wind Engineering and Industrial Aerodynamics*, 73(2):125–144, 1998.

[22] US Congress. United states code: Merchant marine act, 46 usc 5. 2006.

[23] Global Wind Energy Council. Gwec| global wind report 2021. 2021.

[24] A de Gaaij. Applying parametric optimisation in the concept exploration phase on naval support vessels. 2019.

[25] R de Winter. Designing ships using constrained multi-objective efficient global optimization, 05 2018.

[26] Roy de Winter, Bas van Stein, and Thomas Bäck. Samo-cobra: A fast surrogate assisted constrained multi-objective optimization algorithm. In *EMO*, pages 270–282, 2021.

[27] K Deb, Z Lu, C McKesson, C Trumbach, and L DeCan. Towards optimal ship design and valuable knowledge discovery under uncertain conditions. In *2015 IEEE Congress on Evolutionary Computation (CEC)*, pages 1815–1822. IEEE, 2015.

[28] İbrahım Demır, Fatma Corut Ergın, and Berna Kıraz. A new model for the multi-objective multiple allocation hub network design and routing problem. *IEEE Access*, 7:90678–90689, 2019.

[29] S Dhavalikar. Comparative study of seakeeping analysis results from various methods. In *International Conference on Offshore Mechanics and Arctic Engineering*, volume 44335, pages 217–223, 2011.

[30] GL Dnv. Dnv-rp-c205: Environmental conditions and environmental loads. *DNV GL, Oslo, Norway*, 2014.

[31] Huisman Equipment. Technical specification huisman 1200mt motion compensated platform. 2018. Product reference: X0011546.

[32] J Evans. Basic design concepts. *Journal of the American Society for Naval Engineers*, 71(4): 671–678, 1959.

[33] O Faltinsen. *Sea loads on ships and offshore structures*, volume 1. Cambridge university press, 1993.

[34] N Fonseca and C Soares. Sensitivity of the expected ships availability to different seakeeping criteria. In *International Conference on Offshore Mechanics and Arctic Engineering*, volume 36142, pages 595–603, 2002.

[35] H Gaspar, P Brett, S Erikstad, and A Ross. Quantifying value robustness of osv designs taking into consideration medium to long term stakeholders' expectations. In *12th International Marine Design Conference (IMDC)*, volume 2, pages 247–259, 2015.

[36] A Gawad, S Ragab, A Nayfeh, and D Mook. Roll stabilization by anti-roll passive tanks. *Ocean Engineering*, 28(5):457–469, 2001.

[37] T Gourlay, A von Graefe, V Shigunov, and E Lataire. Comparison of aqwa, gl rankine, moses, octopus, pdstrip and wamit with model test results for cargo ship wave-induced motions in shallow water. In *International Conference on Offshore Mechanics and Arctic Engineering*, volume 56598, page V011T12A006. American Society of Mechanical Engineers, 2015.

[38] G Grigoropoulos and D Chalkias. Hull-form optimization in calm and rough water. *Computer-Aided Design*, 42(11):977–984, 2010.

[39] Yue Gu, Evangelos Boulougouris, and Alexander Day. A study on the effects of bilge keels on roll damping coefficient. 2015.

[40] Ra Guanche, M Martini, A Jurado, and I Losada. Walk-to-work accessibility assessment for floating offshore wind turbines. *Ocean Engineering*, 116:216–225, 2016.

[41] M Gutsch, F Sprenger, and S Steen. Influence of design parameters on operability of offshore construction vessels. *Jahrbuch der Schiffbautechnischen Gesellschaft*, pages 230–242, 2016. cited By 1.

[42] M Gutsch, S Steen, and F Sprenger. Operability robustness index as seakeeping performance criterion for offshore vessels. *Ocean Engineering*, 217:107931, 2020.

[43] S Han, Y Lee, and Y Choi. Hydrodynamic hull form optimization using parametric models. *Journal of marine science and technology*, 17(1):1–17, 2012.

[44] S Hannapel. *Development of Multidisciplinary Design Optimization Algorithms for Ship Design Under Uncertainty.* PhD thesis, 2012.

[45] C Ho, D. Okafor, J. DeGregory, N. Tontarski, T. Storey, and Z. Lin. 8520 teu dual fuel container ship for the far east - mediterranean trade route. *2011 - 2012 Dr. James A. Linsnyk student ship design competition*, 2012.

[46] J Holtrop and GGJ Mennen. An approximate power prediction method. *International Shipbuilding Progress*, 29(335):166–170, 1982.

[47] Z Hong, Z Zong, H Li, H Hefazi, and P Sahoo. Self-blending method for hull form modification and optimization. *Ocean Engineering*, 146:59–69, 2017.

[48] F Huang, L Wang, C Yang, et al. Hull form optimization for reduced drag and improved seakeeping using a surrogate-based method. In *The Twenty-fifth International Ocean and Polar Engineering Conference*. International Society of Offshore and Polar Engineers, 2015.

[49] Y Ikeda. A prediction method for ship roll damping. *Report No. 00405 of the Department of Naval Architecture*, 1978.

[50] Y Ikeda. On roll damping force of ship-effect of friction of hull and normal force of bilge keels. *University of Osaka Prefecture, Department of Naval Architecture, Japan, Report No. 00401, Published in: Journal of Society of Naval Architects of Japan, No. 161 (1976)*, 1978.

[51] Y Ikeda. On roll damping force of ship-effect of hull surface pressure created by bilge keels. *University of Osaka Prefacture, Department of Naval Architecture, Japan, Report No. 00402, Published in: Journal of Society of Naval Architects of Japan, No. 165, 1979*, 1979.

[52] Y Ikeda. Prediction methods of roll damping of ships and their application to determine optimum stabilization devices. *Marine technology and SNAME news*, 41(02):89–93, 2004.

[53] Y Ikeda, Y Himeno, and N Tanaka. On eddy making component of roll damping force on naked hull. *Journal of the society of Naval Architects of Japan*, 1977(142):54–64, 1977.

[54] Y Ikeda, Y Himeno, and N Tanaka. Components of roll damping of ship at forward speed. *Journal of the society of Naval Architects of Japan*, 1978(143):113–125, 1978.

[55] J Journée and J Pinkster. Offshore hydromechanics. *TUDelft, Faculty of Marine Technology, Ship Hydromechanics Laboratory, Report No. 1112-K, Lecture Notes*, 1997.

[56] AA Kana and JJ Hopman. State of the art report on design methodology: Design research and practice perspective.

[57] J Kolko. Abductive thinking and sensemaking: The drivers of design synthesis. *Design issues*, 26(1):15–28, 2010.

[58] H Lackenby. On the systematic geometrical variation of ship forms. *Transactions of the TINA, Volume 92, pp. 289-315*, 1950.

[59] E Lewis. Principles of naval architecture second revision. *Jersey: SNAME*, 2, 1988.

[60] B Li. Operability study of walk-to-work for floating wind turbine and service operation vessel in the time domain. *Ocean Engineering*, page 108397, 2020.

[61] A Ljulj, V Slapničar, et al. Multi-attribute concept design procedure of a generic naval vessel. *Alexandria Engineering Journal*, 2020.

[62] A Lloyd. Seakeeping: ship behaviour in rough weather. *Admiralty Research Establishment, Haslar, Gosport, Publisher Ellis Horwood Ltd, John Wiley & Sons, ISBN: 0 7458 0230 3*, 1989.

[63] Baird Maritime. Total awards multi-year charter for two PSVs. *Baird Maritime*, January 2018. URL https://www.bairdmaritime.com/work-boat-world/offshore-world/offshore-operations-maintenance/platform-supply/total-awards-multi-year-charter-for-two-px-121-psvs/.

[64] S Menzel, M Olhofer, and B Sendhoff. Application of free form deformation techniques in evolutionary design optimisation. 02 2021.

[65] F Mistree, W Smith, B Bras, J Allen, D Muster, et al. Decision-based design: a contemporary paradigm for ship design. *Transactions, Society of Naval Architects and Marine Engineers*, 98 (1990):565–597, 1990.

[66] I Nielsen. Assessment of ship performance in a seaway. *Publisher: NORDFORSK, Sortedam Dossering 19, DK-200 Copenhagen, Denmark, ISBN: 87-982637-1-4*, 1987.

[67] H Nowacki. Five decades of computer-aided ship design. *Computer-Aided Design*, 42(11):956–969, 2010.

[68] Quality Systems Group of the 28th ITTC. Recommended procedures-numerical estimation of roll damping. *International Towing Tank Conference*, 26(1):548–549, 2011.

[69] S Özüm, B Şener, and H Yilmaz. A parametric study on seakeeping assessment of fast ships in conceptual design stage. *Ocean Engineering*, 38(13):1439–1447, 2011.

[70] A Papanikolaou. Holistic ship design optimization. *Computer-Aided Design*, 42(11):1028–1044, 2010.

[71] A Papanikolaou. Ship design: methodologies of preliminary design. 2014.

[72] A Papanikolaou. *A Holistic Approach to Ship Design*. Springer, 2019.

[73] R Pawling, V Percival, and D Andrews. A study into the validity of the ship design spiral in early stage ship design. *Journal of Ship Production and Design*, 33(2):81–100, 2017.

[74] Karl Pearson. Vii. note on regression and inheritance in the case of two parents. *proceedings of the royal society of London*, 58(347-352):240–242, 1895.

[75] A Priftis, E Boulougouris, and O Turan. Parametric design and holistic optimisation of post-panamax containerships. *Transport Research Arena (TRA) 2018*, 2018.

[76] A Priftis, E Boulougouris, O Turan, and G Atzampos. Multi-objective robust early stage ship design optimisation under uncertainty utilising surrogate models. *Ocean Engineering*, 197:106850, 2020.

[77] C Rehn, S Pettersen, S Erikstad, and B Asbjørnslett. Investigating tradeoffs between performance, cost and flexibility for reconfigurable offshore ships. *Ocean Engineering*, 147:546–555, 2018.

[78] L Rusu and C Soares. Forecasting fishing vessel responses in coastal areas. *Journal of Marine Science and Technology*, 19(2):215–227, 2014.

[79] T Saaty. Some mathematical concepts of the analytic hierarchy process. *Behaviormetrika*, 18 (29):1–9, 1991.

[80] T Saaty. Decision making with the analytic hierarchy process. *International journal of services sciences*, 1(1):83–98, 2008.

[81] T Scholcz and E van Daalen. Surrogate-based multi-objective optimisation for powering and seakeeping. In *Practical Design of Ships and Other Floating Structures*, pages 477–492. Springer, 2019.

[82] T Sederberg and S Parry. Free-form deformation of solid geometric models. volume 20, pages 151–160, 08 1986. ISBN 0897911962. doi: 10.1145/15886.15903.

[83] C Soares, N Fonseca, and R Centeno. Seakeeping performance of fishing vessels in the portuguese economic zone. 1995.

[84] C Söder, A Rosén, and M Huss. Ikeda revisited. *Journal of Marine Science and Technology*, 24 (1):306–316, 2019.

[85] P Spectre and M Bray. *Planking and Fastening*. WoodenBoat series. WoodenBoat Publications, 1996. ISBN 9780937822418. URL https://books.google.nl/books?id=qVUD70nM898C.

[86] Y Tahara, F Stern, and Y Himeno. Computational fluid dynamics□based optimization of a surface combatant. *Journal of Ship Research*, 48:273–287, 12 2004. doi: 10.5957/jsr.2004.48.4.273.

[87] T Tezdogan, A Incecik, and O Turan. Operability assessment of high speed passenger ships based on human comfort criteria. *Ocean Engineering*, 89:32–52, 2014.

[88] A Van der Loos, H Normann, J Hanson, and M Hekkert. The co-evolution of innovation systems and context: Offshore wind in norway and the netherlands. *Renewable and Sustainable Energy Reviews*, page 110513, 2020.

[89] Manuel Ventura. Estimation methods for basic ship design. *Instituto Superior Tecnico, Technical University of Lisbon, Portugal*, 2011.

[90] Det Norske Veritas. Recommended practice. *Environmental Conditions and Environmental Loads (DNV-RP-C205)*, 2010.

[91] Håvard Vindenes, Kjell Arild Orvik, Henrik Søiland, and Henning Wehde. Analysis of tidal currents in the north sea from shipboard acoustic doppler current profiler data. *Continental Shelf Research*, 162:1–12, 2018.

[92] C Vossen, R Kleppe, and S Randi. Ship design and system integration. 2013.

[93] N Yourkov. Vertical motions of ships with bolbous bows. *TUDelft, Faculty of Marine Technology, Ship Hydromechanics Laboratory Report 320*, 1971.

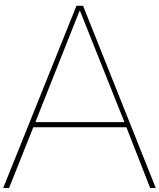

Interview reports C-Job

INTERVIEW REPORT – CONCEPT DESIGN

Subject: Concept design at C-Job
Participants: Geoffrey Smits, Philip Bronkhorst
Time: 10:30-11:30
Date: 08–12-20

Agenda of interview

- Discuss concept design at C-Job,
- Discuss ACD

Interview notes

Concept design at C-Job

- There is no particular definition of concept design at C-Job. Thus, it is largely dependent on the requirements of the client.
    - An concept design might just include a very simple mock up of the vessel, or some principle dimensions. If it is already determined C-Job will also do detail design, the concept design might also include a 3D model, GA and weight calculation. This is partially depended on the time and budget available for concept design.
- At the very least however, the concept design stage contains a feasibility study on the vessel. Hence, can the requirements set by the client be fulfilled by any vessel.
    - Though obviously C-Job strives to design an 100% feasible design, typically some adjustments need to be made. A very rough estimate is that on average a design will be 95% feasible. (This is better interpreted as, there are some adjustments that need to be made during detail design.)
- For an *initial* concept design, main particulars, GM, accommodation sizes and so forth are usually determined based on experience of C-Job naval architects. These aspects are then further refined based with analysis methods such as ACD.

ACD at C-Job

- The foreseen business case for ACD, is to use the method to further refine initial estimates for ship aspects of influence to the vessels ability to meet client requirements.
- Hence, ACD is designed for an optimization role, rather than to fully explore a design space or check feasibility. Though, since ship criteria are also modelled, ACD indirectly also checks a design for feasibility.

INTERVIEW REPORT – OFFSHORE VESSEL DESIGN

Subject: Offshore vessel design drivers
Participants: Alexander van den Ing, Philip Bronkhorst
Time: 10:00-11:00
Date: 09–12-20

Agenda of interview

- Discuss design drivers of offshore vessels

Interview notes

Typical design drivers of offshore vessels

- Time
  - Mostly all clients wish to have their vessel to be available for operation as soon as possible. A ship is capable of fulfilling its function once it has been launched. As such, both the design and building of a ship are under time pressure.
  - Building time can be estimated using steel weight. Time can be correlated with steel weight as the weight gives an indication how many fabrication actions, and thus time, is needed. Steel weight is influenced by the size of the ship.
  - Additionally, the complexity of a vessel impacts the time needed for building, in part by the additional fabrication actions it causes.
- Cost
  - Typically, an optimal ship is able to generate a maximal profit at a minimal cost. This cost can be decamped in CAPEX and OPEX, both of which are to be kept as low as possible.
  - Cost can, similarly to time, be estimated by steel weight and complexity. Both of which impact the fabrication actions and thereby man hours and corresponding cost involved.
- Motions
  - Motion characteristics are of influence on crane ships, W2W-vessels and offshore construction vessels. As such, motion characteristics form a design driver during the design of these vessels.
  - Typically, it is necessitated to keep accelerations to a minimum. The motion amplitude is of less importance. Accelerations can be minimized by:
    - Often, pitch motions are not an issue, and heave, sway and surge motions can be relatively easily motion compensated for. More difficult, and opt
    - Keeping GM low, this increases the roll period, hence the ship rolls (and accelerates) slower. GM is also kept low in an effort to have the roll period far outside the period of a sea state. For example: if the sea state has a significant wave height of 3 [m], and wave period of 10 – 12 [s], a W2W-vessel would be designed to have a roll period around 20 [s]. Note that this is a general example, which purely serves as an example.
    - Accelerations are also kept minimal by the use of a dampening devices. These include appendages such as kim keels and anti-roll tanks.
      - Kim keels increase the added mass thereby resulting in a dampening effect.
      - Anti-roll tanks. These can passively or actively mitigate roll motions

be free surface effects, though this decreases the GM. Active anti-roll tanks also exist, such as U-roll tanks. Hoppe Marine manufactures such tanks.
        - Adjusting inertia effects. A study by MARIN showed this can be done by placing equipment in the front halve of the ship, as far outward as possible.
        - Geometry of the hull
        - Equipment of which its functionality is dependent on motions, can best be placed at roughly 1/3 length of the ship, from aft vessel. Typically, at this point, motions are minimal.
    - Weathervaning capabilities. If a ship is able to lie head into the waves the influence in sway and roll motions are mitigated.
- Station keeping
    - Any vessel requiring DP operations, as is the case by crane ships, W2W-vessels and offshore construction vessels, necessitates good station keeping capabilities
        - This can be achieved by either a more powerful DP system or a minimal size of the vessel. By keeping the vessel as small, or 'compact', as possible, the influence of waves, current and wind, thus external forces, is minimized.
- Ship resistance
    - Ship resistance can be design driver in offshore vessels. Though typically, the transit speeds aren't very high, and the vessel will be capable of satisfying such speeds economically. Whether ship resistance is important is dependent case by case.
        - For a lower ship resistance, it is preferred to keep the ship as slender (=high L/B) as possible.
    - To determine whether ship resistance is a design driver, requires case by case evaluation.

B

Rigid body dynamics

The essence of a 'ship motion' is any movement in six DoF. Namely, a surge, sway, heave, roll, pitch, and yaw movement. These motions concern movement, velocity, or acceleration in - or around - the x-, y- and z-axis of a vessel. The movements are visualized on a ship hull in figure B.1.

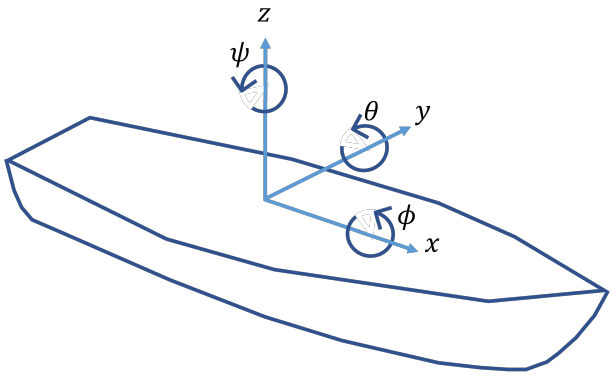

$$x = surge \qquad y = sway \qquad z = yaw$$
$$\phi = roll \qquad \theta = pitch \qquad \psi = heave$$

Figure B.1: Definition of ship Motions in six degrees of freedom

Furthermore, a particular motion on a vessel, such as a crane tip moving, comprises individual movements in these six DoF. Any motion analysis may calculate motion about the CoG or CoB of the vessel. Rotational motions directly translate to any particular point on the vessel. Translational motions on a particular point are calculated by (for small angles),

$$\begin{aligned} x_P &= x - y_b\psi + z_b\theta \\ y_P &= y + x_b\psi - z_b\phi \\ z_P &= z - x_b\theta + y_b\phi \end{aligned} \tag{B.1}$$

Where,

- x_P, y_P, z_P = Absolute translational motion of point in x-, y- and z-direction
- x_b, y_b, z_b = Position of point in x-, y- and z-direction with respect to the CoG
- x, y, z, ϕ, θ, ψ = surge, sway, heave, roll, pitch and yaw position or rotation of the CoG

comprise equation B.1 [55].
The specific definition of each ship motion is,

- Translational movements:
  - x, surge: movement in longitudinal x-direction, positive in forward direction ship,
  - y, sway: movement in lateral y-direction, positive in direction port side,

  - z, heave: movement in vertical z-direction, positive upwards.
- Rotational movements:
  - ϕ, roll: rotation around the x-axis, positive right turning,
  - θ, pitch: rotation around the y-axis, positive right turning,
  - ψ, yaw: rotation around the z-axis, positive right turning.

A ship motion response is an interaction between environment induced forces and the ship's reactionary attributes. This motion response is represented by the ships the ship's equations of motion (EoM),

$$[M + A]\,\ddot{x} + B\dot{x} + Cx = F \tag{B.2}$$

Where,

- x, $\dot{x}$, $\ddot{x}$ = Motion terms: position, velocity and acceleration respectively in six DoF
- M = Mass and inertia terms
- A = Hydrodynamic added mass and inertia terms
- B = Hydrodynamic damping terms
- C = Restoring force terms
- F = Force due vessel motion

comprise equation EoM. The individual components account for the following effects:

- The most left term, $[M + A]\,\ddot{x}$, originates from Newton's second law. Newtown's second law states that acceleration of mass equates to a force. The first two items, M, and A represent the ship's mass and the added mass respectively [59]. Added mass concerns the mass of water which accelerated due to vessel movement. The term $\ddot{x}$ represents the rotational or translational acceleration in any of the six DoF.

- The second term on the left-hand side of the equation, $B\dot{x}$, accounts for forces resulting from hydrodynamic damping, namely due to two physical events. Firstly, if a ship moves, the ship itself will generate waves. Hence, energy is dissipated into the water, damping the motion. Secondly, due to the viscosity of the fluid, friction, the generation of vortexes, and fluid separation also cause damping effects. Consequently, velocity or rotational speed results in a force on the ship or vice versa.

- The third term on the left-hand side of the equation, Cx, characterizes restoring forces of the ship. Ship motions heave, roll, and pitch are accompanied by a 'restoring' force. If the ship undergoes one of these motions, the restoring force results in the ship eventually moving back to its original position. Surge, sway, and yaw responses do not have a restoring force. Hence, a ship laying stationary without a DP system moves due to the wave forces (in addition to current and wind forces).

- The term on the right-hand side of equation B.2, $\mathbf{F}$ is the resultant motion force.

The force term in equation B.2 comprises partially of forces due to encountered waves. As a ship spends the majority of its life-cycle in a body of water with waves, the vessel response against waves is therefore considered equally important in the definition of ship motions and is mostly considered together. This is done by a response amplitude operator or RAO.

C

Calculation of ocean wave parameters

C.1. Wave spectrum

The wave spectrum used in the framework is the Pierson-Moskowitz (PM) spectrum, whereby,

$$S_{PM}(\omega) = \frac{5}{16} \cdot H_S^2 \omega_p^4 \cdot \omega^{-5} \exp\left(-\frac{5}{4}\left(\frac{\omega}{\omega_p}\right)^{-4}\right) \tag{C.1}$$

defines the spectrum. In this equation, $\omega_p = 2\pi/T_p$ is the angular spectral peak frequency. If to be calculated based on the H_S and T_Z found in a scatter diagram, the spectral peak frequency is calculated based on the following relationship,

$$1.407 \cdot T_Z = T_p \rightarrow \omega_p = \frac{2\pi}{T_p} = \frac{2\pi}{1.407 \cdot T_Z} \tag{C.2}$$

For fetch limited seas, the PM spectrum is modified to a JONSWAP spectrum, which is formulated as,

$$S_J(\omega) = A_\gamma S_{PM}(\omega) \gamma^{\exp\left(-0.5\left(\frac{\omega-\omega_p}{\sigma\omega_p}\right)^2\right)} \tag{C.3}$$

In this equation γ is a non-dimensional peak shape parameter, σ the spectral width parameter and A_γ a normalizing factor.

C.2. Scatter diagram

The scatter diagram is calculated by a three-parameter Weibull probability density function. This function defines the probability for significant wave height and zero-crossing wave period as,

$$f_{H_s}(h) = \frac{\beta_{Hs}}{\alpha_{Hs}}\left(\frac{h-\gamma_{Hs}}{\alpha_{Hs}}\right)^{\beta_{Hs}-1} \exp\left\{-\left(\frac{h-\gamma_{Hs}}{\alpha_{Hs}}\right)^{\beta_{Hs}}\right\} \tag{C.4}$$

and,

$$f_{T_Z|H_s}(t \mid h) = \frac{1}{\sigma t\sqrt{2\pi}} \exp\left\{-\frac{(\ln t - \mu)^2}{2\sigma^2}\right\} \tag{C.5}$$

respectively. α_{Hs} and β_{Hs} are shape parameters. Distribution parameters μ and σ are defined as,

$$\mu = E\left[\ln T_z\right] = a_o + a_1 h^{a_2} \tag{C.6}$$

$$\sigma = std\left[\ln T_z\right] = b_0 + b_1 e^{b_2 h} \tag{C.7}$$

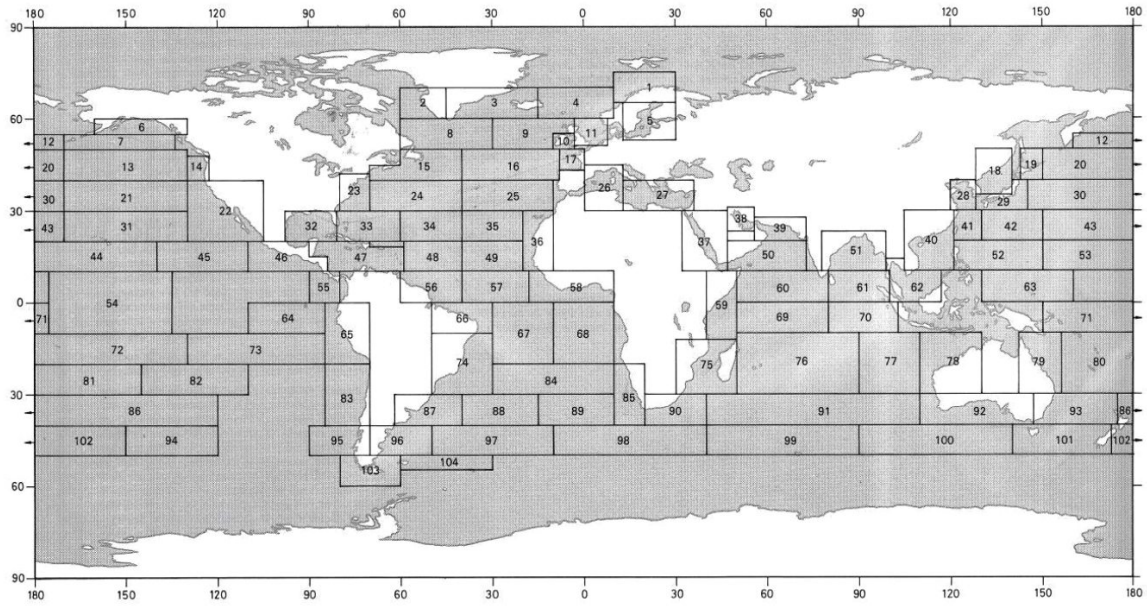

Figure C.1: Nautic zones for estimation of long-term wave distribution parameters

where the coefficients $a_i, b_i, i = 0, 1, 2$ are determined from actual measured data. The input parameters are available for the areas as shown in figure C.1.

Based on the input data, a scatter diagram is calculated, providing input to the calculation of the Operability Robustness Index.

D

Paper describing SAMO-COBRA algorithm

memetic computing manuscript No.
(will be inserted by the editor)

Constrained Multi-objective Optimization with a Limited Budget of Function Evaluations

SAMO-COBRA: Self Adaptive Multi-objective Constrained Optimization by using Radial Basis Function Approximations

Roy de Winter[1,2] · Philip Bronkhorst[2] · Bas van Stein[1] · Thomas Bäck[1]

Received: 16-07-21 / Accepted: **Under review as of 06-08-21**

Abstract This paper proposes the Self-Adaptive algorithm for Multi-Objective Constrained Optimization by using Radial Basis Function Approximations, SAMO-COBRA. This algorithm automatically determines the best Radial Basis Function-fit as surrogates for the objectives as well as the constraints, to find new feasible Pareto-optimal solutions.

SAMO-COBRA is compared to a wide set of other state-of-the-art algorithms (IC-SA-NSGA-II, SA-NSGA-II, NSGA-II, NSGA-III, CEGO, SMES-RBF) on 18 constrained multi-objective problems. In the first experiment SAMO-COBRA outperforms the other algorithms in terms of achieved Hypervolume (HV) after given a fixed small evaluation budget on the majority of test functions. In the second experiment, SAMO-COBRA outperforms the majority of competitors in terms of required function evaluations to achieve 95% of the maximum achievable Hypervolume. Showing that SAMO-COBRA outperforms both in final HV as well as in the number of evaluations required to reach the solutions.

In addition to academic test functions, SAMO-COBRA has been applied on a real-world ship design optimization problem with three objectives, two complex constraints and five decision variables.

Keywords Constrained optimization · Multi-objective optimization · Optimization under limited budgets · Real-world application.

1 Introduction

Real-world optimization problems often have multiple conflicting objectives, several constraints, and decision variables in the continuous domain [4,16,42]. Without loss of generality, a constrained multi-objective optimization problem can be defined as follows [13]:

$$\begin{aligned} &\text{minimize: } f : \Omega \to \mathbb{R}^k \ , \ f(\mathbf{x}) = (f_1(\mathbf{x}), \ldots, f_k(\mathbf{x}))^\top \\ &\text{subject to: } g_i(\mathbf{x}) \leq 0 \ \forall i \in \{1, \ldots, m\} \\ &\qquad\qquad \mathbf{x} \in \Omega \subset \mathbb{R}^d. \end{aligned}$$

In this formulation k is the number of objectives, m is the number of constraints and d is the number of parameters in the optimization problem. Solving this problem type can be done by searching for *feasible Pareto-optimal solutions*. The definition of a solution that is feasible and Pareto-optimal can be found in Def. 1.

Definition 1 (**Feasible Pareto-optimal solution**): $\mathbf{x} \in \Omega$ is called *feasible Pareto-optimal* with respect to Ω and $g_i(\mathbf{x}) \leq 0 \ \forall i \in \{1, \ldots, m\}$, if and only if there is no solution $\mathbf{x}'$ for which $\mathbf{v} = f(\mathbf{x}') = (f_1(\mathbf{x}'), \ldots, f_k(\mathbf{x}'))^\top$ dominates $\mathbf{u} = f(\mathbf{x}) = (f_1(\mathbf{x}), \ldots, f_k(\mathbf{x}))^\top$ where $g_i(\mathbf{x}) \leq 0$ and $g_i(\mathbf{x}') \leq 0 \ \forall i \in \{1, \ldots, m\}$.

✉ Roy de Winter
r.de.winter@liacs.leidenuniv.nl

Philip Bronkhorst
p.bronkhorst@c-job.com

Bas van Stein
b.van.stein@liacs.leidenuniv.nl

Thomas Bäck
t.h.w.baeck@liacs.leidenuniv.nl

[1] Leiden Institute of Advanced Computer Science, Leiden University, Niels Bohrweg 1, 2333 CA Leiden, The Netherlands

[2] Research and Development, C-Job Naval Architects, Regulusplein 1, 2132 JN Hoofddorp, The Netherlands

On top of the already complex constrained multi objective optimization problem characteristics, there is also a need to reduce the computational and licensing cost involved. There are many engineering examples which require expensive function evaluations [34], and special hardware or software licences [36]. Practical examples of such problems can be found in the automotive industry, aerospace engineering, and the maritime industry.

Handling constraints in optimization problems can be done in several ways, using penalty functions, separation of constraints and objectives, treating constraints as additional objectives, or hybrid methods [3,16]. In our approach we only consider separation of constraints and objectives because the main issue with penalty functions is that the ideal penalty factors cannot be known in advance and tuning the parameters requires a lot of additional function evaluations. The issue with treating constraints as additional objectives is that it makes the objective space unnecessarily more complex with a too strong bias towards the constraints.

An algorithm which uses the separation of constraints and objectives in combination with surrogates is SAMO-COBRA [40]. SAMO-COBRA which is an abbreviation for Self Adaptive Multi-Objective Constrained Optimization by using Radial Basis Function Approximations owes its name to the very efficient constraint handling algorithms: COBRA [30] and Self Adjusting-COBRA [3]. Besides constraint handling, SAMO-COBRA shows to be efficient in finding Pareto-optimal solutions and thereby solving constrained multi-objective problems using a limited number of function evaluations.

Compared to our previous work describing SAMO-COBRA [40], in this paper the SAMO-COBRA algorithm is described in more detail, SAMO-COBRA is compared to two new state-of-the-art algorithms, additional experiments are conducted to evaluate its performance, and SAMO-COBRA has been used in practice on to solve a real-world optimization problem. In the real-world application SAMO-COBRA is used to solve a real-world ship design optimization problem with five variables, two complex constraints, and three objectives.

1.1 Outline

The remainder of this paper is organized as follows. In Sect. 2 related work is discussed. In Sect. 3 the SAMO-COBRA algorithm is proposed and described in detail. In Sect. 4 the experimental setup is given on how SAMO-COBRA is compared to other state of the art algorithms. In Sect. 5 the results of the experiments are reported. In Sect. 6 an example is given of a real-world application of SAMO-COBRA. The final concluding remarks are given in Sect. 7.

2 Related work

Existing work on surrogate assisted optimization is typically limited to a subset of three relevant requirements (multi-objective, constrained, and speed). For example, methods exist for solving constrained single objective problems fast (e.g. SACOBRA [3]), for multi-objective optimization without efficient constraint handling techniques (e.g. SMS-EGO [28] and PAREGO [24]), or for constrained multi-objective optimization without using meta-models, leading to a lot of required function evaluations (e.g. NSGA-II [14], NSGA-III [23], SPEA2 [43], and SMS-EMOA [6]). Some recently proposed algorithms address all three requirements, however with computational efforts that grows cubically in iterations and exponentially for each additional decision parameter due to the use of Kriging surrogates (e.g. CEGO [41], ECMO [35]).

Only very occasionally a surrogate based algorithm is published that deals with both constraints and multiple objectives in an effective manner without using a Kriging surrogate (e.g., Datta's and Regis' SMES-RBF [11], Blank and Deb's SA-NSGAII [8], and Blank's and Deb's IC-SA-NSGAII [8]).

SMES-RBF is a surrogate-assisted evolutionary strategy that uses cubic Radial Basis Functions as a surrogate for the objectives and constraints to estimate the actual function values. The most promising solution(s) according to a non-dominated sorting procedure are then evaluated on the real objective and constraint function until the evaluation budget limit has been reached.

SA-NSGA-II is the surrogate assisted NSGA-II algorithm that exploits the Cubic Radial Basis Functions with a linear tail as a surrogate to find the Pareto frontier. SA-NSGA-II starts with a Latin Hypercube Sample to train the surrogates. Next, in every iteration the surrogates are updated and used by the NSGA-II algorithm to determine the next to be evaluated solutions.

IC-SA-NSGA-II assumes that the constraints are inexpensive and exploits this assumption by only evaluating the objective functions if the constraints are satisfied. IC-SA-NSGA-II starts by creating a Riesz s-Energy sample (Energy) [21], which results in a well-spaced feasible point set. After the initial sample is evaluated, cubic Radial Basis Functions with a linear tail are fitted as surrogates for the objective and constraint functions. The surrogates are then used by the NSGA-II algorithm to find novel solutions. The con-

straint functions are evaluated first, the objective functions are only evaluated if the constraints are not violated. The novel evaluated solutions are added to the archive which is used in the next iteration to retrain the surrogates. This continues until the objective evaluation budget has been exhausted.

3 Constrained Multi-objective Optimization Algorithm

In this section, the new SAMO-COBRA algorithm is introduced. It is designed for dealing with continuous decision variables, multiple objectives, and multiple complex constraints, and expensive objective function evaluations in an efficient manner. The idea behind the algorithm is that in every iteration, for each objective and for each constraint independently, the best transformation and the best RBF kernel is sought. In each iteration the best fit is used to search for a new unseen feasible Pareto efficient point that contributes the most to the HyperVolume (HV) which is computed between a reference point and the Pareto-frontier (PF). The pseudocode of SAMO-COBRA can be found in Algorithm 1, a Python implementation can be found on the Github page [38]. In the subsections below, the algorithm is explained in more detail.

3.1 Initial Design

Bossek et al. showed empirically that when dealing with sequential-model based optimization in most cases it is best to use the Halton sampling strategy with an as small as possible initial sample [9]. Several experiments confirmed the hypothesis that a small initial sample size and a more adaptive sampling steps also leads to the best results when applied on most constrained multi-objective problems from Section 4.

An RBF model that models the relationship between the input space and the output space can already be trained with $d+1$ initial samples. It is therefore advised when using SAMO-COBRA to create an initial Halton sample of size $d+1$ before the sequential optimization procedure starts. Every sample in the initial design is then evaluated (line 2-4 of Algorithm 1) so that all samples have their corresponding constraint and objective scores.

3.2 Radial Basis Function Fitting and Interpolation

RBF interpolation approximates a function by fitting a linear weighted combination of RBFs [3]. The challenge is to find correct weights ($\boldsymbol{\theta}$) and a good RBF kernel $\varphi(\|\mathbf{x}-\mathbf{c}\|)$. An RBF is only dependent on the distance between the input point $\mathbf{x}$ to the center $\mathbf{c}$. The RBFs used in this work take each evaluated point as the centroid of the function, and the weighted linear combination of RBFs always produces a perfect fit through the training points. Besides the perfect fit on the training points, the linear combination of the RBFs can also give a reasonable approximation of the unknown area.

Any function which is only dependent on the distance from a specific point to another point belongs to the group of RBFs. The RBF kernels (φ) considered in this work are the *cubic* with $\varphi(r) = r^3$, *Gaussian* with $\varphi(r) = \exp\left(-(\epsilon \cdot r)^2\right)$, *multiquadric* with $\varphi(r) = \sqrt{1+(\epsilon \cdot r)^2}$, *inverse quadratic* with $\varphi(r) = (1+(\epsilon \cdot r)^2)^{-1}$, *inverse multiquadric* with $\varphi(r) = (\sqrt{1+(\epsilon \cdot r)^2})^{-1}$, and *thin plate spline* with $\varphi(r) = r^2 \log r$. Note that the shape/width parameter ϵ for every individual RBF is kept constant such as proposed by Urquhart et al. [37]. Moreover, all shape parameters are fixed to $\epsilon = 1$.

Finding suitable linear weighted combinations $\boldsymbol{\theta}$ of the RBFs can be done by inverting $\boldsymbol{\Phi} \in \mathbb{R}^{n \times n}$ where $\boldsymbol{\Phi}_{i,j} = \varphi(\|\mathbf{x}_i - \mathbf{x}_j\|)$:

$$\boldsymbol{\theta} = \boldsymbol{\Phi}^{-1} \cdot \mathbf{f} \tag{1}$$

Here $\mathbf{f}$ is a vector of length n with the function values belonging to one of the objectives or constraints. Because $\boldsymbol{\Phi}$ is not always invertible, Micchelli introduced RBFs with a polynomial tail, better known as augmented RBFs [25]. In this work augmented RBFs are used with a second order polynomial tail. The polynomial tail is created by extending the original matrix $\boldsymbol{\Phi}$ with $\mathbf{P} = (1, x_{i1}, \ldots, x_{id}, x_{i,1}^2, \ldots, x_{id}^2)$, in its ith row, where x_{ij} is the jth component of vector $\mathbf{x}_i$, for $i = 1, \ldots, n$ and $j = 1, \ldots, d$, $\mathbf{P}^\top$, and zeros $\mathbf{0}_{(2d+1)\times(2d+1)}$, leading to $1+2d$ more weights $\boldsymbol{\mu}$ to learn.

$$\begin{bmatrix} \boldsymbol{\Phi} & \mathbf{P} \\ \mathbf{P}^\top & \mathbf{0}_{(2d+1)\times(2d+1)} \end{bmatrix} \begin{bmatrix} \boldsymbol{\theta} \\ \boldsymbol{\mu} \end{bmatrix} = \begin{bmatrix} \mathbf{f} \\ \mathbf{0}_{2d+1} \end{bmatrix} \tag{2}$$

Now that the weights $\boldsymbol{\theta}$ can be computed and $\boldsymbol{\mu}$ with Eq. 1 (Lines 16, 17, 20, 21 of Algorithm 1), for each unseen input $\mathbf{x}'$ the function value (f') can be interpolated/predicted by using Eq. (3).

$$\begin{aligned} f' &= \boldsymbol{\Phi}' \cdot [\boldsymbol{\theta}\boldsymbol{\mu}] \\ f' &= \sum_{i=1}^{n} \theta_i \varphi(\|\mathbf{x}' - \mathbf{x}_i\|) + \mu_0 + \sum_{l=1}^{d} \mu_l \mathbf{x}'_l + \sum_{l=1}^{d} \mu_l \mathbf{x}'^2_l, \\ \mathbf{x} &\in \mathbb{R}^d \end{aligned} \tag{3}$$

Algorithm 1: SAMO-COBRA. **Input:** Objective functions $f(\mathbf{x})$, constraint function(s) $g(\mathbf{x})$, decision parameters' lower and upper bounds $[\mathbf{lb}, \mathbf{ub}] \subset \mathbb{R}^d$, reference point $\mathbf{ref} \in \mathbb{R}^k$, number of initial samples N, maximum evaluation budget N_{max}, $RBF_{kernels}$ $(\varphi) = \{cubic, gaussian, multiquadric, invquadric, invmultiquadric, thinplatespline\}$ **Output:** Evaluated feasible Pareto efficient solutions.

1 **Function** SAMO-COBRA(f, g, $[\mathbf{lb}, \mathbf{ub}]$, **ref**, N, N_{max}, $RBF_{kernels}$):
2 $\quad \mathbf{X} \leftarrow \{\mathbf{x}_1, \cdots, \mathbf{x}_N\}$ ▷ Generate initial design, $\mathbf{X} \in \mathbb{R}^{d \times N}$
3 $\quad \mathbf{F} \leftarrow f(\mathbf{X})$ ▷ Obtain objective scores, $\mathbf{F} \in \mathbb{R}^{k \times N}$
4 $\quad \mathbf{G} \leftarrow g(\mathbf{X})$ ▷ Obtain constraint scores, $\mathbf{G} \in \mathbb{R}^{m \times N}$
5 $\quad$ **for** $i \leftarrow 1$ **to** $k + m$ **do**
6 $\quad\quad RBF_i^* \leftarrow (kernel = cubic,$ PLOG$=True)$ ▷ Initialize best RBF configuration
7 $\quad$ **end**
8 $\quad$ **while** $N < N_{max}$ **do**
9 $\quad\quad \hat{\mathbf{X}} \leftarrow$ SCALE$(\mathbf{X}, [-1, 1]^d)$ ▷ Scale input space to $[-1, 1]^d$
10 $\quad\quad \tilde{\mathbf{F}} \leftarrow$ PLOG$(\mathbf{F})$ ▷ See function plog in Eq. (5)
11 $\quad\quad \tilde{\mathbf{G}} \leftarrow$ PLOG$(\mathbf{G})$ ▷ See function plog in Eq. (5)
12 $\quad\quad \hat{\mathbf{F}} \leftarrow$ STANDARDIZE$(\mathbf{F})$ ▷ Standardize objective space
13 $\quad\quad \hat{\mathbf{G}} \leftarrow$ SCALE CONSTRAINT$(\mathbf{G})$ ▷ 0 remains feasibility boundary
14 $\quad\quad$ **for** $\varphi \in RBF_{kernels}$ **do** ▷ For each kernel
15 $\quad\quad\quad$ **for** $i \leftarrow 1$ **to** k **do** ▷ For each objective
16 $\quad\quad\quad\quad \hat{S}_i^{\varphi} \leftarrow$ FITRBF$(\hat{\mathbf{X}}, \hat{\mathbf{F}}_{(i,\cdot)}, \varphi)$ ▷ Fit RBF with standardized objective values
17 $\quad\quad\quad\quad \tilde{S}_i^{\varphi} \leftarrow$ FITRBF$(\hat{\mathbf{X}}, \tilde{\mathbf{F}}_{(i,\cdot)}, \varphi)$ ▷ Fit RBF with PLOG transformed objective values
18 $\quad\quad\quad$ **end**
19 $\quad\quad\quad$ **for** $j \leftarrow 1$ **to** m **do** ▷ For each constraint
20 $\quad\quad\quad\quad \hat{S}_{k+j}^{\varphi} \leftarrow$ FITRBF$(\hat{\mathbf{X}}, \hat{\mathbf{G}}_{(j,\cdot)}, \varphi)$ ▷ Fit RBF with scaled constrained scores
21 $\quad\quad\quad\quad \tilde{S}_{k+j}^{\varphi} \leftarrow$ FITRBF$(\hat{\mathbf{X}}, \tilde{\mathbf{G}}_{(j,\cdot)}, \varphi)$ ▷ Fit RBF with PLOG transformed constraint values
22 $\quad\quad\quad$ **end**
23 $\quad\quad$ **end**
24 $\quad\quad S^* \leftarrow \left\{ S_i^{(RBF_i^*)} \mid \forall i = 1, \ldots, (k+m) \right\}$ ▷ Apply best RBF configuration defined on line 32
25 $\quad\quad \mathbf{PF} \leftarrow$PARETO$(\mathbf{X}, \mathbf{F}, \mathbf{G})$ ▷ PF indicator see Def. 1, $\mathbf{PF} \in \{0, 1\}^N$
26 $\quad\quad \mathbf{x}^* \leftarrow$ MAXIMIZE(HV, **PF**, **ref**, S^*) ▷ Get best solution based on HV contribution, see Section 3.4
27 $\quad\quad \mathbf{x}_{new} \leftarrow$ SCALE$(\mathbf{x}^*, [\mathbf{lb}, \mathbf{ub}])$ ▷ Scale to original scale
28 $\quad\quad N \leftarrow N + 1$ ▷ Increase iteration counter to new matrix sizes
29 $\quad\quad \mathbf{X} \leftarrow [\mathbf{X}\ \mathbf{x}_{new}]$ ▷ Add new solution, $\mathbf{X} \in \mathbb{R}^{d \times N}$
30 $\quad\quad \mathbf{F} \leftarrow [\mathbf{F}\ f(\mathbf{x}_{new})]$ ▷ Add evaluated objectives, $\mathbf{F} \in \mathbb{R}^{k \times N}$
31 $\quad\quad \mathbf{G} \leftarrow [\mathbf{G}\ g(\mathbf{x}_{new})]$ ▷ Add evaluated constraints, $\mathbf{G} \in \mathbb{R}^{m \times N}$
32 $\quad\quad RBF^*, \mathbf{SE} \leftarrow$SELECTBESTRBF$(\mathbf{SE}, S, \mathbf{x}^*, \mathbf{F}, \mathbf{G}, \mathbf{PF}, N)$ ▷ Get best RBF configuration, see Section 3.6
33 $\quad$ **end**
34 **return** $(\mathbf{F}_{(\cdot,\mathbf{PF})}, \mathbf{G}_{(\cdot,\mathbf{PF})}, \mathbf{X}_{(\cdot,\mathbf{PF})})$

3.3 Scaling

In SAMO-COBRA, various scaling and transformation functions are used in lines 9-13 of the algorithm. This is done to improve the predictive accuracy of the RBF surrogate models. The four functions SCALE, PLOG, STANDARDIZE and the SCALE CONSTRAINT are described below.

SCALE: The input space/decision variables are scaled into the range $[-1, 1]$ with $x = 2 \cdot (x - x_{lb})/(x_{ub} - x_{lb}) - 1$. By scaling large values in the input space, computationally singular (ill-conditioned) coefficient matrices in Eq. (1) can be prevented. In case the large values in the input space are kept, the linear equation solver will terminate with an error, or it will result in a large root mean square error [3]. Additionally, when fitting the RBFs, a small change in one of the variables, is relatively the same small change in all the other variables, making each variable in the basis equally important and equally sensitive.

STANDARDIZE: The relationship between the input space and the objective function values is modelled with RBF surrogates. Besides this relationship, Bagheri et al. also exploited similarities between RBF and Kriging surrogates to come up with an uncertainty quantification method [2]. The formula for this uncertainty quantification method is given in Eq. (4).

$$\widehat{U}_{RBF} = \varphi(\|\mathbf{x}' - \mathbf{x}'\|) - \mathbf{\Phi}'^{\top} \mathbf{\Phi}^{-1} \mathbf{\Phi}' \tag{4}$$

The uncertainty ($\widehat{U}_{RBF}$) of solutions far away from earlier evaluated solutions is higher compared to so-

lutions close to earlier evaluated solutions. This uncertainty quantification method can therefore help in exploration and prevent the algorithm from getting stuck in a local optimal solution. However, as can be derived from Eq. (4), the uncertainty quantification method is only dependent on the input space and not on the scale of the objective and/or weights of the RBF models. The objective values are therefore standardized as $y' = (y - \bar{y})/\sigma$ so that the uncertainty scale and the objective scale match. Here σ is the standard deviation of y, and $\bar{y}$ the mean of y.

Scale Constraint: The constraint evaluation function should return a continuous value, namely the amount by which the constraint is violated. Since it is possible to have multiple constraints, and each constraint is equally important, every constraint output is scaled with $c' = c/(\max(c) - \min(c))$, where $\max(c)$ is the maximum constraint violation encountered so far, and $\min(c)$ is the smallest constraint value seen so far. After scaling, the difference between $\min(c)$ and $\max(c)$ becomes 1, for all constraints, making every constraint equally important while 0 remains the feasibility boundary.

Plog: In cases where there are very steep slopes, a logarithmic transformation of the objective and/or constraint scores can be beneficial for the predictive accuracy [31]. Therefore, the scores are transformed with the Plog transformation function. The extension to a matrix argument $\mathbf{Y}$ is defined componentwise, i.e., each matrix element y_{ij} is subject to Plog.

$$\text{Plog}(y) = \begin{cases} +\ln(1+y), & \text{if} \quad y \geq 0 \\ -\ln(1-y), & \text{if} \quad y < 0 \end{cases} \tag{5}$$

3.4 Maximize Hypervolume Contribution

After modelling the relationship between the input space and the response variables with the RBFs, the RBFs are used as cheap surrogates. For each constraint and objective the best RBF configuration is chosen as described in Section 3.6. By using Eq. (3) for each unseen input $\mathbf{x}'$ every corresponding constraint and objective prediction can be calculated. The COBYLA (Constrained Optimization BY Linear Approximations) algorithm [29] is then used to search for a new feasible Pareto-optimal solution $\mathbf{x}' \in [\mathbf{lb}, \mathbf{ub}]$. This is achieved by maximizing the HV a solution $\mathbf{x}'$ adds to the HV between a predefined reference point and the already evaluated solutions on the PF (Line 26 of Algorithm 1). The HV contribution of a solution to the PF is computed with two infill criteria:

1. Compute all objective scores for a given solution $\mathbf{x}'$ with Eq. (3). Then with the interpolated objective scores compute the additional Predicted HV (PHV) score this solution adds to the PF.
2. Compute all objective scores for a given solution $\mathbf{x}'$ with Eq. (3) and subtract the uncertainty of each objective given $\mathbf{x}'$ and Eq. (4), which is similar to the Kriging $\mathcal{S}$-metric Selection (SMS) criterion from Emmerich et al. [6].

Besides the highest possible SMS or PHV score, the potential solution should not violate any of the constraints. This can easily be checked by using the RBF surrogates of the constraints and Eq. (3). COBYLA then searches for a solution which does not violate any of the constraints and has the highest SMS or PHV score. If no feasible solution can be found, the solution with the smallest constraint violation is evaluated. The best candidate is then evaluated on the real objective and constraint functions (Lines 27-31 of Algorithm 1).

3.5 Surrogate Exploration and RBF adaptation Rules

The surrogate search budget and the number of starting points are updated and optimized every iteration. This is done to limit the time spend on exploring the surrogates and to further increase the chance of finding a solution that adds the most HV to the PF. The problem characteristics (number of variables, constraints, and objectives) influences the optimization problem complexity. Therefore, in the first iteration of SAMO-COBRA, the surrogate evaluation budget and number of starting points are empirically chosen and set at $50 \cdot (d+m+k)$ and $2 \cdot (d+m+k)$ respectively. In every iteration of SAMO-COBRA the convergence of COBYLA is checked. If COBYLA converges every time to a feasible solution, the number of randomly generated points is increased by 10% and the surrogate search budget is decreased by 10%. The opposite update is done if COBYLA did not converge from one of the starting points.

Because in the first iterations, the RBFs do not model the constraints very well yet, an allowed error (ϵ) of 1% for each constraint is built in. If the solution, evaluated on the real constraint function, is feasible, the error margin of this constraint approximation is reduced by 10%. If a solution is infeasible the RBFs surrogate approximation is clearly still wrong, so the error margin of the corresponding constraint is increased by 10%.

Algorithm 2: SelectBestRBF **Input: SE** Historic squared RBF approximation error, per RBF kernel, with and without PLOG transformation, for each objective, and for each constraint. S surrogate models for each kernel, with and without PLOG transformation, for each objective, and for each constraint. $\mathbf{x}^*$ last evaluated solution. **F** objective scores, **G** constraint scores, **PF** Pareto-frontier indicator vector. N number of function evaluations. **Output:** best RBF kernel, and PLOG strategy for each objective and constraint separately, and historic squared approximation errors.

Function SelectBestRBF($(\mathbf{SE}, S, \mathbf{x}^*, \mathbf{F}, \mathbf{G}, \mathbf{PF}, N)$):
  $\mathbf{ID} \leftarrow \mathbf{PF} \cup \{\mathbf{ID}_i \leftarrow 1 \mid \forall i = N-4, \ldots, N\}$ ▷ Mark last 4 and Pareto Efficient Solutions in vector
  $T \leftarrow \{T_i \leftarrow \infty \mid \forall i = 1, \ldots, (k+m)\}$ ▷ Temporary vector for smallest sum of approximation errors
  for $\varphi \in RBF_{kernels}$ **do** ▷ For each kernel
    for $i \leftarrow 1$ **to** k **do** ▷ For each objective
      $\hat{\mathbf{SE}}^{\varphi}_{i,N} \leftarrow \left(\text{INTERPOLATE}(\hat{S}^{\varphi}_i, \mathbf{x}^*) - \mathbf{F}_{i,N}\right)^2$ ▷ Error^2 of RBF trained with standardized values
      $\tilde{\mathbf{SE}}^{\varphi}_{i,N} \leftarrow \left(\text{INTERPOLATE}(\tilde{S}^{\varphi}_i, \mathbf{x}^*) - \mathbf{F}_{i,N}\right)^2$ ▷ Error^2 of RBF trained with PLOG transformed values
    end
    for $j \leftarrow 1$ **to** m **do** ▷ For each constraint
      $\hat{\mathbf{SE}}^{\varphi}_{k+j,N} \leftarrow \left(\text{INTERPOLATE}(\hat{S}^{\varphi}_{k+j}, \mathbf{x}^*) - \mathbf{G}_{j,N}\right)^2$ ▷ Error^2 of RBF trained with standardized values
      $\tilde{\mathbf{SE}}^{\varphi}_{k+j,N} \leftarrow \left(\text{INTERPOLATE}(\tilde{S}^{\varphi}_{k+j}, \mathbf{x}^*) - \mathbf{G}_{j,N}\right)^2$ ▷ Error^2 of RBF trained with PLOG transformed values
    end
    for $i \leftarrow 1$ **to** $k+m$ **do** ▷ For each constraint and objective find best RBF kernel and PLOG strategy
      if $(\sum_{n=1}^{N} \mathbf{ID}_n \cdot \hat{\mathbf{SE}}^{\varphi}_{i,n}) < T_i$ **then** ▷ If cumulative sum of marked solutions is smaller then temp
        $T_i \leftarrow \sum_{n=1}^{N} \mathbf{ID}_n \cdot \hat{\mathbf{SE}}^{\varphi}_{i,n}$ ▷ Store sum of smallest approximation errors in temp
        $RBF^*_i \leftarrow (kernel = \varphi, \text{PLOG}{=}False)$ ▷ Store best RBF kernel and PLOG strategy
      if $(\sum_{n=1}^{N} \mathbf{ID}_n \cdot \tilde{\mathbf{SE}}^{\varphi}_{i,n}) < T_i$ **then** ▷ If cumulative sum of marked solutions is smaller then temp
        $T_i \leftarrow \mathbf{ID}_n \cdot \tilde{\mathbf{SE}}^{\varphi}_{i,n}$ ▷ Store sum of smallest approximation errors in temp
        $RBF^*_i \leftarrow (kernel = \varphi, \text{PLOG}{=}True)$ ▷ Store best RBF kernel and PLOG strategy
    end
  end
return $(RBF_*, \mathbf{SE})$

3.6 Select Best RBF

In every iteration, the best RBF kernel and transformation strategy is chosen (Line 32 of Algorithm 1). The pseudocode of this function can be found in Algorithm 2. Finding the best RBF kernel and transformation strategy is done by computing the difference between the RBF interpolated solution and the solution computed with the real constraint and objective functions. This difference is computed every iteration, resulting in a list of historical RBF approximation errors for each constraint and objective function, for each kernel, with and without the PLOG transformation.

Based on the RBF approximation errors, the best RBF kernel and transformation are chosen. Bagheri et al. show empirically that if only the last approximation error is considered, in the single objective case, the algorithm converged to the best solution faster [1]. This is the case because when closer to the optimum, the vicinity of the last solution is the most important. In the multi-objective case, the vicinities of all the feasible Pareto-optimal solutions are important. We therefore experimented with this and confirmed that the approximation errors of the feasible Pareto-optimal solutions and the last four solutions should be considered. The approximation error of the last four solutions make sure that the algorithm does not get stuck on one RBF configuration and the error of the Pareto efficient solutions make sure that all the vicinity of the optimal solutions are considered. The Mean Squared Error measure is used to quantify which RBF kernel and which transformation function in the previous iterations resulted in the smallest approximation error.

4 Experimental Setup

Two experiments are setup to compare SAMO-COBRA with other state of the art algorithms. In these experiments, two variants of the SAMO-COBRA algorithm are tested, one without the uncertainty quantification method (PHV), and one with the uncertainty quantification method (SMS). The performance of the two variants are compared to the performance of the following algorithms: CEGO [41], IC-SA-NSGA-II [8], SA-NSGA-II [8], NSGA-II [14], NSGA-III [23], and SMES-RBF [11]. All the algorithms except for SMES-RBF are tested on 18 academic benchmark functions. SMES-RBF is not tested on all functions since the implementa-

Table 1 Test functions with citation, the reference points, the number of objectives k, number of parameters d, number of constraints m and feasibility percentage $P(\%)$ based on 1 million random samples.

Function	Reference point	k	d	m	P(%)
BNH [10]	(140, 50)	2	2	2	96.92
CEXP [12]	(1, 9)	2	2	2	57.14
SRN [15]	(301, 72)	2	2	2	16.18
TNK [15]	(2, 2)	2	2	2	5.05
CTP1 [12]	(1, 2)	2	2	2	92.67
C3DTLZ4 [36]	(3, 3)	2	6	2	22.22
OSY [10,15]	(0,386)	2	6	6	2.78
TBTD [18]	(0.1, 50000)	2	3	2	19.46
NBP [17]	(11150, 12500)	2	2	5	41.34
DBD [18]	(5,50)	2	4	5	28.55
SPD [27]	(16, 19000, -260000)	3	6	9	3.27
CSI [23]	(42, 4.5, 13)	3	7	10	18.17
SRD [26]	(7000, 1700)	2	7	10	96.92
WB [18]	(350, 0.1)	2	4	5	35.28
BICOP1 [11]	(9, 9)	2	10	1	100
BICOP2 [11]	(70, 70)	2	10	2	10.55
TRIPCOP [11]	(34, -4, 90)	3	2	3	15.85
WP [23]	(83000, 1350, 2.85, 15989825, 25000)	5	3	7	92.06

tion of SMES-RBF has not been made available and as such it could only be compared to the results reported in the SMES-RBF publication.

The 18 test functions and there characteristics are listed in Table 1. Some of the problems are real-world-like-problems while others are artificially created benchmark problems proposed by several authors over the past years [36]. Each algorithm is tested 10 times on every test function to get a trustworthy result. The results for NSGA-II, and NSGA-III had a high variance, we therefore used 100 runs for those algorithms. In the first experiment, the algorithms are given a fixed budget to find a feasible Pareto-frontier. In the second experiment the algorithms are evaluated to see how many function evaluations they require to achieve a predefined threshold performance.

Hyper Parameter Settings

In the experiments for each algorithm either the original implementation is used or an implementation which was readily available in Python. For all algorithms, the recommended hyper parameters from the original implementations are used. Since there are no clear recommendations for the hyper parameters of NSGA-II and NSGA-III a grid search is conducted. In the grid search the optimal population size and number of generations is determined for NSGA-II. For NSGA-III a grid search is done to find the best parameter value for the number of divisions that influence the spacing of the reference points of NSGA-III. For the sake of brevity, only the results with the best scores from this grid search are reported.

The implementations of the different algorithms are listed here: The original implementation of CEGO can be found on the dedicated Github page[1]. The original implementation of IC-SA-NSGA-II and SA-NSGA-II can be found on the personal page of Julian Blank[2]. For NSGA-II, and NSGA-III the implementation of Platypus is used[3]. The implementation of the SMES-RBF algorithm is not provided. Therefore only the reported results from the SMES-RBF paper [11] can be compared.

More details concerning the implementation of SAMO-COBRA, the experiments, and the statistical comparison can be found on Github [38].

4.1 Fixed Budget Experiment

In the first experiment, each algorithm was given a limited fixed number of function evaluation after which the HV performance metric is computed [7]. Each algorithm is allowed to do $40 \cdot d$ function evaluations, here d is the number of decision variables of the optimization test function.

The HV metric is selected as the performance metric to quantify the results. The HV metric is selected because it simultaneously measures accuracy and diversity, and because it is the most common performance metric [33]. The HV is computed between the obtained Feasible Pareto-optimal solutions and the reference point reported in Table 1. Higher HV scores mean that more HV is covered and therefore a better approximation is found of the Pareto-frontier.

4.2 Convergence Experiment

In the second experiment, each algorithm is tested to see when it reaches a threshold value of the HV metric. The threshold is set to 95% of the maximum achievable HV per test function between the reference points in Table 1 and the Pareto-frontier. Since the Pareto-front is not known for every function, NSGA-II is used to find the maximal HV between a reference point and the Pareto-frontier by running it with a population size of $100 \cdot d$ and allowing the algorithm to run for 1000 generations.

For each algorithm, after each iteration or generation the HV is computed. As soon as the threshold value is achieved the number of function evaluations are used as the evaluation metric.

[1] `https://github.com/RoydeZomer/CEGO`

[2] `https://julianblank.com/static/misc/pycheapconstr.zip`

[3] `https://platypus.readthedocs.io/`

4.2.1 SMES-RBF Convergence Experiment

To be able to compare the results of SMES-RBF with the results of SAMO-COBRA, a different experiment is conducted. In this experiment the number of function evaluations are compared between SAMO-COBRA and SMES-RBF to achieve the HV as reported in the SMES-RBF paper [11].

5 Results

The complete set of results from the experiments can be found on Github [38]. It is important to keep in mind when analysing the results that IC-SA-NSGA-II in contrary to the other algorithms uses much more constraint function evaluations.

5.1 Fixed Budget Experiment Results

The results of the first experiment, in which the HV is computed after $40 \cdot d$ function evaluations, can be found in Table 2. A Wilcoxon rank-sum test with Bonferroni correction is used to determine if there is a significant difference between the algorithm with the best results compared to the algorithm with the lesser results.

Interestingly enough, the SAMO-COBRA with the predicted HV infill criterion (PHV) is in 16 out of the 18 test functions outperforming most of the state-of-the art algorithms with the exception of the SAMO-COBRA SMS variant. Only on the *WB* and *C3DTLZ4* test function the IC-SA-NSGA-II algorithm finds a significantly larger HV score. However, for the IC-SA-NSGA-II algorithm only the objective function evaluations are counted and not the constraint function calls. It is therefore not remarkable that for some test functions IC-SA-NSGA-II finds a higher HV.

Inspection showed that IC-SA-NSGA-II uses 10 000 constraint function evaluations to find a well spread feasible initial sample, after which IC-SA-NSGA-II starts optimizing. In total IC-SA-NSGA-II used on average 10537 and 10776 constraint function evaluations for respectively the *WB* and *C3DTLZ4* test functions to obtain the Pareto-frontier.

5.2 Convergence Experiment Results

In Table 3 the number of function evaluations are reported that are required to achieve the 95% threshold value of the maximum HV. For some test functions this was very easy to achieve since it only required to evaluate the initial sample. On other test functions the algorithms required much more evaluations to achieve the threshold. Important to note is that again for IC-SA-NSGA-II only the objective function calls are reported and not the constrained function evaluations.

NSGA-II and NSGA-III are terminated after 5000 function evaluations on the *C3DLTZ4*, *OSY*, *SPD*, and *SRD* test function. CEGO was not able to obtain the threshold value for the *SPD* and *CSI* function within 24 hours.

As can be seen in Table 3, SAMO-COBRA with the Predicted HV (PHV) infill criterion again outperforms the other algorithms for the majority of the test functions. This is interesting since this infill criterion is designed to be exploitative.

5.2.1 SMES-RBF Convergence Experiment Results

As mentioned before, the implementation of SMES-RBF is not provided, therefore the reported results of SMES-RBF are compared with the results of SAMO-COBRA. In Table 4 the number of function evaluations are reported that are required to obtain the same hypervolume as reported in the SMES-RBF paper.

As you can see in Table 4, the number of function evaluations of SAMO-COBRA is much smaller. Remarkable enough the HV results for the BICOP1 test function after 1000, 2000, and 5000 function evaluations of SMES-RBF reported in the original paper are, given the Nadir point, not possible.

To further inspect the performance of the algorithms over time, convergence plots are made for the BNH and TRICOP test function. The convergence plots show the HV computed in each iteration. In this experiment the same estimation of Nadir points as in the original SMES-RBF paper [11] are used as the reference points. The convergence of the HV on the BNH test function can be found in Figure 1. The convergence of the HV on the TRICOP test function can be found in Figure 2.

5.3 PHV vs SMS infill criterion

Interesting conclusion from all the experiments is that that the exploiting strategy of the PHV infill criterion leads in most cases to the highest HV and to the least number of required function evaluations to obtain the 95% threshold. It is no surprise that this exploiting strategy works well in a constrained multi-objective setting since a similar effect was already shown by Rehbach et al. [32]. In this paper, the authors show that in the single objective case, it is only useful to include an expected improvement infill criterion, if the dimensionality of the problem is low, if it is multimodal, and if the algorithm can get stuck in a local optimum. With the results as presented in Table 2 and Table 3 we

Table 2 Mean HV after $40 \cdot d$ function evaluations for each algorithm on each test function. Note that for IC-SA-NSGA-II only the objective function evaluations are counted. PHV and SMS represents the SAMO-COBRA variants. The highest mean HV per test function are presented in **bold**. The Wilcoxon rank-sum test (with Bonferroni correction) significance is represented with a grayscale. Background colours represent: $p \leq 0.001$, $p \leq 0.01$, $p \leq 0.05$. Red shows that the algorithm took more than 24 hours.

Function	PHV	SMS	CEGO	IC-SA-NSGA-II	SA-NSGA-II	NSGA-II	NSGA-III
BNH	**5256.0**	5251.0	5218.0	5154.6	5158.3	5089.7	4848.8
CEXP	**3.7968**	3.7967	3.7658	3.7072	3.6749	3.1544	2.9561
SRN	**62385**	62377	62307	61074	60767	54233	52585
TNK	8.0430	**8.0474**	8.0309	8.0033	7.8031	6.4282	6.2948
CTP1	**1.3026**	1.3023	1.2972	1.2941	1.2924	1.1929	1.1864
C3DTLZ4	6.3016	6.4697	6.2664	**6.6326**	5.9269	5.2489	5.2500
OSY	**100577**	100458	100181	96978	96889	46631	42204
TBTD	4029.3	4027.5	**4055.0**	4026.3	3841.9	3421.5	3446.0
NBP	$\mathbf{1.0785 \cdot 10^{8}}$	$1.0785 \cdot 10^{8}$	$1.0784 \cdot 10^{8}$	$1.0740 \cdot 10^{8}$	$1.0552 \cdot 10^{8}$	$9.8573 \cdot 10^{7}$	$9.5816 \cdot 10^{7}$
DBD	**228.77**	228.34	227.85	227.25	227.80	218.47	218.33
SPD	$\mathbf{3.8859 \cdot 10^{10}}$	$3.7602 \cdot 10^{10}$	$3.4057 \cdot 10^{10}$	$3.6956 \cdot 10^{10}$	$3.6939 \cdot 10^{10}$	$2.6069 \cdot 10^{10}$	$2.5689 \cdot 10^{10}$
CSI	**27.800**	25.167	*terminated*	25.605	25.532	17.296	16.993
SRD	**4205165**	4164992	4148333	4200148	4198861	2766367	2673599
WB	34.395	34.392	34.522	**34.618**	34.457	34.0270	33.995
BICOP1	**80.664**	78.160	*terminated*	80.618	80.635	67.6506	70.911
BICOP2	**4834.33**	4822.13	*terminated*	4826.74	4816.30	4816.12	4816.72
TRIPCOP	20610	**20611**	20609	20568	20544	20101	19982
WP	$\mathbf{1.5991 \cdot 10^{19}}$	$1.5698 \cdot 10^{19}$	$1.5350 \cdot 10^{19}$	$1.4173 \cdot 10^{19}$	$1.3903 \cdot 10^{19}$	$1.1623 \cdot 10^{19}$	$1.1797 \cdot 10^{19}$

Table 3 Test Function, Threshold Hypervolume, and number of function evaluations required to achieve this threshold per optimization algorithm. The results of the algorithm with the smallest number of function evaluations are reported in bold and accompanied with a ↑. PHV and SMS represents the SAMO-COBRA variants. Experiments that required more than 5000 function evaluations or more than 24 hours are terminated.

Function	Threshold	PHV	SMS	CEGO	IC-SA-NSGA-II	SA-NSGA-II	NSGA-II	NSGA-III
BNH	5005.5	**11** ↑	16	12	31	36	56	114
CEXP	3.6181	**13** ↑	16	23	61	71	392	404
SRN	59441	**15** ↑	**15** ↑	17	36	66	200	227
TNK	7.6568	11	**9**↑	**9** ↑	21	66	432	586
CTP1	1.2398	**10** ↑	14	14	26	36	140	170
C3DTLZ4	6.4430	179	181	226	**100** ↑	275	+5000	+5000
OSY	95592	**15** ↑	31	16	110	105	+5000	+5000
TBTD	3925	**31** ↑	58	49	47	357	324	369
NBP	1.024E8	**5** ↑	9	6	21	36	102	206
DBD	217.31	**13** ↑	19	16	43	48	112	142
SPD	3.6887E10	**43** ↑	125	-	185	205	+5000	+5000
CSI	25.717	**59** ↑	484	-	276	376	+5000	+5000
SRD	3997308	**17** ↑	55	28	81	81	952	1357
WB	32.9034	**7** ↑	10	10	43	43	24	24
BICOP1	76.6328	**22** ↑	25	35	114	119	1700	1975
BICOP2	4606.57	17	18	18	109	109	**10** ↑	12
TRIPCOP	19578.0	**7** ↑	8	**7** ↑	21	21	42	8
WP	1.5147E19	**48** ↑	66	111	232	292	3120	3876

can give an advice based on empirical results, as follows: When searching for a set of Pareto-optimal solutions, an uncertainty quantification method should not be used. This is due to the fact that, when searching for a trade-off between objectives, the algorithm is forced to explore more of the objective space in the different objectives, making it less likely to get stuck in a local optimum, and making the uncertainty quantification method redundant.

6 Real World Application

SAMO-COBRA has been used in practice to design a wind feeder vessel to support the installation of windmills on sea. Although strong winds are good for power production, they usually also result in rough seas. These rough seas around the wind park installation sites increases the demand for reliable vessels. An example of such a reliable vessel (See Figure 3) has been designed and later optimized with SAMO-COBRA at C-

Table 4 Number of function evaluations after which SAMO-COBRA with PHV infill criterion achieved same hypervolume for test functions as SMES-RBF.

Function	SMES-RBF	PHV-SAMO-COBRA
BNH	200	50
BNH	500	122
SRN	200	23
SRN	500	27
TNK	200	24
TNK	500	194
OSY	500	14
OSY	1000	14
OSY	2000	14
TRICOP	200	12
TRICOP	500	12
BICOP1	500	56
BICOP2	500	31
BICOP2	1000	31
BICOP2	2000	38
BICOP2	5000	82

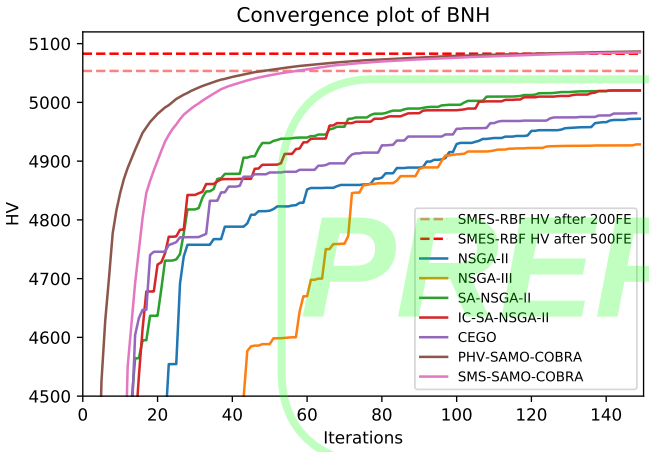

Fig. 1 Convergence plot of BNH test problem for NSGA-II, NSGA-III, SA-NSGA-II, IC-SA-NSGA-II, CEGO, PHV-SAMO-COBRA, SMS-SAMO-COBRA. The dashed lines represents final obtained Hypervolume of SMES-RBF after 200 and 500 function evaluations.

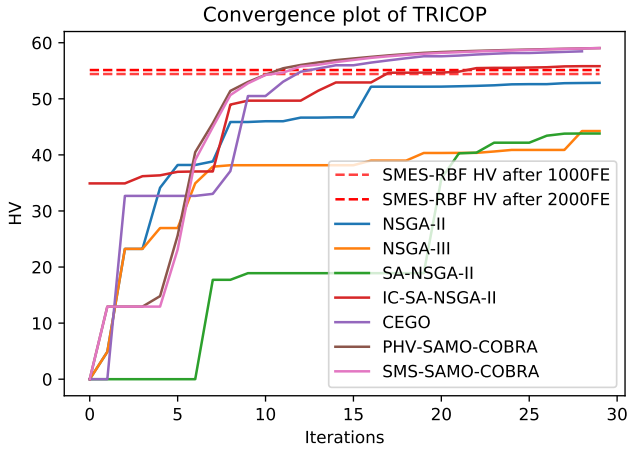

Fig. 2 Convergence plot of TRICOP test problem for NSGA-II, NSGA-III, SA-NSGA-II, IC-SA-NSGA-II, CEGO, PHV-SAMO-COBRA, SMS-SAMO-COBRA. The dashed lines represents final obtained Hypervolume of SMES-RBF after 1000 and 2000 function evaluations.

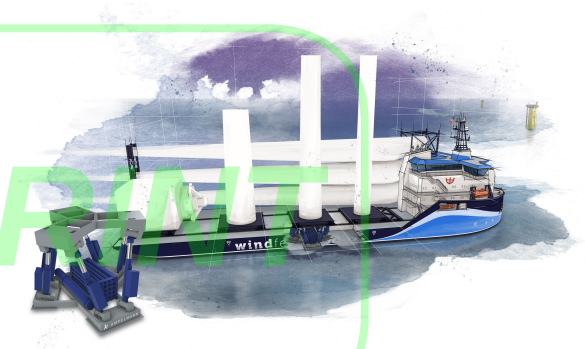

Fig. 3 Impression of Wind Feeder Vessel design by C-Job Naval Architects.

Job Naval Architects[4]. This vessel is designed to support the construction of wind farms and for the transportation of goods from shore to the installation sites.

The objectives of the optimization case of the wind feeder vessel are to have a robust seakeeping performance to maximize the year-round operability while keeping the operational cost and capital expenses at a minimum. The operability can be optimized by maximizing the so-called Operability Robustness Index (ORI) [20]. The seakeeping assessment is done with a strip theory code of NAPA[5]. Strip theory is proven to be fast and reliable with a sufficient accuracy for conventional hull forms [5,19]. The capital expenses can be translated into the cost of steel that is required to build the vessel; this is roughly equal to the Lightship Weight (LSW) of the vessel. The LSW is calculated by summing the weight of all the equipment plus the minimum amount of steal that is required to fulfil the longitudinal strength requirements. The operational expenses can be dealt with by minimizing the ship resistance in the water at service speed (Rt[kN]). This resistance is calculated with the Holtrop Mennen method [22].

All objectives, practical constraints, relevant rules, regulations, and loading conditions can be evaluated with the modular Accelerated Concept Design framework [39]. In this software a parametric 3D model of the ship is set up by a naval architect after which automated software tools can evaluate different design variations. In the wind feeder vessel case, five design variables are defined: *Aftship Length*, *Midship Length*, *Foreship length*, *Beam at Waterline*, and *Draught*. Since sea-

[4] Dedicated Naval Architects, https://c-job.com/

[5] Intelligent solutions for the maritime industry, https://www.napa.fi/

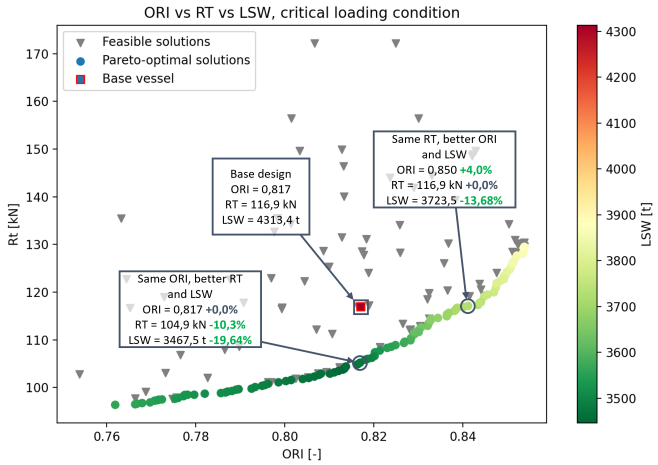

Fig. 4 Pareto Frontier of Ship Design case with Original Design by human expert represented by a square. Objectives are maximize the Operability Robustness Index (ORI[-]), minimize ship resistance (Rt [kN]), and minimize Lightship Weight (LSW[t]).

keeping and longitudinal strength are already captured in the objectives, only two constraints are needed. The two constraints are for space reservation of the wind turbine blades, and there is a constraint on the metacentric height for intact stability of the vessel.

SAMO-COBRA is then used to optimize this ship design optimization problem. To enhance the exploration in this case study, SAMO-COBRA started with 50 initial Halton samples, and the PHV infill criterion is used in the following 250 iterations to obtain a final Pareto frontier.

After analysing the results from the optimization study, the base design by the naval architect was shown to be much too large causing the ship to be too heavy, with a sub-optimal performance. If we zoom in on two solutions and compare them with the original, then the solution with the same ORI score has a 10.3% smaller resistance value, and 19.64% less light ship weight. The solution with the same resistance score has a 4% better ORI score, and 13.68% less light ship weight. All the evaluated feasible solutions are visualized on the Pareto frontier in Figure 4.

7 Conclusion and Future Work

In this paper, two variants of the SAMO-COBRA algorithm are introduced, based on using two different infill criteria: S-Metric-Selection and Predicted Hypervolume (PHV), of which the latter is considered to be more exploitative than the former. The performance of the two SAMO-COBRA variants is compared to six other state of the art algorithms: IC-SA-NSGA-II, SA-NSGA-II, NSGA-II, NSGA-III and SMES-RBF. On 16 out of the 18 test functions, SAMO-COBRA with the PHV infill criterion showed comparative or better results. On two test functions IC-SA-NSGA-II obtained significantly better results which can be explained by the fact that IC-SA-NSGA-II uses at least 10 000 more constraint function evaluations.

The SAMO-COBRA algorithm with the PHV infill criterion showed to be very efficient in terms of function evaluations at solving constrained multi-objective optimization problems. We speculate that this exploiting infill criterion works best in most cases because of the characteristics of multi-objective problems. Because we are dealing with multi-objective problems, the algorithm is already forced to explore more of the objective space, making the uncertainty quantification method redundant.

Besides such a performance comparison on test functions, SAMO-COBRA has also already been used in practice on a ship design optimization problem with three objectives, two constraints, and five decision variables. In this application, the algorithm demonstrates its ability to outperform the human expert in all objectives simultaneously.

Further research efforts will be put into creating infill criteria which can propose multiple solutions simultaneously. This way, in each iteration evaluations can be run in parallel and wall clock time can be reduced even further. Besides parallelization, effort will be put into dealing with mixed integer decision parameters and solving multi-fidelity optimization problems.

References

1. Bagheri, S., Konen, W., Bäck, T.: Online selection of surrogate models for constrained black-box optimization. In: 2016 IEEE Symposium Series on Computational Intelligence (SSCI), pp. 1–8. IEEE (2016)
2. Bagheri, S., Konen, W., Bäck, T.: Comparing kriging and radial basis function surrogates. In: Proc. 27. Workshop Computational Intelligence, pp. 243–259 (2017)
3. Bagheri, S., Konen, W., Emmerich, M., Bäck, T.: Self-adjusting parameter control for surrogate-assisted constrained optimization under limited budgets. Applied Soft Computing **61**, 377–393 (2017). DOI 10.1016/j.asoc.2017.07.060
4. Bandaru, S., Ng, A.H., Deb, K.: Data mining methods for knowledge discovery in multi-objective optimization: Part a-survey. Expert Systems with Applications **70**, 139–159 (2017)
5. BECK, R.F., REED, A.M., SCLAVOUNOS, P.D., HUTCHISON, B.L.: Modern computational methods for ships in a seaway. discussion. author's closure. Transactions-Society of Naval Architects and Marine Engineers **109**, 1–51 (2001)
6. Beume, N., Naujoks, B., Emmerich, M.: SMS-EMOA: Multiobjective selection based on dominated hypervol-

ume. European Journal of Operational Research **181**(3), 1653–1669 (2007). DOI 10.1016/j.ejor.2006.08.008
7. Beume, N., Naujoks, B., Emmerich, M.: Sms-emoa: Multiobjective selection based on dominated hypervolume. European Journal of Operational Research **181**(3), 1653–1669 (2007)
8. Blank, J., Deb, K.: Constrained bi-objective surrogate-assisted optimization of problems with heterogeneous evaluation times: Expensive objectives and inexpensive constraints. In: H. Ishibuchi, Q. Zhang, R. Cheng, K. Li, H. Li, H. Wang, A. Zhou (eds.) Evolutionary Multi-Criterion Optimization, pp. 257–269. Springer International Publishing, Cham (2021)
9. Bossek, J., Doerr, C., Kerschke, P.: Initial design strategies and their effects on sequential model-based optimization. arXiv preprint arXiv:2003.13826 (2020)
10. Coello, C.A.C., Lamont, G.B., Van Veldhuizen, D.A., et al.: Evolutionary algorithms for solving multi-objective problems, vol. 5. Springer (2007)
11. Datta, R., Regis, R.G.: A surrogate-assisted evolution strategy for constrained multi-objective optimization. Expert Systems with Applications **57**, 270–284 (2016). DOI 10.1016/j.eswa.2016.03.044
12. Deb, K.: Multi-objective optimization using evolutionary algorithms, vol. 16. John Wiley & Sons (2001)
13. Deb, K.: Multi-objective optimisation using evolutionary algorithms: an introduction. In: Multi-objective evolutionary optimisation for product design and manufacturing, pp. 3–34. Springer (2011)
14. Deb, K., Pratap, A., Agarwal, S., Meyarivan, T.: A fast and elitist multiobjective genetic algorithm: NSGA-II. IEEE transactions on evolutionary computation **6**(2), 182–197 (2002). DOI 10.1109/4235.996017
15. Deb, K., Pratap, A., Meyarivan, T.: Constrained test problems for multi-objective evolutionary optimization. In: International conference on evolutionary multi-criterion optimization, pp. 284–298. Springer (2001). DOI 10.1007/3-540-44719-9_20
16. Fan, Z., Fang, Y., Li, W., Lu, J., Cai, X., Wei, C.: A comparative study of constrained multi-objective evolutionary algorithms on constrained multi-objective optimization problems. In: 2017 IEEE congress on evolutionary computation (CEC), pp. 209–216. IEEE (2017)
17. Forrester, A., Sobester, A., Keane, A.: Engineering design via surrogate modelling: a practical guide. John Wiley & Sons (2008). DOI 10.2514/4.479557
18. Gong, W., Cai, Z., Zhu, L.: An efficient multiobjective differential evolution algorithm for engineering design. Structural and Multidisciplinary Optimization **38**(2), 137–157 (2009). DOI 10.1007/s00158-008-0269-9
19. Gourlay, T., von Graefe, A., Shigunov, V., Lataire, E.: Comparison of aqwa, gl rankine, moses, octopus, pdstrip and wamit with model test results for cargo ship wave-induced motions in shallow water. In: International Conference on Offshore Mechanics and Arctic Engineering, vol. 56598, p. V011T12A006. American Society of Mechanical Engineers (2015)
20. Gutsch, M., Steen, S., Sprenger, F.: Operability robustness index as seakeeping performance criterion for offshore vessels. Ocean Engineering **217**, 107931 (2020)
21. Hardin, D., Saff, E.: Minimal riesz energy point configurations for rectifiable d-dimensional manifolds. Advances in Mathematics **193**(1), 174–204 (2005)
22. Holtrop, J., Mennen, G.: An approximate power prediction method. International Shipbuilding Progress **29**(335), 166–170 (1982)
23. Jain, H., Deb, K.: An evolutionary many-objective optimization algorithm using reference-point based nondominated sorting approach, part II: Handling constraints and extending to an adaptive approach. IEEE Trans. Evolutionary Computation **18**(4), 602–622 (2014). DOI 10.1109/tevc.2013.2281534
24. Knowles, J.: ParEGO: a hybrid algorithm with on-line landscape approximation for expensive multiobjective optimization problems. IEEE Transactions on Evolutionary Computation **10**(1), 50–66 (2006). DOI 10.1109/tevc.2005.851274
25. Micchelli, C.A.: Interpolation of scattered data: distance matrices and conditionally positive definite functions. Constructive approximation **2**(1), 11–22 (1986)
26. Mirjalili, S., Jangir, P., Saremi, S.: Multi-objective ant lion optimizer: a multi-objective optimization algorithm for solving engineering problems. Applied Intelligence **46**(1), 79–95 (2017). DOI 10.1007/s10489-016-0825-8
27. Parsons, M.G., Scott, R.L.: Formulation of multicriterion design optimization problems for solution with scalar numerical optimization methods. Journal of Ship Research **48**(1), 61–76 (2004). DOI 10.1007/s10489-016-0825-8
28. Ponweiser, W., Wagner, T., Biermann, D., Vincze, M.: Multiobjective optimization on a limited budget of evaluations using model-assisted $\mathcal{S}$-metric selection. In: International Conference on Parallel Problem Solving from Nature, pp. 784–794. Springer (2008). DOI 10.1007/978-3-540-87700-4_78
29. Powell, M.J.D.: A direct search optimization method that models the objective and constraint functions by linear interpolation. In: Advances in Optimization and Numerical Analysis, pp. 51–67. Springer Netherlands (1994). DOI 10.1007/978-94-015-8330-5_4
30. Regis, R.G.: Constrained optimization by radial basis function interpolation for high-dimensional expensive black-box problems with infeasible initial points. Engineering Optimization **46**(2), 218–243 (2014)
31. Regis, R.G., Shoemaker, C.A.: A quasi-multistart framework for global optimization of expensive functions using response surface models. Journal of Global Optimization **56**(4), 1719–1753 (2013). DOI 10.1007/s10898-012-9940-1
32. Rehbach, F., Zaefferer, M., Naujoks, B., Bartz-Beielstein, T.: Expected improvement versus predicted value in surrogate-based optimization. arXiv preprint arXiv:2001.02957 (2020). DOI 10.1145/3377930.3389816
33. Riquelme, N., Von Lücken, C., Baran, B.: Performance metrics in multi-objective optimization. In: 2015 Latin American Computing Conference (CLEI), pp. 1–11. IEEE (2015)
34. Santana-Quintero, L.V., Montano, A.A., Coello, C.A.C.: A review of techniques for handling expensive functions in evolutionary multi-objective optimization. Computational intelligence in expensive optimization problems pp. 29–59 (2010)
35. Singh, P., Couckuyt, I., Ferranti, F., Dhaene, T.: A constrained multi-objective surrogate-based optimization algorithm. In: 2014 IEEE Congress on Evolutionary Computation (CEC). IEEE (2014). DOI 10.1109/cec.2014.6900581
36. Tanabe, R., Oyama, A.: A note on constrained multi-objective optimization benchmark problems. In: 2017 IEEE Congress on Evolutionary Computation (CEC), pp. 1127–1134. IEEE (2017)
37. Urquhart, M., Ljungskog, E., Sebben, S.: Surrogate-based optimisation using adaptively scaled radial basis functions. Applied Soft Computing **88**, 106050 (2020)

38. de Winter, R.: Roydezomer/samo-cobra: Release with new experiments (2020). DOI 10.5281/zenodo.5105636. URL `https://doi.org/10.5281/zenodo.5105636`
39. de Winter, R., Furustam, J., Bäck, T., Muller, T.: Optimizing ships using the holistic accelerated concept design methodology. In: T. Okada, K. Suzuki, Y. Kawamura (eds.) Practical Design of Ships and Other Floating Structures, pp. 38–50. Springer Singapore, Singapore (2021)
40. de Winter, R., van Stein, B., Bäck, T.: Samo-cobra: A fast surrogate assisted constrained multi-objective optimization algorithm. In: H. Ishibuchi, Q. Zhang, R. Cheng, K. Li, H. Li, H. Wang, A. Zhou (eds.) Evolutionary Multi-Criterion Optimization, pp. 270–282. Springer International Publishing, Cham (2021)
41. de Winter, R., van Stein, B., Dijkman, M., Bäck, T.: Designing ships using constrained multi-objective efficient global optimization. In: International Conference on Machine Learning, Optimization, and Data Science, pp. 191–203. Springer (2018). DOI 10.1007/978-3-030-13709-0_16
42. Yang, Y., Liu, J., Tan, S.: A multi-objective evolutionary algorithm for steady-state constrained multi-objective optimization problems. Applied Soft Computing **101**, 107042 (2021)
43. Zitzler, E., Laumanns, M., Thiele, L.: SPEA2: Improving the strength pareto evolutionary algorithm. TIK-report **103** (2001)

E

Input US Wind Feeder Concept case study

E.1. Base hull shape

See figure E.1 for the base hull shape used in the case study.

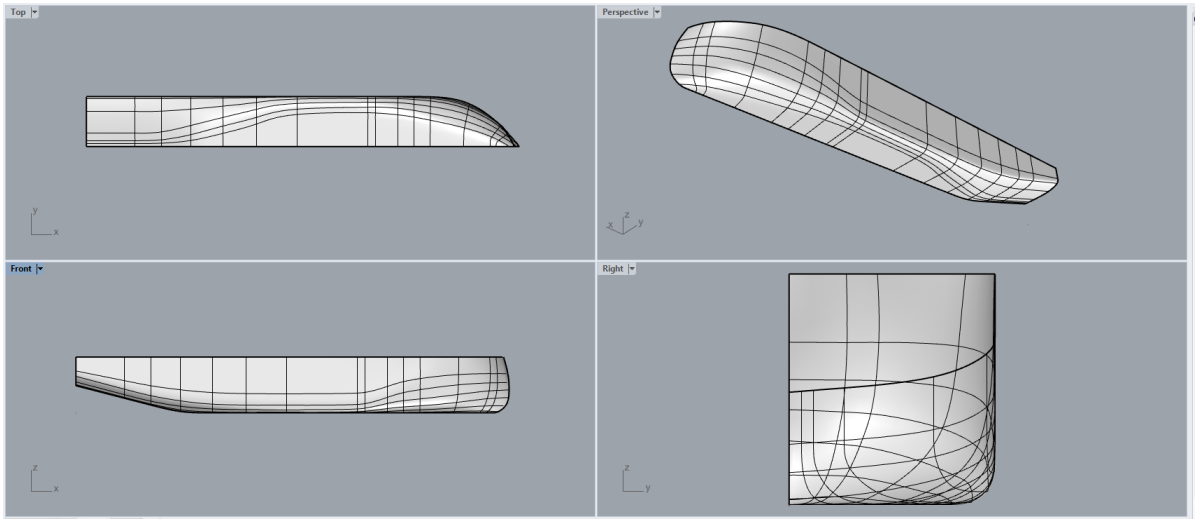

Figure E.1: Base hull shape used for US Wind Feeder case study

E.2. General parameters

Base vessel, input parameters that require to be defined			
Variable	*Symbol*	*Value*	*Unit*
Aft location midship	-	46.0	m
Forward location midship	-	69.0	m
Length between perpendiculars	L_{PP}	103.5	m
Length midship/ base bilge keel length	-	23	m
Draught	T	5.5	m
Service speed	V_S	10	kn
Height of bilge keel	$HBILGE$	0.7	m
Factor lengthening of bilge keel	-	0	%
Linear part of roll damping	$RLD1$	0.05	–
Non-linear part of roll damping	$RLD2$	0.1	–
Wave steepness factor	α	0.5	°

Table E.1: General input parameters for US Wind Feeder case study

E.3. Environmental conditions

E.3.1. Parameters for station keeping force

Station keeping force input			
Variable	*Symbol*	*Value*	*Unit*
Heading of wind and current w.r.t. aft of vessel	–	150	°
Densitiy air	ρ_{air}	0.0013	kg/m^3
Relative wind velocity	V_{air}	7.80	m/s
Transverse project wind area superstructure and load	$A_{transverse}$	650	m^2
Lateral project wind area superstructure and load	$A_{lateral}$	2400	m^2
Density water	ρ_{water}	1025	kg/m^3
Dynamic viscosity	μ	0.00089	$pa \cdot A \cdot s$
Current velocity	$V_{current}$	0.75	m/s

Table E.2: Station keeping force parameters

The significant wave height based on scatter diagram is calculated from the scatter diagram. The velocities have been based on average values [21], [91]. The air and water properties are based on values from engineering toolbox [5].

E.4. Algorithm settings

Algorithm settings		
Item	*Setting*	*Unit*
Algorithm	SAMO-COBRA	–
Initial sample generation	HALTON	–
Spreading function	PHV	–
Maximum iterations	300	#

Table E.3: Optimization settings, for more information, see appendix D. The choice of algorithm, sample generation function and spreading function is based on recommendations by R. de Winter.

E.4.1. Scatter diagram

See figure E.2 on next page.

Scatter diagram North Atlantic - Area 23, created using 2-parameter Weibull distribution based on recommendations by DNV GL DNV-RP-C205

Hs[m] \ Tz[s]	0,5	1	1,5	2	2,5	3	3,5	4	4,5	5	5,5	6	6,5	7	7,5	8	8,5	9	9,5	10	10,5	11	11,5	12	12,5	13	13,5	14	14,5	15	15,5	16	16,5	17	17,5	18	18,5	19	19,5	20	Sum	Perc
0,5	0	0	0	0	2	37	244	715	1190	1326	1103	737	418	209	94	40	16	6	2	1	0	0	0	0	0	0	0	0	0	0	0	0	0	0	0	0	0	0	0	0	6140	16%
1	0	0	0	0	0	5	60	280	698	1114	1278	1444	846	540	307	159	77	35	15	6	3	1	0	0	0	0	0	0	0	0	0	0	0	0	0	0	0	0	0	0	6568	17%
1,5	0	0	0	0	0	1	17	108	351	709	1005	1088	957	716	471	280	153	78	38	18	8	3	1	1	0	0	0	0	0	0	0	0	0	0	0	0	0	0	0	0	6002	16%
2	0	0	0	0	0	0	5	42	168	408	679	851	855	721	531	349	210	118	62	31	15	7	3	1	1	0	0	0	0	0	0	0	0	0	0	0	0	0	0	0	5058	13%
2,5	0	0	0	0	0	0	2	17	79	222	423	598	669	624	503	360	234	141	80	43	22	11	5	2	1	0	0	0	0	0	0	0	0	0	0	0	0	0	0	0	4037	11%
3	0	0	0	0	0	0	0	3	16	60	141	243	326	357	333	274	202	136	86	51	29	15	8	4	2	1	0	0	0	0	0	0	0	0	0	0	0	0	0	0	3091	8%
3,5	0	0	0	0	0	0	1	7	36	117	249	391	482	489	426	328	228	146	87	49	27	14	7	3	2	1	0	0	0	0	0	0	0	0	0	0	0	0	0	0	2288	6%
4	0	0	0	0	0	0	0	1	7	30	78	145	210	247	245	213	166	118	77	48	28	16	8	4	2	1	1	0	0	0	0	0	0	0	0	0	0	0	0	0	1646	4%
4,5	0	0	0	0	0	0	0	0	3	15	42	84	130	163	172	157	128	95	65	42	25	15	8	4	2	1	1	0	0	0	0	0	0	0	0	0	0	0	0	0	1154	3%
5	0	0	0	0	0	0	0	0	1	7	22	47	78	104	115	111	95	73	52	35	22	13	7	4	2	1	1	0	0	0	0	0	0	0	0	0	0	0	0	0	791	2%
5,5	0	0	0	0	0	0	0	0	1	3	11	26	46	64	75	75	67	54	40	27	18	11	6	4	2	1	1	0	0	0	0	0	0	0	0	0	0	0	0	0	531	1%
6	0	0	0	0	0	0	0	0	0	2	6	14	26	38	47	49	46	38	29	21	14	9	5	3	2	1	0	0	0	0	0	0	0	0	0	0	0	0	0	0	350	1%
6,5	0	0	0	0	0	0	0	0	0	1	3	7	14	22	29	32	30	26	21	15	10	7	4	2	1	1	0	0	0	0	0	0	0	0	0	0	0	0	0	0	227	1%
7	0	0	0	0	0	0	0	0	0	1	1	4	8	13	17	20	19	17	14	11	7	5	3	2	1	1	0	0	0	0	0	0	0	0	0	0	0	0	0	0	144	0%
7,5	0	0	0	0	0	0	0	0	0	0	1	2	4	7	10	12	12	11	9	7	5	4	2	1	1	0	0	0	0	0	0	0	0	0	0	0	0	0	0	0	91	0%
8	0	0	0	0	0	0	0	0	0	0	0	1	2	4	6	7	8	7	6	5	4	2	1	1	0	0	0	0	0	0	0	0	0	0	0	0	0	0	0	0	56	0%
8,5	0	0	0	0	0	0	0	0	0	0	0	0	1	2	3	4	5	4	4	3	2	2	1	1	0	0	0	0	0	0	0	0	0	0	0	0	0	0	0	0	34	0%
9	0	0	0	0	0	0	0	0	0	0	0	0	1	1	2	2	3	3	2	2	2	1	1	0	0	0	0	0	0	0	0	0	0	0	0	0	0	0	0	0	21	0%
9,5	0	0	0	0	0	0	0	0	0	0	0	0	0	1	1	2	2	2	1	1	1	1	1	0	0	0	0	0	0	0	0	0	0	0	0	0	0	0	0	0	12	0%
10	0	0	0	0	0	0	0	0	0	0	0	0	0	0	1	1	1	1	1	1	1	0	0	0	0	0	0	0	0	0	0	0	0	0	0	0	0	0	0	0	7	0%
10,5	0	0	0	0	0	0	0	0	0	0	0	0	0	0	0	1	1	1	1	0	0	0	0	0	0	0	0	0	0	0	0	0	0	0	0	0	0	0	0	0	4	0%
11	0	0	0	0	0	0	0	0	0	0	0	0	0	0	0	0	0	0	0	0	0	0	0	0	0	0	0	0	0	0	0	0	0	0	0	0	0	0	0	0	2	0%
11,5	0	0	0	0	0	0	0	0	0	0	0	0	0	0	0	0	0	0	0	0	0	0	0	0	0	0	0	0	0	0	0	0	0	0	0	0	0	0	0	0	1	0%
12	0	0	0	0	0	0	0	0	0	0	0	0	0	0	0	0	0	0	0	0	0	0	0	0	0	0	0	0	0	0	0	0	0	0	0	0	0	0	0	0	1	0%
12,5	0	0	0	0	0	0	0	0	0	0	0	0	0	0	0	0	0	0	0	0	0	0	0	0	0	0	0	0	0	0	0	0	0	0	0	0	0	0	0	0	0	0%
13	0	0	0	0	0	0	0	0	0	0	0	0	0	0	0	0	0	0	0	0	0	0	0	0	0	0	0	0	0	0	0	0	0	0	0	0	0	0	0	0	0	0%
13,5	0	0	0	0	0	0	0	0	0	0	0	0	0	0	0	0	0	0	0	0	0	0	0	0	0	0	0	0	0	0	0	0	0	0	0	0	0	0	0	0	0	0%
14	0	0	0	0	0	0	0	0	0	0	0	0	0	0	0	0	0	0	0	0	0	0	0	0	0	0	0	0	0	0	0	0	0	0	0	0	0	0	0	0	0	0%
14,5	0	0	0	0	0	0	0	0	0	0	0	0	0	0	0	0	0	0	0	0	0	0	0	0	0	0	0	0	0	0	0	0	0	0	0	0	0	0	0	0	0	0%
15	0	0	0	0	0	0	0	0	0	0	0	0	0	0	0	0	0	0	0	0	0	0	0	0	0	0	0	0	0	0	0	0	0	0	0	0	0	0	0	0	0	0%
15,5	0	0	0	0	0	0	0	0	0	0	0	0	0	0	0	0	0	0	0	0	0	0	0	0	0	0	0	0	0	0	0	0	0	0	0	0	0	0	0	0	0	0%
16	0	0	0	0	0	0	0	0	0	0	0	0	0	0	0	0	0	0	0	0	0	0	0	0	0	0	0	0	0	0	0	0	0	0	0	0	0	0	0	0	0	0%
16,5	0	0	0	0	0	0	0	0	0	0	0	0	0	0	0	0	0	0	0	0	0	0	0	0	0	0	0	0	0	0	0	0	0	0	0	0	0	0	0	0	0	0%
17	0	0	0	0	0	0	0	0	0	0	0	0	0	0	0	0	0	0	0	0	0	0	0	0	0	0	0	0	0	0	0	0	0	0	0	0	0	0	0	0	0	0%
17,5	0	0	0	0	0	0	0	0	0	0	0	0	0	0	0	0	0	0	0	0	0	0	0	0	0	0	0	0	0	0	0	0	0	0	0	0	0	0	0	0	0	0%
18	0	0	0	0	0	0	0	0	0	0	0	0	0	0	0	0	0	0	0	0	0	0	0	0	0	0	0	0	0	0	0	0	0	0	0	0	0	0	0	0	0	0%
18,5	0	0	0	0	0	0	0	0	0	0	0	0	0	0	0	0	0	0	0	0	0	0	0	0	0	0	0	0	0	0	0	0	0	0	0	0	0	0	0	0	0	0%
19	0	0	0	0	0	0	0	0	0	0	0	0	0	0	0	0	0	0	0	0	0	0	0	0	0	0	0	0	0	0	0	0	0	0	0	0	0	0	0	0	0	0%
19,5	0	0	0	0	0	0	0	0	0	0	0	0	0	0	0	0	0	0	0	0	0	0	0	0	0	0	0	0	0	0	0	0	0	0	0	0	0	0	0	0	0	0%
20	0	0	0	0	0	0	0	0	0	0	0	0	0	0	0	0	0	0	0	0	0	0	0	0	0	0	0	0	0	0	0	0	0	0	0	0	0	0	0	0	0	0%
Sum	0	0	0	0	2	43	330	1173	2553	4013	5042	5384	5073	4325	3388	2474	1701	1111	693	417	242	137	75	40	21	11	6	3	1	1	0	0	0	0	0	0	0	0	0	Total sum	
Perc	0%	0%	0%	0%	0%	0%	1%	3%	7%	10%	13%	14%	13%	11%	9%	6%	4%	3%	2%	1%	1%	0%	0%	0%	0%	0%	0%	0%	0%	0%	0%	0%	0%	0%	0%	0%	0%	0%	0%	0%	38258	

Figure E.2: Scatter diagram area 23, calculated according to the method described in appendix C